8-2018

DEVELOPMENT AND IMPLEMENTATION OF A HOMOGENEOUS AND A HETEROGENEOUS ANTHROPOMORPHIC END TO END QUALITY ASSURANCE AUDIT SYSTEM PHANTOM FOR MAGNETIC RESONANCE GUIDED RADIOTHERAPY MODALITIES RANGING FROM 0.35 T TO 1.50 T

Angela Steinmann

TMC LIBRARY
Health Sciences Resource Center

DEVELOPMENT AND IMPLEMENTATION OF A HOMOGENEOUS AND A

HETEROGENEOUS ANTHROPOMORPHIC END TO END QUALITY

ASSURANCE AUDIT SYSTEM PHANTOM FOR MAGNETIC RESONANCE

GUIDED RADIOTHERAPY MODALITIES RANGING FROM 0.35 T TO 1.50 T

By

Angela Kay Steinmann, M.S.

APPROVED:

_____
David Followill, Ph.D.
Supervisory Professor

_____
Laurence Court, Ph.D.

_____
Clifton Fuller, M.D., Ph.D.

_____
Gabriel Sawakuchi, Ph.D.

_____
R. Jason Stafford, Ph.D.

_____
Zhifei Wen, Ph.D.

APPROVED:

_____
Dean, The University of Texas
MD Anderson Cancer Center UT Health Graduate School of Biomedical
Sciences

DEVELOPMENT AND IMPLEMENTATION OF A HOMOGENEOUS AND A HETEROGENEOUS ANTHROPOMORPHIC END TO END QUALITY ASSURANCE AUDIT SYSTEM PHANTOM FOR MAGNETIC RESONANCE GUIDED RADIOTHERAPY MODALITIES RANGING FROM 0.35 T TO 1.50 T

A

DISSERTATION

Presented to the Faculty of
The University of Texas
Health Science Center at Houston
Graduate School of Biomedical Sciences

in Partial Fulfillment

of the Requirements

for the Degree of

DOCTOR OF PHILOSOPHY

By

Angela Kay Steinmann, M.S.

Houston, Texas
August, 2018

Dedication

This dissertation could not be possible without the never-ending support of my humble and loving parents. Mama and Daddy, ***we did it***.

To Daddy- For your endless and selfless sacrifices to ensure your children's needs were first taken care of before your own. Thank you for instilling in me that positive attitude, hard work and persistence does pay off.

To Mama- For always being my life cheerleader and always believing in me (even when I couldn't see it in myself). Thank you always being just one phone call away and for teaching me to be kind to everyone.

"The brick walls are there for a reason. The brick walls are not there to keep us out. The brick walls are there to give us a chance to show how badly we want something. Because the brick walls are there to stop the people who don't want it badly enough. They're there to stop the other people." ― Randy Pausch

Acknowledgements

First and foremost, I would like to thank my gracious advisor, Dr. David Followill, for his never-ending guidance and encouragement throughout each part of my graduate journey. Thank you Dr. Followill for showing me what an effective leader, a supportive mentor and a distinctive medical physicist looks like. I am forever grateful for having you as an advisor and working with such a positive person every day. Thank you for creating a supportive educational environment where I could excel professionally. I am truly fortunate to call Dr. Followill my graduate advisor, a life mentor and a long lasting friend.

I would also like to thank the rest of my advisor committee: Dr. Laurence Court, Dr. Clifton Fuller, Dr. Gabriel Sawakuchi, Dr. Jason Stafford, and Dr. Zhifei Wen. All of my committee members played an intricate role in my research. Thank you all for believing in me and for always taking time out of your hectic schedules to meet with me. My project excelled as a consequence of having your support and guidance during each stage of my research.

Additionally, I would like to thank several other people at IROC-Houston, MD Anderson and The University of Wisconsin who played a crucial role in my project. Interacting with IROC-Houston's physicists, physics assistants, graduate students and the TLD staff members were always positive and they all had willing-to-help attitudes. A very special thank you to John Costales, IROC's phenomenal machinist, who graciously helped construct many of my projects including manufacturing the MRgRT phantoms. Another special thank you to Paola Alvarez who spent countless hours with me to discuss my project and TLDs. Thank you, Hunter Mehrens and Blake Lewis, two of IROC-Houston's physics assistants, for being great friends and always going the extra mile to help me understand IROC-Houston's phantom analysis process. Thanks to all the IROC-Houston's graduate students, physicists and staff for being wonderful colleagues and friends. A special thank you to Mary Carroll for editing this dissertation. I am so grateful for your comments and recommendations. Thanks, also to Gary Bosco, Mo Kadbi, and Drs. John Bayouth,

Kate Mittauer, Daniel O'Brien, Hannah Lee, Geoff Ibbott for helping me with the MRIdian and Unity systems.

I would like to thank my entire family for their endless support and encouragement during my graduate career. I would have not achieved a doctoral degree had it not been for my sweet parents. Thank you for cheering me on and supporting me no matter what. I am forever grateful for your commitment to teach me the value of hard work, persistence and kindness. Thank you Allie, my sister and bestie since birth, for encouraging and reminding me to enjoy the little things in life. Thank you Cliff, my kind hearted brother, for helping me during all of my car problems in graduate school and thank you for your guidance when I *finally* bought a new one. I am truly so thankful to have all your support and love. I love you all so much!

I am forever grateful for meeting my best friend and endearing boyfriend, Dr. Mitchell Carroll, in graduate school. Thank you for your friendship, patience, kindness, encouragement, support and love. You always know how to make me laugh and smile even during the super stressful moments of our graduate careers. Thank you for making me a better person, enriching my life and loving me for who I am. I love you so much! Specifically for this dissertation, thank you for taking the time to edit/discuss my papers, and persevering with me during our graduate careers.

Above all, I thank ***Jesus Christ*** for working through me and always placing the right people in my life to help teach, motivate, encourage and support me. May this document be a true testament of God's love and faithfulness. After all, anything is possible if you have faith as small as a mustard seed (Matthew 17:20).

DEVELOPMENT AND IMPLEMENTATION OF A HOMOGENEOUS AND
HETEROGENEOUS ANTHROPOMORPHIC END TO END QUALITY
ASSURANCE AUDIT SYSTEM PHANTOM FOR MAGNETIC RESONANCE
GUIDED RADIOTHERAPY MODALITIES RANGING FROM 0.35 T TO 1.50 T

Angela Kay Steinmann, M.S.

Supervisory Professor: David S. Followill, Ph.D.

Abstract

Introduction: Magnetic resonance (MR) guided radiation therapy (MRgRT) is

an emerging field that integrates an MR imager with either a linear accelerator or three

radioactive cobalt-60 sources. Before institutions participate in multi-institutional NCI-

sponsored clinical trials, they are required to perform a credentialing test provided by

IROC-Houston. During the credentialing test, end-to-end phantoms are used to evaluate

the institution's ability to perform consistent and accurate radiation treatments. IROC-

Houston's conventional anthropomorphic phantoms are not visible in MR, thus they are

insufficient for MRgRT systems. The purpose of this work was to create an

anthropomorphic thorax and a head and neck (H&N) phantom for MRgRT systems

with magnetic fields ranging from 0.35T to 1.5T.

Methods: Over 80 synthetic materials were examined as potential materials

used to construct the MRgRT thorax and H&N phantoms. Materials were characterized

by: 1) measuring Hounsfield units, 2) visualizing in MR and CT imagers and 3)

evaluating their dosimetric characteristics. Once materials were selected for the

MRgRT phantoms, radiochromic film and double-loaded TLDs were then characterized

in a 1.5T and a 0.35T MR environment. Reproducibility measurements on double-

loaded TLDs were performed by using an acrylic block and irradiating it in 0T/1.5T

and 0T/0.35T configurations on the Unity system and the MRIdian Cobalt 60 system,

respectively. Geometrical thorax and H&N phantom slabs were designed to mimic similar interface conditions seen in anthropomorphic phantoms, but were simplified to reduce manufacturing time. The geometrical phantoms were designed with a rectangular tumor centrally located around surrounding tissue. These two phantoms were used to characterize radiochromic EBT3 film and TLDs by comparing beam profiles and point dose measurements irradiated with and without magnetic fields, respectively. GEANT4 Monte Carlo simulations validated the detectors in both Unity 0T/1.5T and MRIdian 0T/0.35T configurations. Two MRgRT anthropomorphic (H&N and thorax) phantoms were designed, manufactured and evaluated. A reproducibility and feasibility study was conducted to evaluate the phantom's performance on MRgRT systems.

Results: This study found four materials which were tissue equivalent and visible on both MR and CT. Additionally, this study showed negligible difference in dose response between TLDs and radiochromic film when irradiated in 0.35T and 1.5T magnetic field environments. Two anthropomorphic phantoms were constructed and evaluated. The anthropomorphic thorax and H&N phantoms passed IROC-Houston's 7%/5mm and 7%/4mm gamma passing criteria, respectively.

Conclusions: An anthropomorphic thorax and an H&N phantom were tissue equivalent, compatible with MR and CT workflows and could be used as end-to-end QA tools for MRgRT systems with magnetic fields ranging from 0.35T to 1.5T.

Table of Contents

NOMENCLATURE

2D	Two-dimensional
3D	Three-dimensional
3D-CRT	Three-dimensional Conformal Radiation Therapy
^{60}Co	Cobalt 60
CBCT	Cone-beam Computer Tomography
CT	Computer Tomography
DTA	Distance to Agreement
EPID	Electronic Portal Imaging Device
ERE	Electron Return Effect
ETL	Echo Train Length
FA	Flip Angle
GTV	Gross Tumor Volume
H&N	Head and Neck
HIPS	High Impact Polystyrene
HU	Hounsfield Unit
IAEA	International Atomic Energy Agency
IMRT	Intensity-Modulated Radiation Therapy
IGRT	Image-guided radiotherapy
IROC-Houston	Imaging and Radiation Oncology Core in Houston
LiF	Lithium Fluoride
NCI	National Cancer Institute
NCTN	National Clinical Trial Networks

M	Magnesium
MLC	Multi Leaf Collimator
MR	Magnetic Resonance Imaging
MRgRT	Magnetic Resonance guided Radiation Therapy
MVCT	Megavoltage Computed Tomography
NEX	Number of Excitations
OAR	Organ at Risk
OD	Optical Density
PDD	Percent Depth Dose
PTV	Planning Target Volume
PVC	Polyvinyl Chloride
QA	Quality Assurance
RT	Radiation Therapy
RTOG	Radiation Therapy Oncology Group
SBRT	Stereotactic Body Radiation Therapy
SRS	Stereotactic Radiosurgery
STE	Synthetic Tissue Equivalent
Ti	Titanium
TE	Echo Time
TL	Thermoluminescent
TPS	Treatment Planning System
TR	Repetition Time

TrueFISP	True Fast Imaging with Steady-state free Precession (MRIdian)
TRUFI	True Fast Imaging with Steady-state free Precession (GE)
VR-TPDS	ViewRay System Treatment Planning and Delivery Software
Zeff	Effective atomic number

LIST OF ILLUSTRATIONS

LIST OF TABLES

Chapter 1:   Introduction

1.1   BACKGROUND

1.1.1   Imaging Guidance in Radiation Therapy

Most modern radiotherapy systems are equipped with image-guided radiotherapy (IGRT) devices to verify patient setup and manage intrafraction and interfraction motion[1-3]. IGRT devices can broadly be categorized into either radiation or non-radiation based systems. Some radiation-based systems include: electronic portal imaging device (EPID), Computed Tomography (CT) on rails, Megavoltage CT (MVCT), and cone beam CT (CBCT); common non-radiation based IGRT devices are ultrasound and camera-based systems. Modern treatment vaults can be equipped with either a single IGRT system or multiple IGRT systems used in conjunction with one another.

Gantry-mounted electronic portal imaging systems, commonly known as EPID systems, are equipped with a flat-panel imager mounted parallel to an in-field linear accelerator. These systems are used to verify patient setup from the treatment field's orientation by capturing a single two-dimensional (2D) MV image. Modern EPID systems are readily available since they use the same beam path and energy as the linear accelerator. Compton interaction dominates during MV imaging. Consequently, these 2D images produce poor contrast between tissues that have similar effective atomic numbers (Zeff)[4]. Structure interfaces that have large Zeff deviations, such as bony anatomy or fiducial markers next to soft tissue, will have high contrast delineation in MV images. Therefore, EPID images are primarily used to verify patient setup by comparing gross anatomy (i.e., bony anatomy) to CT images. While EPID systems are convenient and use

the same photon beam, they are a limiting IGRT system since they mostly are used to align rigid structures. EPID systems (unless imaged multiple times) are also limited since they only capture a 2D image at a single point in time.

Another IGRT system, known as MVCT, captures a three-dimensional (3D) image by using an in-field MV beam parallel to a fan beam detector. Helical TomoTherapy is the most commonly known MVCT system used in the clinic and was specially designed to alleviate 2D setup errors. During imaging acquisition, the beam energy is reduced from 6 MV to 3.5 MV and both detector and beam rotate around a single isocenter as a treatment couch travels through the bore. The reduced beam energy allows for greater soft tissue contrast compared to a normal 6 MV image and eliminates streaking artifacts caused in lower KV images[5]. While MVCT soft tissue contrast is enhanced, acquired images have poor delineation between tumor and surrounding tissues. Additionally, MVCT requires more time to acquire an image and can only capture a single-frame image[6].

To produce diagnostic-quality images, a conventional CT can be installed inside the treatment vaults. Commonly referred to as, CT on rails, a treatment couch is rotated 180 degrees where a mobile diagnostic CT scanner slides across a pair of rails and captures a 3D image which is then used to verify patient setup[3]. Diagnostic-quality 3D CT images permit better soft tissue contrast than MV generated images, thus improving soft tissue localization. CT on rails has a few limitations: 1) images are only captured pre or post treatment, 2) large vaults are required to hold both systems, and 3) CT on rails is incapable of tracking intrafraction motion.

CBCT is currently a popular IGRT system which is typically mounted onto the treatment gantry and installed orthogonal to the treatment beam. This system is equipped

with a retractable x-ray tube parallel to a flat panel imager[7]. KV energies are used to acquire a single-frame volumetric image by rotating the gantry around the treatment couch[2-4]. CBCT images produce superior soft tissue contrast compared to common MV IGRT systems. While CBCT is currently considered the most universal 3D IGRT system used for pre-treatment setup verification, there are limitations prevent CBCT from being the absolute universal IGRT system[3]. The cone beam geometry in CBCT contributes to larger radiation scatter which consequently affects the image quality. Therefore, diagnostic-quality CT images are not captured in CBCT imagers. This degrade in image quality can impair soft-tissue delineation that is required to accurately verify treatment setup. Similar to other IGRT systems, CBCT is limited to only capturing a single-frame image and is unable to track intrafraction motion without capturing multiple images that would then increase patient dose.

Ultrasound imaging can also be used as an IGRT system for radiotherapy. In-room ultrasound image guidance is inexpensive, non-ionizing and is used as a site-specific tumor localization method. Ultrasound captures a 2D image which is used to localize soft tissue organs such as a liver, a breast or a prostate. In-room ultrasound image guidance verifies patient setup by mapping a 2D ultrasound image to the treatment room's coordinate system[3-5]. Other than being restricted to soft tissue organs, there are two limiting factors: 1) inter-user variability and 2) the inability to capture real-time images[4; 5]. Ultrasound images are hard to reproduce since the acquisition is highly dependent on the transducer's angle relative to the patient. Secondly, images are not captured during treatment since these systems are not automatized and therefore require a sonographer to operate the equipment. Since the transducer is required to be close to

the patient, any automated system would generally be within the treatment field and ultimately might alter the dose deposition.

Camera-based systems are another non-ionizing radiation imaging technique. These systems are used to verify setup positions through visible or infrared cameras. In-room camera based systems are relatively cheap to install and have a live feedback mechanism used to correct setup errors occurring at any point during treatment[7]. Some of these systems are used for site specific locations. These systems mostly commonly are used to account for intrafraction motion by implying either gating or external surrogating techniques. The major limitation of camera-based systems is the lack of visualizing internal structures such as the disease site and surrounding normal tissues. Camera-based systems assume exterior surface motion directly correlates with tumor motion. For some tumors, measured surface movements do not accurately resemble the same motion a tumor experiences. Inability to visualize internal soft tissues prevents the system from accurately track tumor motion, and internal organ deformations[7; 8].

1.1.1.1 Benefits of On-board MR imaging

Current IGRT systems have greatly improved dose delivery accuracy in radiation therapy by reducing interfraction setup errors; however, these systems all have limitations that either are incapable of distinguishing the disease site from surrounding normal tissue, visualizing the tumor in real-time or capturing images to be used for online adapted radiotherapy. Recently, there have been attempts to mitigate these limitations by integrating a magnetic resonance (MR) system with either a linear accelerator or a radioactive cobalt 60 source. MR provides superior soft tissue contrast compared to images acquired from either KV or MV imagers. This improved ability to visualize soft

tissue would consequently increase the accuracy of delineating the tumor boundary from normal tissue (Figure 1)[9]. Better target delineation could be used to reduce margins or increase the gross tumor volume (GTV) radiation boost, which could potentially increase local tumor control and reduce normal tissue toxicities. Another advantage is that MR does not contribute to the absorbed dose; so, a patient is not restricted to a single-frame setup image but rather could be image during the entire treatment. Fast sequence protocols used in on-board MR scanners enable 2D and 3D cine images during treatment. This eliminates the need for external surrogates and improves gating techniques by tracking the disease site in real-time. Online adapted radiotherapy could be implemented in the clinic since images with superior contrast would be used to localize the disease site. The newly captured MR image would then be used to adjust the treatment plan to the disease site's current location. On-board MR imagers could potentially be used to capture functional imaging information which then could be used to quantify and evaluate the overall tumor progression during treatment. Therefore, on-board MR imagers could revolutionize radiation treatment by improving the certainty of delivering radiation.
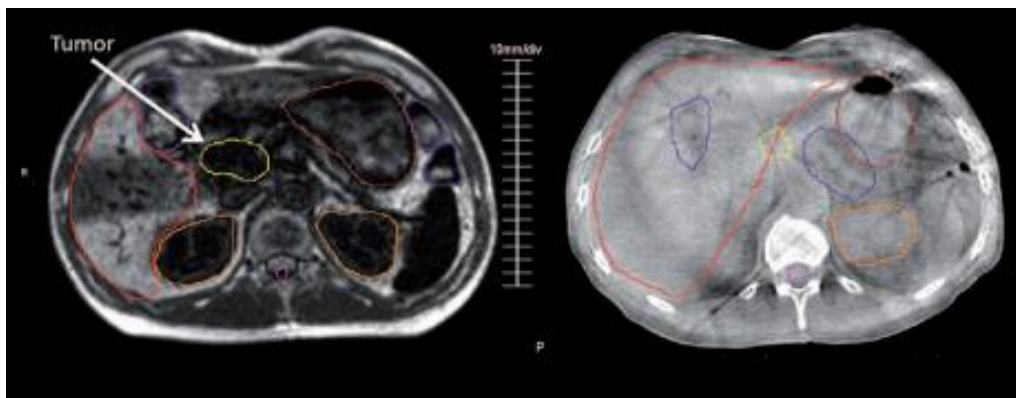
Figure 1: A comparison between abdominal images captured on a 0.35T on-board MR imager (left) and CBCT (right). The low field MRI provides high soft tissue contrast to distinguish between a pancreas tumor and surrounding organs, whereas the CBCT shows insignificant contrast between the two[9].

1.1.2   MR guided Radiation Therapy Systems

Magnetic resonance guided radiotherapy (MRgRT) is a rapidly emerging field which integrates a fully functional MR imager in conjunction with either a linear accelerator or a radioactive Cobalt 60 (^{60}Co) source. Presently, there are a total of six different MRgRT prototypes: two are still in the research stage and four have been fully implemented into the clinic[10-16]. Pre-clinical MRgRT systems are: the Australian MR-Linac (Ingham Institute, Liverpool, Australia) and Aurora RT (MagnetTx Oncology Solutions, Alberta, Canada) and clinically implemented MRgRT systems are: MRgRT suite (Varian, Palo Alto, California, USA and Siemens, Erlangen, Germany), Unity (Elekta, Crawley, United Kingdom and Philips, Amsterdam, Netherlands). MRIdian ^{60}Co (ViewRay, Oakwood Village, Ohio), and MRIdian Linac (ViewRay, Oakwood Village, Ohio).

In short, the Australian MRI-Linac is an inline MRgRT system equipped with a 6 MV linear accelerator and a 1.0 T open bore magnet[11]. This system was designed to have a fixed 6 MV beam with a mobile treatment couch that was capable of rotating 360 degrees inside the bore[11; 17]. The Aurora RT system was first designed to have a 6 MV beam only; however, additional research has been performed to create a versatile MRgRT system that has four possible (4 MV, 6 MV, 8 MV and 10 MV) discrete energies[13; 18-20]. This system was designed such that a linear accelerator can rotate around a biplanar 0.5T magnet, thus allowing a photon beam to transmit in either parallel or perpendicular directions from the magnetic field[13; 21]. The first MRgRT system used to treat patients was developed at the Princess Margaret Cancer Centre and is commonly known as the

MRgRT suite. This suite interconnects three rooms which allow a Siemen's MRI on rails system to travel to either a Varian TrueBeam vault or a Nucletron brachytherapy suite[10]. Elekta's Unity system started treating patients in 2017 and is equipped with a 7 MV linear accelerator located above a modified 1.5T Philip's MR scanner. The ViewRay system currently has two models: ViewRay MRIdian and ViewRay MRIdian Linac, both of which are FDA cleared and have been fully implemented into the clinic to treat patients. The MRIdian system, which started treating patients in 2014, is equipped with three ^{60}Co radioactive head sources located in between a split 0.35T magnet. The MRIdian Linac, which started treating patients in 2017, is a modification to the original ^{60}Co MRIdian system[22]. In this upgraded MRgRT system, the three radioactive sources were replaced with a single 6 MV beam. Table 1 is a summary of all MRgRT systems and their technical specifications.

While there are several different emerging MRgRT devices (Table 1), the only systems currently used within the United States are the Elekta/Philip's Unity, the ViewRay's MRIdian ^{60}Co, and the ViewRay's MRIdian Linac MRgRT system. Both MRIdian and Unity systems are capable of intrafractional and interfractional monitoring, cine images during treatment, and adaptive radiation therapy[15; 23]. These systems were used to develop and characterize the Imaging and Radiation Oncology Core Quality Assurance Center in Houston's (IROC-Houston) MRgRT QA phantoms. These three MRgRT systems' configurations will further be discussed in the following subsections.

MRgRT Systems	Energy	Magnetic Field Strength	Bore Diameter	Beam Direction to Magnetic Field	First Treated Patients
Australian MRI-Linac[a]	6 MV	1.0T	82 cm	Parallel or Perpendicular	n/a
Aurora RT[b]	4, 6, 8 and 10 MV	0.5 T	60 cm	Parallel or Perpendicular	n/a
MRI on Rails[c]	6 MV	1.5T	70 cm	n/a	2014 *(Princess Margret Cancer Centre, Canada)*
Unity[d]	7 MV	1.5T	70 cm	Perpendicular	2017 *(UMC Utrecht, Netherlands)*
MRIdian[e]	3 Co-60	0.35T	70 cm	Perpendicular	2014 *(Washington University, USA)*
MRIdian Linac[e]	6 MV	0.35T	70 cm	Perpendicular	2017 *(Henry Ford Health Systems, USA)*

a: Ingham Institute, Liverpool, Australia b: MagnetTx Oncology Solutions, Alberta, Canada c: Varian, Palo Alto, California, USA and Siemens, Erlangen, Germany d: Elekta, Crawley, United Kingdom and Philips, Amsterdam, Netherlands e: ViewRay Oakwood Village, Ohio, USA

Table 1: Summary of the current MRgRT systems. Among all MRgRT systems, two are in the clinical development stage (Australian MRI-Linac and Aurora RT) and four have been used to treat patients (MRI on Rails, Unity, MRIdian, and MRIdian Linac).

1.1.2.1 Elekta Unity System

The Unity system was equipped with a flattening filter free (FFF) 7 MV standing waveguide attached to a slip ring gantry centrally located above a modified 1.5T MR system (Figure 2). The magnet was redesigned to have a 15 cm gap free of coils in the center of the magnet. Additionally, active shielding was modified to create a low field toroidal ($<10^{-3}$T magnetic field) in the center of the magnet[24; 25]. The 7 MV linear accelerator was centrally installed above the magnet, where both systems could be magnetically decoupled from one another. The MR component works independently of the linear accelerator and can be used to capture real-time diagnostic-quality 2D and 3D

images at 8 frames per second. The linear accelerator was designed to have a 160-leaf multi-leaf collimator (MLC) system and could be extended to have a maximum field size of 57 cm (sagittal) by 22 cm (axial) [23; 26]. The Unity system is presently not FDA cleared to treat patients in the United States; however, the first patient treated on the Unity system was at The University Medical Center Utrecht in 2017[23].

Figure 2: Elekta's Unity system, which is the first high magnetic field (1.5T) system integrated with a 7 MV linear accelerator.

1.1.2.2 ViewRay MRIdian System

The ViewRay MRIdian is the first single-room integrated MRgRT system to simultaneously treat and image patients. The MRIdian system was FDA cleared in 2012 and began treating patients in 2014. The MRIdian system (Figure 3) delivers modulated radiation therapy using three independent ^{60}Co head sources equally spaced 120-degrees from each other. The radioactive sources are centrally located in between a split 0.35T

superconducting magnet[27]. All three ^{60}Co head sources simultaneously rotate 240-degrees around a ring gantry to provide 360-degree coverage and can be used individually or simultaneously with one another. The head sources can be used together to provide a dose rate comparable to a typical 6 MV linear accelerator (550 cGy/min at installation) [15; 28]. Each source was equipped with a 60 leaf double-focus MLC to provide comparable penumbras that are typically seen in a 6 MV linear accelerator[15; 28]. Using radioactive head sources in between a split magnet eliminated the need for electronics, which allowed the two systems to work independently of one another.
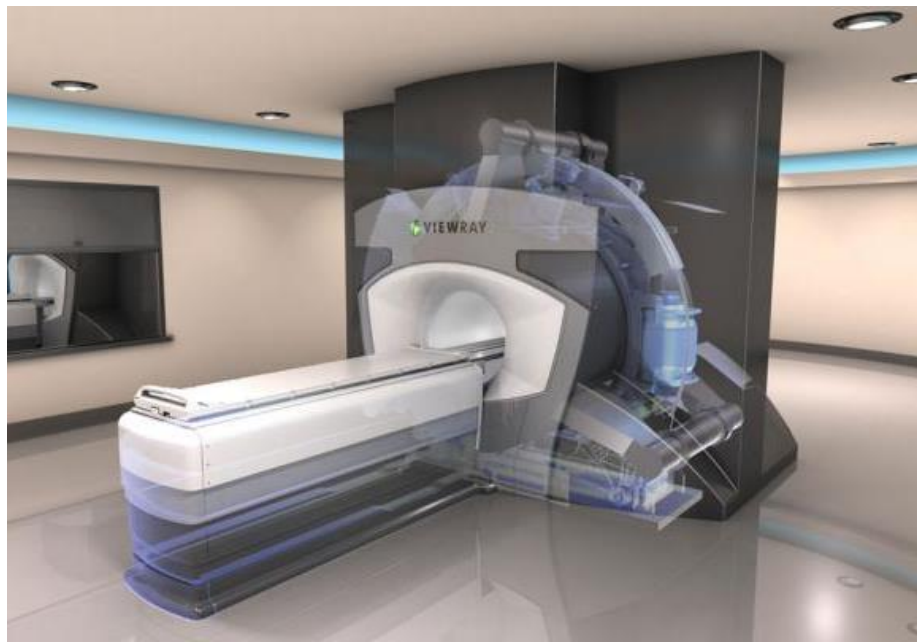
Figure 3: ViewRay's first MRgRT system. The MRIdian Co-60 is comprised of three equally spaced cobalt 60 head sources centrally located in between a spilt 0.35T semiconducting magnetic. In 2014, the first patient was treated on the MRIdian Co-60 system at Washington University School of Medicine in St. Louis, Missouri, USA[27].

The MRIdian Linac (Figure 4) is an upgraded MRgRT system that replaced three radioactive ^{60}Co sources with a single compact inline S-band 6 MV standing waveguide[29; 30]. Similar to ViewRay's first generation MRgRT system, the linear accelerator is centrally located in between a split 0.35T superconducting magnet. The

compact linear accelerator is enclosed around a magnetic and RF shield, thus allowing the two systems to work independently of each other[30]. The FFF linear accelerator was designed to produce dose rates greater than 600cGy/min and was constructed with 138-leaf double-focused double-stacked MLC system. The two sets of MLC are used to create a sharp penumbra and to reduce interleaf leakage[30]. The MRIdian Linac was granted FDA clearance in early 2017 and started treating patients that summer[22].
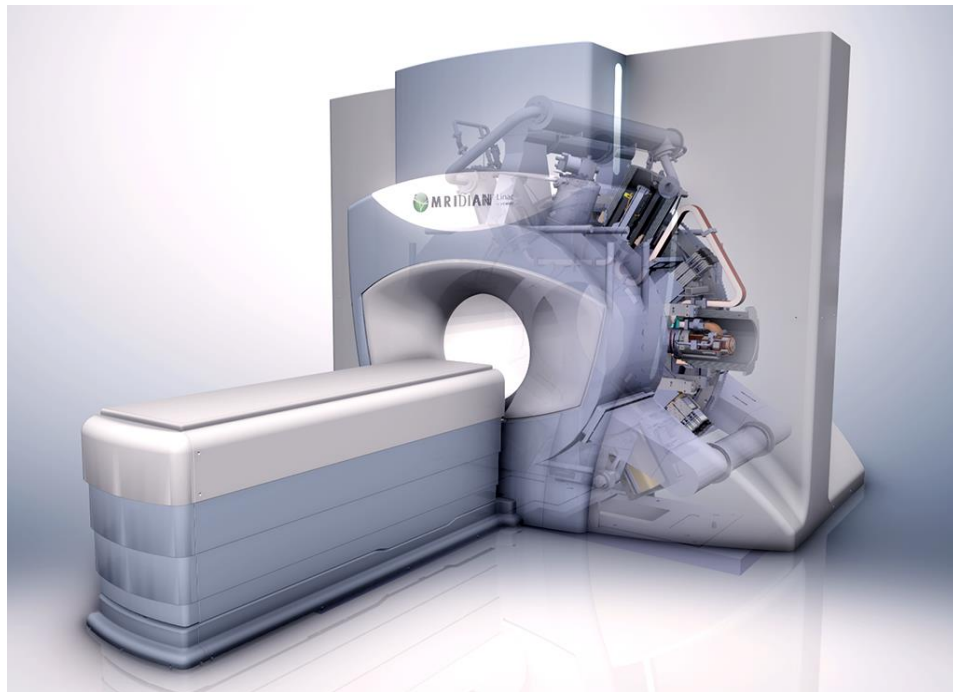
Figure 4: ViewRay's upgraded MRgRT system. The MRIdian Linac is comprised of a 6 MV linear accelerator centrally located in between a spilt 0.35T semiconducting magnetic. The first patient treated on the MRIdian Linac was in 2017 at Henry Ford Health Center, Gross Point, Michigan, USA[29].

Both MRIdian and MRIdian Linac systems use a Monte Carlo based treatment planning system known as the ViewRay System Treatment Planning and Delivery Software (VR-TPDS). The VR-TPDS is capable of creating 3D conformal radiation therapy (3D-CRT), intensity modulated radiation therapy (IMRT), stereotactic body radiation therapy (SBRT), stereotactic radiosurgery (SRS) and IGRT plans. At 4 frames

per second, both systems can acquire a single sagittal image using a single true fast imaging with a steady state precession MR sequence[31].

1.1.3 Dosimetric Challenges in MRgRT systems

Secondary electrons, set into motion from photon interactions, are affected by magnetic field environments. This phenomenon can be explained by the Lorentz force (Equation 1). When charge particles (q) with a velocity (v) experience a magnetic field (B), the Lorentz force causes the charge particle's trajectory to curve perpendicularly from the magnetic field direction and velocity direction.

$$\boldsymbol{F} = q(\boldsymbol{v} \times \boldsymbol{B}) \tag{Eq.1}$$

The magnetic field affects the trajectories of secondary electrons which, specific to radiotherapy, will consequently affect dose being deposited into a tissue. Figure 5 visually describes how a single electron's point spread kernel is affected in different magnetic field strengths perpendicular to a 6 MV photon beam inside a homogenous water phantom[32]. In low magnetic field environments (i.e., 0.2T), the electron's trajectory is generally unaffected by the magnetic field and creates similar radiation deposition seen in zero magnetic field environments. In high field environments (i.e., 3.0T), the electron's trajectory is greatly influenced by the magnetic field and, as a result, deposits dose in an arc-shape pattern. The radius of an electron's arc-shape trajectory is proportional to the electron's energy and inversely proportional to the experienced magnetic field strength[32]. Therefore, the point spread kernels are more asymmetrically pronounced for higher magnetic fields and lower electron energies.
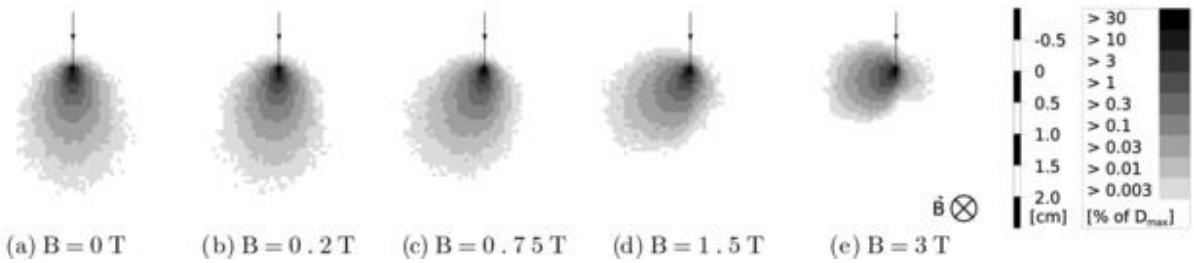
Figure 5*: Point spread kernels for a single electron trajectory in a homogenous medium under a 6MV beam perpendicular to (a) 0T, (b) 0.2T, (c) 0.75T, (d) 1.5T and (e) 3T magnetic field strengths. Point spread kernels become more asymmetric in larger magnetic field environments*[32].

Secondary electrons traveling through heterogeneous materials in the presence of a magnetic field will experience what is known as the electron return effect (ERE). The ERE is most prominent at interfaces with high density variations such as: air cavities or patient exteriors. As the electron exits from a higher-density material and enters into a lower-density material, the electron will curve back into the high-density material and deposit dose (Figure 6). In Monte Carlo studies, dose deposited in complex heterogeneous systems generally showed that the dose decreased in low-density to high-density interfaces but increased in high-density to low-density interfaces[33]. Further investigation also showed that, at first order, opposing photon beams could counterbalance the ERE effect in heterogeneous materials[33].
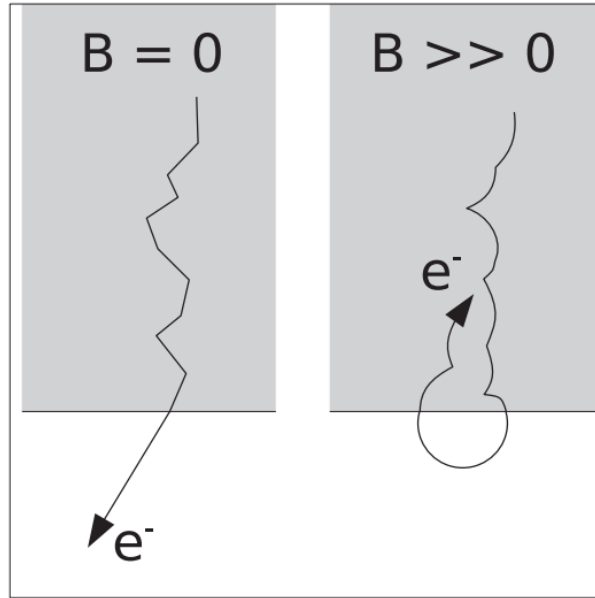
Figure 6: A single electron trajectory propagating through high to low density medium in absence (left) and presence (right) of a magnetic field[34].

High magnetic field can also affect general radiation beam characteristic, namely, percent depth dose (PDD) curves and beam profiles. In general, the secondary electron's helical-shape trajectories reduce the overall path, causing the PDD to shift. Specifically in a 7 MV photon beam perpendicular to a 1.5T magnetic field configuration, the PDD is modified causing a shorter build-up region, a 4-5 mm shift in the depth of maximum dose (d_{max}) towards the surface, and an approximately 0.5% reduction in dose beyond build up region (Figure 8)[35; 36]. In the presence of a 1.5T magnetic field, the output at dmax is enhanced by 1.9%[36]. For a 7 MV beam the dmax was measured at 1.3 cm and 1.7 cm for 1.5T and 0T configurations, respectively[36].
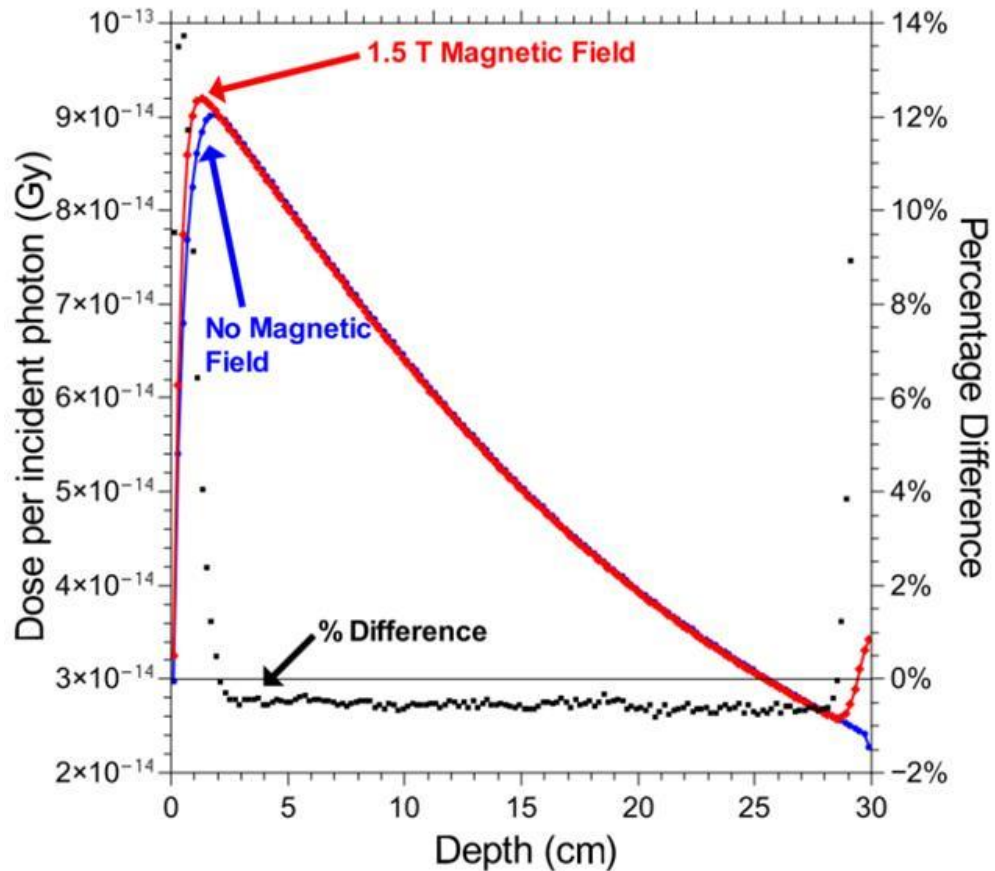
Figure 7: Geant4 Monte Carlo measurements comparing PDD curves under the presence of 0T and 1.5T magnetic field strengths for a 7 MV photon beam with a 10x10 cm² field size[35].

Magnetic fields also affect beam profiles by creating asymmetric dose deposition in the lateral direction. The entire field, towards the Lorentz force direction, shifts approximately 1 mm for all field sizes at the 50% level[35; 37]. A more dramatic shift was seen in the shoulder region of the profiles due to the magnetic field influence. As shown in Figure 8, the general shape of beam profiles measured in a 1.5T magnetic field are asymmetric and more pronounced in smaller field sizes. From the central axis, the disproportional penumbras are less pronounced on the right side and vice versa, more pronounced on the left side due to the effects of the magnetic field. In general, smaller fields (1x1cm²) are affected more by a magnetic field than larger field sizes (i.e., 10 x 10cm²)[32].
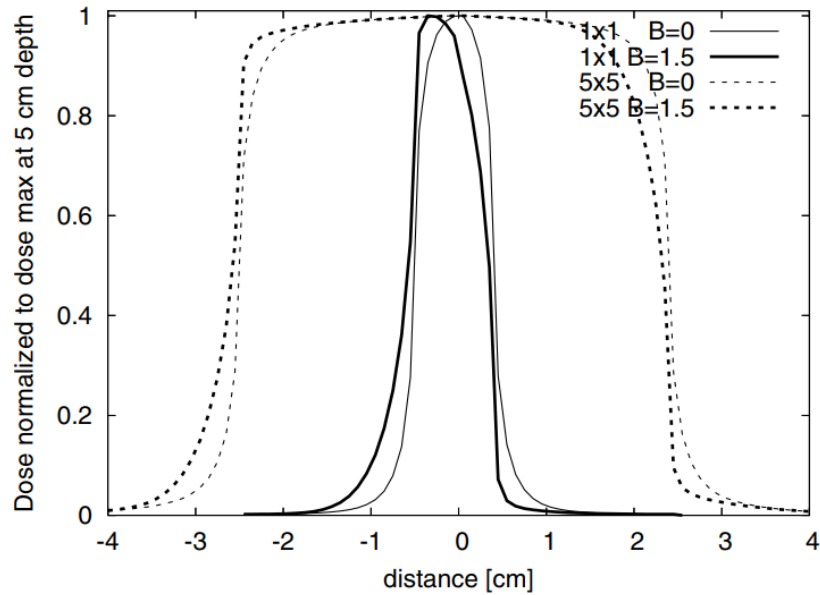
Figure 8: GEANT4 Monte Carlo generated beam profiles for a 6 MV radiation beam incident perpendicular to 1.5T and 0T magnetic field strengths for 1.0 cm x 1.0 cm² and 5.0 x 5.0 cm² field size[34].

1.1.4 Conventional IROC Phantoms

IROC-Houston, formally known as Radiological Physics Center or RPC, has been funded by the National Cancer Institute (NCI) since 1968 to help credential and audit institutions participating in NCI sponsored clinical trials. IROC monitors NCI participating institutions' performances through either on-site dosimetry visits or off-site auditing methods.

Among various off-site quality assurance (QA) programs, IROC-Houston implemented an anthropomorphic program designed to evaluate multi-institutions' performances through an end-to-end examination. The main purpose of this off-site QA program was to ensure that all institutions participating in NCI clinic trials could deliver comparable and consistent radiation treatments. During the examination, the anthropomorphic phantom will experience the same clinical workflow (i.e., CT imaging, treatment planning, treatment setup, and dose delivery) as a patient, thus analyzing the

institution's capability of delivering radiation based on their expected treatment plan. IROC-Houston's current site-specific phantoms used in photon beams include: SRS Head, IMRT Head and Neck (H&N), IMRT Thorax, 3D CRT Thorax, IMRT Spine, liver and pelvis/prostate. Most of IROC-Houston's phantoms are similarly designed consisting of a water-fillable shell and a removable insert which contains: dosimeters, tumor targets and organ(s) at risk (OAR) structures.

IROC-Houston's most widely used phantoms are the H&N and thorax anthropomorphic phantoms and are, respectively, visualized in Figure 10 & Figure 9. The materials used to manufacture these phantoms are described in Table 2. In short, the H&N phantom insert consists of an acrylic spinal cord representing an OAR, surrounding tissue constructed of high impact polystyrene (HIPS), and two (primary and secondary) planning target volumes (PTV) constructed from solid water. The thorax phantom utilizes a programmable stepper motor to reflect normal inhale/exhale physiology and consists of an acrylic spinal cord, nylon heart, two lungs constructed from compressed cork, and HIPS representing a PTV centrally located inside the left lung. Substituted materials used in the H&N and thorax phantoms are tissue equivalent and have similar density as corresponding human tissues (Table 3).

Structure	H&N Materials	Thorax Materials
Tumor	Solid Water	HIPS
Surrounding Tissue	HIPS	Compressed Cork
OAR: Spinal Cord	Acrylic	Acrylic
OAR: Heart	n/a	Nylon

Table 2: Material assigned to IROC-Houston's conventional thorax and H&N phantom.

Figure 9: IROC-Houston's water-fillable anthropomorphic lung phantom contains a nylon heart, an acrylic spinal cord, two compressed cork lungs and a centrally located HIPS tumor inside the left-side lung. The left-sided lung is created from an external insert that is mounted to a motion table to simulate breathing.

Figure 10: IROC-Houston's conventional H&N phantom is constructed using solid HIPS and is equipped with a centrally located single insert. The insert has two parts that combine to create an acrylic spinal cord, a semi-circle primary PTV and a circular secondary PTV constructed of solid water.

Material	Density [g/cm3]
Acrylic	1.17
Compressed Cork	0.33
HIPS	1.20
Nylon	1.08
Solid Water	1.04

Table 3: Density of substituted materials used in IROC-Houston's conventional H&N and thorax phantoms.

1.1.5   Detectors used in IROC Phantoms

IROC-Houston's anthropomorphic phantoms use thermoluminescent detectors (TLD) and radiochromic film. The measured doses on these detectors are compared with the expected treatment planning data. In total, eight double-loaded TLDs and three planar films were inserted into the H&N phantom. Similarly, the thorax phantom was equipped with four double-loaded TLDs and three planar films. TLDs are used as an absolute point dose measurement at a specific location and radiochromic films are used to describe planar relative dose distributions across a specific region within the insert.

1.1.5.1   Thermoluminescent Detectors

Thermoluminescent (TL) is a phenomenon in which inorganic crystals absorb radiation energy and proportionally emit energy in the form of light when heated. The generally accepted TL model theorizes that the impurities from the inorganic crystal causes electron traps in the forbidden energy bands[38]. These energy traps are located in between the "allowable" conduction (excited state) and valence (ground state) energy bands. When an inorganic material is irradiated, electrons in the ground state can absorb enough energy to rise to the excited state; thereby creating a vacancy (knowns as a

positive hole) in the ground state (Figure 11). Both excited electrons and positive holes move around in the conduction and valence bands until they recombine, respectively. Recombination can occur in two ways: 1) the excited electron can recombine with the positive hole in the ground state or 2) the excited electron and positive hole can get "trapped" respectively in an electron trap and hole trap[38; 39]. When the inorganic crystal is heated, electrons and positive holes receive enough energy to excite out of their traps, recombining and emitting one light photon per recombination[39]. The light photon is converted into an electrical current through a photomultiplier tube, and then read out. The intensity of light photons emitted is a function of temperature and is displayed on a glow curve. Figure 12 shows a typical example of a glow curve for TLD-100s. The area under the glow curve represents the signal which is the total number of light photons emitted[39].
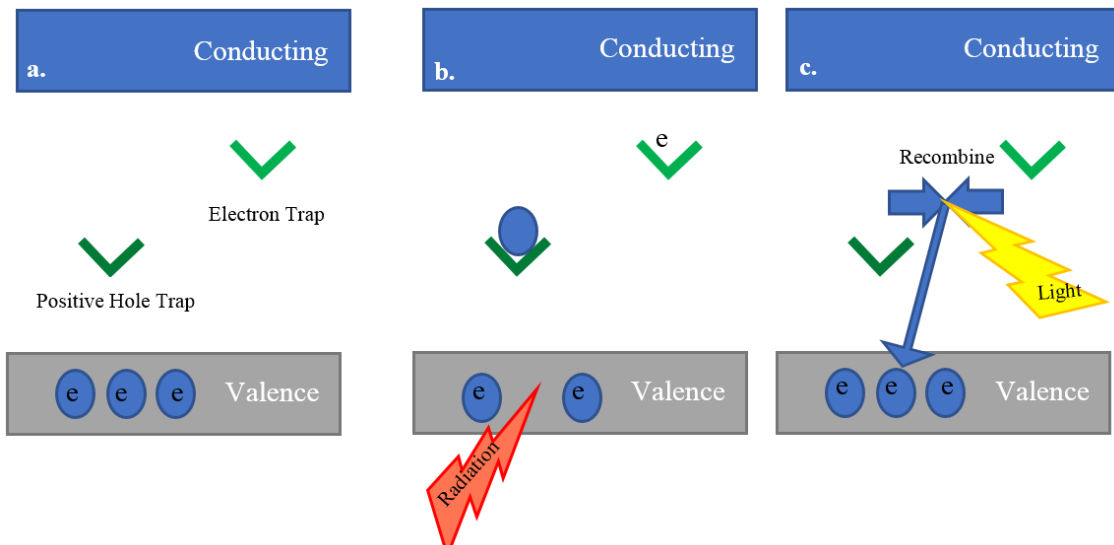
Figure 11: The physics behind TL phenomena. Impurities in lithium fluoride doped with magnesium and titanium (LiF: M, Ti) structures create positive hole and electron traps (a). When radiation passes through a TL structure, the electrons will be excited to a higher energy state and will leave holes in the valence band. Both holes and electrons will move around the valence and conduction bands, respectively, until they are either recombined or trapped (b). The electrons and holes are trapped until a source of heat simulates the structure. Heat energy is transferred to the electrons and holes thereby releasing them from their traps and allowing for them to recombine (c). Energy is conserved in the recombination process. The excess energy is released in the form of a visible light photon.
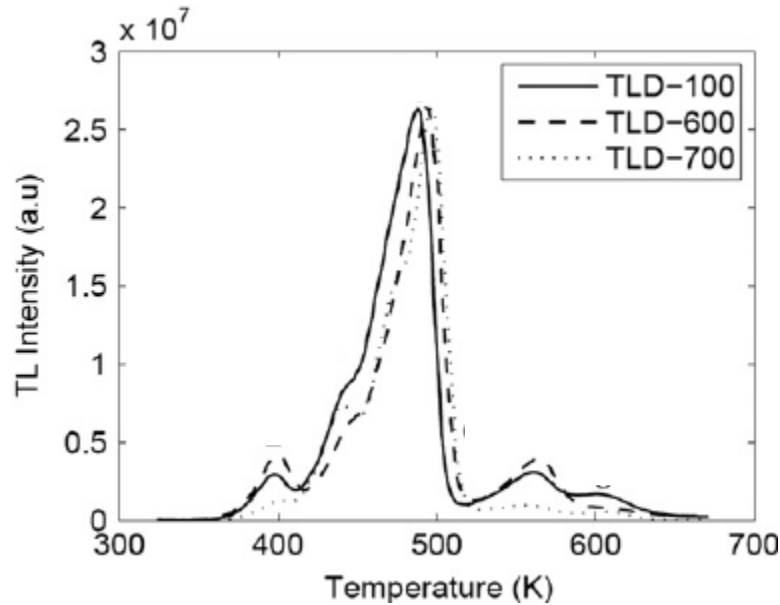
Figure 12: Typical Glow Curve for a TLD-100. The intensity represents the total light emitted as the material is heated[40].

Dose measurements from TLDs can be converted into absorbed dose by applying several correction factors to the average TL response from photomultiplier readout. Some of these correction factors include: system sensitivity, dose-response linearity, fading and energy response. System sensitivity correction factor accounts for the readout system. Since TLDs are linear up to 4 Gy, a linearity correction factor is used to account for superlinearity corrections at higher doses. At shallow traps, electrons and holes may recombine at room temperature and can "fade" the signal. Fading corrections are a factor of time and are implemented to account for reductions in the signal from irradiation time to read-out time.

The most extensive TLDs used in radiation therapy are TLD-100s and are composed of lithium fluoride (LiF) and doped with titanium (Ti) and magnesium (M). TLD-100s are popular clinical dosimeters since they are nearly tissue equivalent (effective atomic number of: 6.06) and have deep traps which prevent extreme fading[39; 41]. Impurities, caused from doping with Ti and M, allow for trap structures. TLDs can

come in various forms (i.e., powder, rod, chip, and disk). IROC-Houston purchases powder-form TLDs (ThermoFisher Scientific, Waltham, Massachusetts, USA) which come in cylindrical capsules that have a 4 mm diameter and 15 mm length. Double-loaded TLDs are filled with approximately 22 mg of LiF: M, Ti and is produced with no air gaps inside the TLD capsule. These TLDs have a linear range of 10 µGy to 1 Gy and provide two absolute point dose measurements. Previous studies, concluded by Kirby et al. 1992, showed TLDs to have a 3% precision and a dosimetrically accuracy of 5% (at 93% confidence interval) compared to measured ion chambers readings[42].

1.1.5.2   Radiochromic EBT3 Film

In addition to TLDs, IROC-Houston inserts radiochromic film into anthropomorphic phantoms to analyze the relative 2D radiation dose distributions. Currently, IROC-Houston uses GafChromic EBT3 (International Specialty Products Ashland Inc., Covington, Kentucky, USA) film for all anthropomorphic phantom studies. As shown in Figure 13, EBT3 film is manufactured with three main layers. A thin active layer (28µm) is located in between two transparent, matte polyester base sheets each having 125µm thickness. The two identical polyester base sheets that are directly attached to the active layer prevents the user from keeping track of what side the film was placed on the light source of a densitometer. According to the manufacturer, the active layer is comprised of marker dye, stabilizers, active component and aluminum oxide to minimize low-energy dependence[43; 44]. EBT3 is nearly tissue equivalent with an effective atomic number of 6.71 and is generally used to measure radiation dose from 0.01Gy to 10Gy[43]. EBT3 film is extremely useful for IROC-Houston since it can easily

be modified to fit inside an insert, does not require wet-post-processing methods, and is nearly insensitive to light.
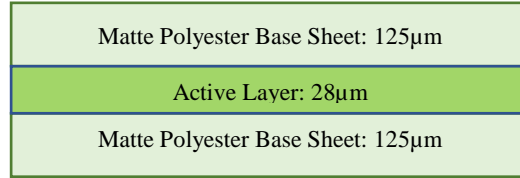
Figure 13: Cross-section describing Gafchromic EBT3 film component layers. Two 125μm polyester base sheets protecting a 28μm active layer.

1.1.6   Dosimetric End-to-End Evaluations

Gamma Analysis, first developed by Low et al. 1998, is a quantitative method which compares two distributions (calculated treatment planning dose distribution vs. measured dose distribution) using a point-by-point methodology. Specifically, this technique uses 3D spatial coordinates to align the two dose distributions and phantom dimensions to perform the comparison. The gamma comparison is a measure of the agreement in dose distributions (DD) considering dose delivered (percent difference criterion) and position of the dose [distance to agreement (DTA) criterion]. The percent criterion dominates in regions of shallow to no dose gradient, whereas the DTA criterion applies to dose distribution areas where there are steep dose gradients. IROC-Houston's common evaluation criterion for H&N is 7% dose delivery and 4mm DTA (also written as 7%/4mm) and for the thorax phantom is 7%/5mm. During evaluation the normalized gamma-index (γ) will measure the smallest length between the reference point and the evaluation distributions. If the smallest length in the voxel is >1 (i.e., γ<1), then it said to be outside the assigned normalized criterion. Vice versa, if the smallest length is <1 (i.e., γ>1), then it is within the criteria tolerance. The distributions of all γ values are

collectively used as a composite to determine whether the measured dose passes or fails the gamma analysis. This means that for each point in the measured volume, the measured dose must closely agree with the expected dose to within 7% or it must be nominally within 4mm of a point dose. For IROC-Houston's H&N phantom, film is said to have a gamma passing rate when at least 85% of pixels have $\gamma>1$ for sagittal and axial film dose distribution. Similarly, IROC-Houston's thorax phantom was said to pass if the individual axial and sagittal films had at least 80% of pixel passing and if the combined films had greater than 85% of pixels passing.

1.2   STATEMENT OF PROBLEM

The NCI requires participating institutions that intend to use IMRT techniques to first become credentialed by demonstrating their ability to accurately deliver radiation[45; 46]. IROC-Houston has developed various site-specific anthropomorphic phantoms that are used to credential participating institutions. These phantoms were designed as end-to-end QA tests used in a traditional radiotherapy workflow. To complete an end-to-end test, the institution was required to capture a CT image, create an individual treatment plan based on IROC-Houston's dose criteria, and irradiate the phantom using a conventional linear accelerator. IROC-Houston's conventional phantoms are insufficient end-to-end QA tools for MRgRT systems.

Unlike conventional linear accelerators, MRgRT systems use MR images to verify treatment setup, treatment guidance and online adapted radiotherapy. Using one phantom to perform an end-to-end test means the phantom must be used and visualized in both CT and MR imagers. IROC-Houston's current phantoms are constructed of rigid materials that lack MR signal. Consequently, the lack of signal causes the tumor and surrounding tissue to be indistinguishable (Figure 14).   With future developments of MR-only workflows, IROC-Houston's phantoms must be visible in MR to be used for end-to-end tests. Therefore, new MRgRT phantoms must be constructed with tissue equivalent materials that are visible in both CT and MR imagers.

The goal of this project was to create two anthropomorphic phantoms, one being a homogenous H&N phantom and the other being a motion enabled heterogeneous thoracic phantom. These phantoms were designed for MRgRT systems that have a magnetic field ranging from 0.35T to 1.50T. The two phantoms will be used as remote

end-to-end auditing tools to credential institutions wishing to use MRgRT systems in

NCI-sponsored clinical trials.

1.3 HYPOTHESIS AND SPECIFIC AIMS

Hypothesis: A homogeneous head and neck (H&N) and dynamic heterogeneous thoracic anthropomorphic phantom can be designed to evaluate MRgRT which will assure agreements between the measured and calculated doses within ±7%/4mm and ±7%/5mm, respectively.

Specific Aim 1:

Identify synthetic tissue substitutes that are visible in MR, share common tissue equivalent properties in CT and are accurately modeled in a treatment planning system.

Specific Aim 2:

Characterize radiochromic EBT3 film, and thermoluminescence detectors (TLD) in the presence of a magnetic field and validate the detector characterizations using a Monte Carlo model.

Specific Aim 3:

Design and construct a homogeneous H&N and a dynamic heterogeneous thoracic anthropomorphic QA phantom; which will be used to verify the dose delivery with the characterized dosimeters while under the presence of a magnetic field ranging from 0.35T to 1.50T.

Specific Aim 4:

Conduct a feasibility study for the homogeneous head and dynamic heterogeneous thoracic anthropomorphic phantoms while under the presence of 0.35T and 1.50 T magnetic field strengths.

1.4   BENEFITS TO SCIENCE

End-to-end tests are performed with IROC-Houston's phantoms to ensure all NCI participating institutions are delivering radiation accurately and in a comparable manner. Implementing MR into the clinical workflow will require new CT/MR visible anthropomorphic H&N and thorax phantoms. These specially designed MRgRT QA phantoms will be used as tools to credential institutions wishing to use MRgRT systems in NCI-sponsored clinical trials. MR/CT visible phantoms will be used to benefit the advancement of radiotherapy in two ways: 1) ensuring safe radiation delivery using MRgRT systems and 2) contributing to the general understanding of the advantages/disadvantages of MRgRT systems.

A single QA device must be used to evaluate the overall treatment workflow in MRgRT systems. MRgRT systems have altered the conventional radiotherapy workflow. On-board MR imagers in MRgRT systems will be used to verify treatment setup, treatment guidance and online adapted radiotherapy. Some MRgRT systems are not equipped with lasers in the treatment room and solely depend on MR guidance to correctly setup a patient. Some systems will require reoptimizing the plan based on MR images acquired the day of treatment. The overall workflow uncertainty will be evaluated comprehensively by using IROC-Houston's MRgRT phantoms as end-to-end test.

MRgRT H&N and thorax phantoms will be essential tools used to credential institutions participating in NCI sponsored clinical trials. Ultimately, the NCI-sponsored clinical trials will be used to quantify the benefits of MRgRT systems. The MRgRT phantoms will contribute to the overall understanding of using on-board MR imagers in the clinic.

Chapter 2:   Developing and Characterizing MR/CT visible materials used in QA phantoms for MRgRT systems

A substantial portion of this chapter is written or based on the following publication:

A.Steinmann, R. Stafford, L. Court, Z. Wen, G. Sawakuchi, D. Fuller, D. Followill, "Developing and characterizing MR/CT visible materials used in QA phantoms for MRgRT systems," *Medical Physics.* Doi: 10.1002/mp.12700. (2018). © John Wiley and Sons.

The permission for reuse of this material was obtained from John Wiley and Sons.

2.1   ABSTRACT

Purpose: Synthetic tissue equivalent (STE) materials currently used to simulate tumor and surrounding tissues for IROC-Houston's anthropomorphic head and thorax QA phantoms cannot be visualized using magnetic resonance (MR) imaging. The purpose of this study was to characterize dual MR/CT visible STE materials that can be used in an end-to-end QA phantom for MR guided radiotherapy (MRgRT) modalities.

Methods: Over 80 materials' MR, CT, and dosimetric STE properties were investigated for use in MRgRT QA phantoms. The materials tested included homogeneous and heterogeneous materials to simulate soft-tissue/tumor and lung tissues. Materials were scanned on a Siemens' Magnetom Espree 1.5T using four sequences, which showed the materials visual contrast between T1 and T2 weighted images. Each material's Hounsfield number and electron density data was collected using a GE's CT Lightspeed Simulator. Dosimetric properties were examined by constructing a 10 x 10 x 20 cm^3 phantom of the selected STE materials that was divided into three sections: anterior, middle, and posterior. Anterior and posterior pieces were composed of polystyrene, whereas the middle section was substituted with the selected STE materials. EBT3 film was inserted into the phantom's midline and was irradiated using an Elekta's

Versa 6 MV beam with a prescription of 6 Gy at 1.5 cm and varying field size of: 10 x 10 cm^2, 6 x 6 cm^2, and 3 x 3 cm^2. Measured film PDD curves were compared to planning system calculations and conventional STE materials' percent depth dose (PDD) curves.

Results: The majority of the tested materials showed comparable CT attenuation properties to their respective organ site; however, most of the tested materials were not visible on either T1 or T2 weighted MR images. Silicone, hydrocarbon, synthetic gelatin and liquid PVC plastic-based materials showed good MR image contrast. In-house lung equivalent materials made with either silicone or hydrocarbon-based materials had HUs ranging from: -978 to -117 and -667 to -593, respectively. Synthetic gelatin and PVC plastic-based materials resembled soft tissue/tumor equivalent materials and had HUs of: -175 to -170 and -29 to 32, respectively.

PDD curves of the selected MR/CT visible materials were comparable to IROC-Houston's conventional phantom STE materials. The smallest field size showed the largest disagreements, where the average discrepancies between calculated and measured PDD curves were 1.8% and 5.9% for homogeneous and heterogeneous testing materials, respectively.

Conclusions: Gelatin, liquid plastic, and hydrocarbon-based materials were determined as alternative STE substitutes for MRgRT QA phantoms.

2.2 INTRODUCTION

Advances in radiation oncology have drastically evolved over the past decade. Among the many changes, one of the most prominent additions is the use of on board imaging in conjunction with a radiation therapy treatment modality (i.e., cone-beam CT guided linear accelerator). While the integration of cone-beam CT (CBCT) with a modern linear accelerator enables patient set-up verification and target localization; this imaging modality is often limited to interfraction setup verifications [47-49]. Several research collaborations were initiated several years ago to integrate a magnetic resonance imager (MR) with either a ^{60}Co unit or a linear accelerator as a new form of image guided radiation therapy [13; 48]. In comparison with CBCT, the integrated MR can provide images with superior soft tissue contrast, permit real-time imaging, and not cause any additional radiation dose. The incorporation of a magnetic resonance guided radiation therapy (MRgRT) modality into the clinic can provide visualization for both intrafractional and interfractional target motion.

In the United States, there are two MRgRT systems: the Unity developed by Elekta/Philips (Elekta, Crawley, United Kingdom and Philips, Amsterdam, Netherlands) which is not yet in clinical use and the ViewRay MRIdian (ViewRay, Oakwood Village, Ohio) which is in clinical use. The Unity system is equipped with an Elekta 7 MV linear accelerator that is located in between a Philips' 1.5 T MR scanner. Due to the active shielding on the superconducting magnets, a low magnetic field toroid is created, which enables a linear accelerator to be positioned and operate in between the two magnets with only a minimal magnetic effect[10; 12]. In contrast, the MRIdian is a radiation therapy (RT) treatment machine with three independent ^{60}Co sources located in between a split 0.35T

superconducting MR imager[15]. Each of the three ^{60}Co treatment heads are equipped with a double focused multileaf collimator; thus, permitting the MRIdian unit to have a comparable penumbra and dose rate as a conventional 6 MV linear accelerator[15]. Additionally, ViewRay has developed a linac-based version of the MRIdian system. The MRIdian Linac, which was FDA approved in February 2017, is an upgraded system that incorporates a 0.35T superconducting magnetics with a 6 MV linear accelerator.

Both MRgRT systems have the ability to provide real-time imaging and deliver adaptive RT. Despite the innovation and potential benefits of using a MR unit for MRgRT treatments, there are challenges that limit a MR-only RT workflow. Two of these include: 1) the inability to easily determine the patient's electron density for treatment planning dose calculations and 2) geometric distortions produced on MR images [50-54]. Conventionally, the patient's electron density is indirectly determined through a bi-linear relationship between the linear attenuation data collected from a CT and the material's respectively density. Unlike CT, where images are created from back projections of photons penetrating the body, MR does not use radiation to produce an image and solely relies on small fluctuations of the materials' net magnetic moment. Due to the inherent differences in the acquisition process of MR and CT, the linear attenuation data is not collected in MR. Therefore, current MR scanners are unable to indirectly measure electron density from one scan. Additionally, it is critical to know the exact size and location of a patient's anatomy in radiotherapy (RT). MR images commonly misrepresent actual patient anatomy in space (geometric distortion) due to the inherent configuration and design of a MR unit[55]. Nonlinear gradients and heterogeneities in the static magnetic field primarily contribute to geometric distortions in the image[52; 54; 55]. Since geometric distortions and electron densities are limited to the inherent differences

in the acquisition process between MR and CT, it is critical that current MRgRT modalities rely on both CT and MR for treatment planning and treatment verification/treatment adaptation, respectively.

End-to-end QA verifications performed for conventional radiation treatments have routinely focused on using a CT imager in a radiotherapy modality. However, with the incorporation of MR in radiotherapy, it is important that end-to-end QA tests expand to also include MR imagers. Current end-to-end QA phantoms used at the Imaging and Radiation Oncology Core at Houston (IROC-Houston) QA Center for credentialing purposes in National Cancer Institute (NCI) funded clinical trials are not MR visible. As shown in Figure 14, tumor and surrounding tissue in IROC-Houston's anthropomorphic thorax phantom are distinguishable in CT images but are not in T1 and T2 weighted MR images. Dosimetrically the phantoms are accurate, but the plastics used to represent tumor and surround tissue in IROC-Houston's phantoms do not yield any MR signal, which makes these phantoms deficient as end-to-end QA phantoms for MRgRT. Other researchers have attempted to create dual MR/CT phantoms, but the phantoms are limited by either: shelf-life storage, require refrigeration or additives to prevent microorganism growth and therefore were not suitable for shipping to other RT institutions[56-58].

The aim of this study was to identify and characterize STE materials that could be used to develop an anthropomorphic dual MR/CT QA phantom which would require minimal maintenance and be used to credential RT institutions wishing to use MRgRT modalities in NCI funded clinical trials.
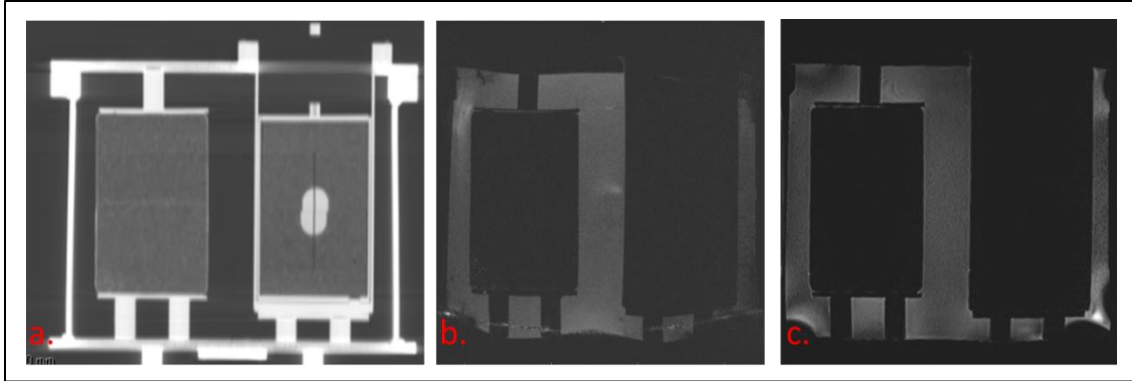
Figure 14: Images a-c are used to illustrate the need for a dual CT/MR visible phantom for MRgRT modalities. This figure displays IROC-Houston's Anthropomorphic Thorax phantom imaged in a GE Lightspeed CT simulator (a.) and Siemen's Magnetom Espree 1.5T MR scanner (b-c). The phantom's tumor and lung were constructed out of polystyrene and compressed cork, respectively. The tumor is located in the phantom's left lung and is completely visible on a CT (a.) however, the tumor and surrounding lung tissue are not visually distinguishable in either a T1-weighted (b.) or T2-weighted (c.) MR image.

2.3   MATERIAL AND METHODS

2.3.1   IROC-Houston's Traditional QA Phantoms

IROC-Houston's two anthropomorphic phantoms used most often are the heterogeneous thorax and homogeneous head and neck (H&N) phantoms. The thorax and H&N phantoms were previously described in detail by Followill and Molineu, respectively[59; 60]. Briefly, the current thorax phantom is a water fillable shell and contains two lungs made of compressed cork (one with a centrally located target made of nylon). Other organs at risk represented in IROC-Houston's thorax phantom include a heart and spinal cord composed of polystyrene and acrylic, respectively. In IROC-Houston's H&N phantom, the primary and secondary targets are constructed out of solid water and are surrounded by polystyrene. The polystyrene/solid water insert is enclosed into a water fillable plastic shell, which is shaped as a human head. For both phantoms, the materials used to simulate the targets and surrounding normal tissues are synthetic, rigid, and hydrogen deficient. These materials are ideal for traditional QA phantoms since they do

not require special storage conditions, require minimal maintenance, can easily hold radiation dosimeters, maintain their shape, are distinguishable using CT, and are dosimetrically similar to human tissue.

2.3.2 *Required Material Properties Used in MRgRT QA Phantoms*

To develop an appropriate MRgRT QA phantom, it is vital that the materials used for this dual modality phantom are: 1) visible on both T1 and T2 weighted MR images, 2) visible on CT images, and 3) have comparable HUs and dosimetrically simulate tumor and surrounding tissue. Since IROC-Houston ships their end-to-end QA phantoms to other institutions, these materials must also satisfy non-dosimetric characteristics. IROC-Houston's MR/CT visible materials must also endure rough shipping conditions, show longevity without adding preservatives, maintain their physical structure (i.e., high melting point) and show a relative ease in manipulating the material to form a realistic tissue shape and hold dosimeters. A wide variety of materials (listed in Table 4) were tested for their dosimetric, MR and CT compatibility. The materials were first imaged using a MR and CT scanner. Based on the material's MR and CT assessment, a decision was made on what materials to continue with dosimetric testing. Potential materials examined for a MR/CT QA phantom included: nylon-based, silicon-based, acrylic-based, and gel-based materials. In addition to commercially purchased materials, some tested materials were manufactured in-house. The in-house mixtures incorporated mini Styrofoam balls with ranging diameters of 2-4mm with either a petroleum or silicone-based material. Combining a based material with Styrofoam balls created a heterogeneous material that could potentially be used to represent a synthetic lung equivalent tissue.

Testing Material	Material Type	HU	T1-Visible	T2-Visible	Tissue Equivalent
Superflab [a]	Plastic	59.9	Y	Y	Y
SuperStuff [a]	Plastic	65.2	Y	Y	-
100% Liquid PVC Plastic [b]	Plastic	-10.4	Y	Y	Y
100% Super Soft PVC Plastic [b]	Plastic	3.70	Y	Y	-
90% Liquid PVC Plastic & 10% Plastic Softener Mix [b]	Plastic	15.7	Y	Y	-
100% Plastic Hardener [b]	Plastic	32.0	Y	N	-
75% Plastic Hardener & 25% Plastic Softener Mix [b]	Plastic	21.9	Y	Y	-
75% Super Soft Plastic & 25% Softener Mix [b]	Plastic	-29.7	Y	Y	-
75% Liquid PVC Plastic & 25% Plastic Softener Mix [b]	Plastic	-6.5	Y	Y	-
Gel #10 [c]	Synthetic Gelatin	-170	Y	Y	-
Gel #20 [c]	Synthetic Gelatin	-164	Y	Y	Y
Gel #1 [c]	Synthetic Gelatin	-169	Y	Y	-
Gel #2 [c]	Synthetic Gelatin	-172	Y	Y	-
Gel #3 [c]	Synthetic Gelatin	-171	Y	Y	Y
Gel #4 [c]	Synthetic Gelatin	-175	Y	Y	-
Multiwax [h]	Hydrocarbon	-156	N	N	-
Petroleum Jelly [h]	Hydrocarbon	-154	Y	Y	-
91.7% Petroleum Jelly & 8.3% Styrofoam ball Mix [i,‡]	In-House Hydrocarbon Mix	-593	Y	Y	Y
95% Petroleum Jelly & 5% Styrofoam ball Mix [i,‡]	In-House Hydrocarbon Mix	-667	Y	Y	-
Dragon Skin 10 [g]	Silicone	262	Y	Y	-
Dragon Skin 30 [g]	Silicone	294	Y	Y	N
Dragon Skin FX-Pro [g]	Silicone	231	Y	Y	-
Eco Flex 00-10 [g]	Silicone	202	Y	Y	-
EcoFlex 00-30 [g]	Silicone	185	Y	Y	-
EcoFlex 00-50 [g]	Silicone	203	Y	Y	N
PlatSil® Gel 00 [d]	Silicone	275	Y	Y	-
PlatSil® Gel 10 [d]	Silicone	319	Y	Y	-
PlatSil® Gel 25 [d]	Silicone	290	Y	N	-
PlatSil® Gel 00 +H (10:10:10) [d,◊]	In-House Silicone Mix	-978	Y	Y	-
PlatSil® Gel 10 +H (10:10:10) [d,◊]	In-House Silicone Mix	-970	Y	Y	-
PlatSil® Gel 25 +H (10:10:10) [d,◊]	In-House Silicone Mix	-972	Y	N	-
PlatSil® Gel 25 (20:20:0.5) [d,‡]	In-House Silicone Mix	-117	Y	N	-
PlatSil® Gel-00/Styrofoam ball Mix (20g:20g:1g) [d,‡]	In-House Silicone Mix	-510	Y	Y	-
PlatSil® Gel 25 (20:20:1) [d,‡]	In-House Silicone Mix	-358	Y	N	-
PlatSil® Gel-00/Styrofoam ball Mix (20g:20g:1.5g) [d,‡]	In-House Silicone Mix	-406	Y	Y	N
PlatSil® Gel 25 (20:20:1.5) [d,‡]	In-House Silicone Mix	-470	Y	N	-
PlatSil® Gel 25 (20:20:2) [d,‡]	In-House Silicone Mix	-494	Y	N	-
PlatSil® Gel-00/Styrofoam ball Mix (10g:10g:1g) [d,‡]	In-House Silicone Mix	-655	Y	Y	-
PlatSil® Gel-00/Styrofoam ball Mix (40g:40g:1g) [d,‡]	In-House Silicone Mix	-350	Y	Y	N
Nycast ® 6PA- Blue [e]	Nylon	161	N	N	-
Nycast ® 6PA- MoS2 Filled [e]	Nylon	94.2	N	N	-
Nycast ® 6PA-Orange [e]	Nylon	99.2	N	N	-
Nycast CP [e]	Nylon	82.7	N	N	-

Nycast Rx [e]	Nylon	90.9	N	N	-
Nylon Nyloil [e]	Nylon	94.2	N	N	-
EP 30 [f]	Epoxy	72.9	N	N	-
EP424T [f]	Epoxy	63.0	N	N	-
PMC ® 121/30 [g]	Urethane	-10.5	Y	N	-
PMC ® 744 [g]	Urethane	-2.90	N	N	-
PMC ® 746 [g]	Urethane	-11.0	N	N	-
PMC ® 770 [g]	Urethane	78.0	N	N	-
PMC ® 790 [g]	Urethane	66.1	N	N	-
ReoFlex ® 20 [g]	Urethane	-19.5	Y	N	-
ReoFlex ® 30 [g]	Urethane	-45.0	Y	N	-
Simpact® 85 A [g]	Urethane	66.0	N	N	-
Simpact® 60 A [g]	Urethane	71.6	N	N	-
VytalFlex® 10 [g]	Urethane	-9.0	N	N	-
VytalFlex® 20 [g]	Urethane	-18.3	Y	N	-
VytalFlex® 30 [g]	Urethane	-27.0	Y	N	-

a: Radiation Products Design Incorporation, Albertville, Minnesota b: M-F Manufacturing Company, Fort Worth, Texas c: Clear Ballistics, Fort Smith, Arkansas d: Polytek® Development Corporation, Easton, Pennsylvania e: Cast Nylons Limited, Willoughby, Ohio f: MasterBond, Hackensack, New Jersey g: Smooth-On Inc., Macungie, Pennsylvania h: Sonneborn, Parsippany, New Jersey ‡:In-house mixture that used % weight of Styrofoam balls from Steve Spangler Science Styrofoam Beads, Englewood, Colorado.

Table 4: Above is a list of materials tested for a MR/CT visible STE phantom. As displayed in the second column, testing materials were grouped as: plastic, synthetic gelatin, hydrocarbon, urethane, epoxy, silicone, and nylon based materials. These material's HU were measured from a GE LightSpeed CT Simulator and are displayed in the third column. The materials were also imaged on a Siemen's Magnetom Espree 1.5 MR scanner using T1 and T2 weighted sequences. The fourth and fifth columns display whether the materials could visually be distinguished in T1 and T2 weighted images, respectively. Materials were visualized on a both T1 and T2 weighted sequences, and also shared reasonable HUs for either tumor, soft tissue, and lung materials were then dosimetrically tested. The last column displays whether or not a material was tested dosimetrically. If the material was tested dosimetrically the final column displays if it was considered STE.

2.3.2.1 MR Imaging

All materials listed in Table 4 were submerged in water and were scanned using four MR scanning protocols on a Siemen's Magnetom Espree 1.5T MR scanner (Siemens Healthcare, Erlangen Germany). Common T1 and T2 MR sequences were chosen based on an assumption that similar sequences would be equipped in all of MRgRT treatment's imaging software. MR scans represented four different MR sequences that were either: 1) currently used in an MRgRT modality (TRUFI) or 2) shared similar sequences (T1-

weighted and T2-weighted) that were expected to be equipped in all new MRgRT modalities. All materials were specifically scanned under a TRUFI sequence since ViewRay exclusively uses this sequence.

Four MR sequences, summarized in Table 5, were used to image the testing material's MR properties. The water bath was used as a baseline to assess the material's contrast in various MR sequences. A T1-weighted image was obtained from a 3D gradient echo sequence and used the following parameters: FA= 25°, TR= 9.5 ms, TE= 4.68 ms, ETL= 1, NEX=1. A true fast imaging with steady-state free precession sequence, commonly referred as a TRUFI sequence, was acquired with the following parameters: FA= 70°, TR= 4 ms, TE= 2 ms, ETL= 1, NEX=1. Two additional T2-weighted images were also obtained for each material. The first T2 weighted image was a gradient sequence and had parameters of: FA= 120°, TR= 3200 ms, TE= 245 ms, ETL= 109, NEX=2. The second T2-weighted image used a fluid-attenuated inversion recovery sequence, commonly referred as a FLAIR sequence, and had scanning parameters of: FA= 120°, TR= 5000 ms, TE= 336 ms, ETL= 109, NEX=2.

Scanning Sequence	T1-Weighted Gradient	TRUFI	T2-Weighted Gradient	FLAIR
FA	25°	70°	120°	120°
TR (ms)	9.5	4	3200	5000
TE (ms)	4.68	2	245	336
ETL	1	1	109	109
NEX	1	1	2	2

Table 5: Four MR scanning parameters were used to visually compare the selected material's contrast between water. Among the parameters, a T1 weighted and T2 weighted sequence were scanned based off of the assumption that other MRgRT systems would have the capability to image basic T1 weighted and T2 weighted protocols. A TRUFI sequence was scanned to ensure that the materials could be visualized on ViewRay systems. Since FLAIR sequences are commonly used to enhanced lesions in the clinic, a FLAIR sequence was also used to compare the selected material's contrast.

2.3.2.2   CT Imaging

All of the materials listed in Table 4 were submerged in a water bath and were scanned using a brain protocol on a GE Lightspeed CT simulator (General Electric Company, New York, New York). The scanning parameters were: DFOV= 500.0 mm, 120 kVp, 275 mA, and slice thickness= 3mm. The materials' HU were obtained after exporting the CT images into Philips IntelliSpace PACS Enterprise (Philips, Amsterdam, Netherlands) system.

2.3.2.3   Dosimetric properties

A dual MR/CT visible end-to-end QA anthropomorphic phantom used in radiotherapy must also dosimetrically represent human tissue. Percent depth dose (PDD) curves were obtained to determine the material's dosimetric properties on materials that were MR/CT visible. As shown in Figure 15, a 10 cm x 10 cm x 20 cm rectangular phantom was constructed to determine the PDD for selected MR/CT visible materials. The 20 cm long PDD phantom was divided into three sections: anterior, middle, and posterior, which had lengths of 5.0 cm, 10.0 cm, and 5.0 cm, respectively. The anterior and posterior sections were composed of polystyrene, whereas the middle section was substituted with materials that were visible on both CT and MR. Additionally, two materials commonly used in IROC-Houston's QA phantoms (compressed cork and polystyrene) were included in this study to provide controlled PDD curves.
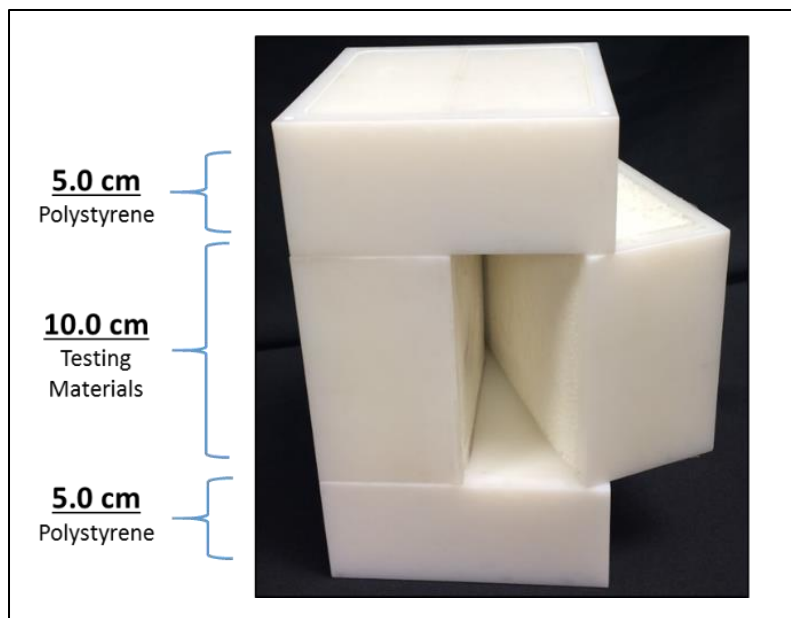
Figure 15: PDD phantom was used to determine the testing material's dosimetric properties. The PDD phantom was divided into three subsections where the anterior and posterior sections were composed of polystyrene and the middle section was interchanged with testing materials. Film was placed in the sagittal plane to measure the material's PDD curve.

The 6 MV beam from an Elekta Versa HD (Elekta, Stockholm, Sweden) was used to irradiate the PDD phantoms with three different field sizes of: 10 x 10 cm^2, 6 x 6 cm^2, 3 x 3 cm^2. During each irradiation, EBT-3 radiochromic film was inserted into the midline of the PDD phantom. Additional 5 cm of polystyrene was placed around the PDD phantom which ensured proper scatter conditions. Within each field size, the PDD phantom was irradiated three times with a prescribed dose of 600 cGy to d$_{max}$ (d=1.5 cm).

It was also important to assess how accurate the experimental PDD curves compared to the treatment planning system (TPS). A treatment plan was created among the testing materials for each of the three field sizes. Using Pinnacle's treatment planning (Philips, Amsterdam, Netherlands), the dose from 0.5 to 17.0 cm was calculated and normalized to a depth of 1.5 cm using the collapsed cone dose algorithm. After the films were irradiated, a photoelectron CCD microdensitometer (Photoelectron Corporation, North Billerica, Massachusetts) was used to capture the optical density of the film at the

different depths of interest. The intensity of the film was then converted into dose and the dose at the varying depths were normalized to the dose at 1.5 cm.

2.4   RESULTS

2.4.1   Tested Material's Properties

2.4.1.1   MR properties

Most plastic, silicone, and gelatin-based materials tested were visible in both T1 and T2 weighted images. In-house mixtures were mostly visible on all four MR sequences. Specifically, testing materials that used either Polytek Development Corporation's Gel 25 or M-F Manufacturing Company's 100% Plastic Hardener were visible on T1-weighted images but were not visible on T2-weighted images. With few exceptions most nylon, urethane, and epoxy-based materials were not visible on either T1 or T2 weighed MR sequences. Specifically, Smooth-On's Reoflex 20, Reoflex 30, VytalFlex 20, VytalFlex 30, and PMC 121/30 materials were all urethane-based materials and were only visible on T1-weighted images.

Materials that were heterogeneous and showed a random absence of signal were more favorable lung materials compared to the homogeneous substitutes since these materials were better representations of lung tissue. Heterogeneous tested materials were constructed in-house and were combined with a base material (either Sonneborn's petroleum jelly or Polytek Development Corporation's silicon gels) and different concentrations of 2-4mm miniature Styrofoam balls. Within the heterogeneous lung materials, miniature Styrofoam balls represented air pockets with no MR signal while the surrounding base materials generated MR signal. MR visibility of potential lung-

equivalent materials greatly depended on the Styrofoam ball concentration. As the concentration of Styrofoam balls increased, the MR visibility greatly decreased since there was less signal from the surrounding materials. Among the in-house mixtures, the most visible lung substitute was a combination of 8.3% weight of Styrofoam balls and 91.7% of petroleum jelly (Figure 16).

Contrary to potential lung candidates, homogeneous materials better represented soft tissue and tumor substitutes. Potential soft tissue and tumor substitutes were not required to have the same grey-scale contrast as their human flesh counterparts, but these materials were required to have visible contrast between water and each other. Taking into account all four MR sequences, three materials (Clear Ballistics' Gel #20, M-F Manufacturing Company's 100% Liquid PVC Plastic, and Radiation Products Design Incorporation's Superflab) were shown to have the most visible contrast between water, each other and other testing materials. Therefore, Gel #20, 100% Liquid PVC Plastic and Superflab were chosen to be tested further as suitable soft tissue or tumor substitutes (Figure 16).
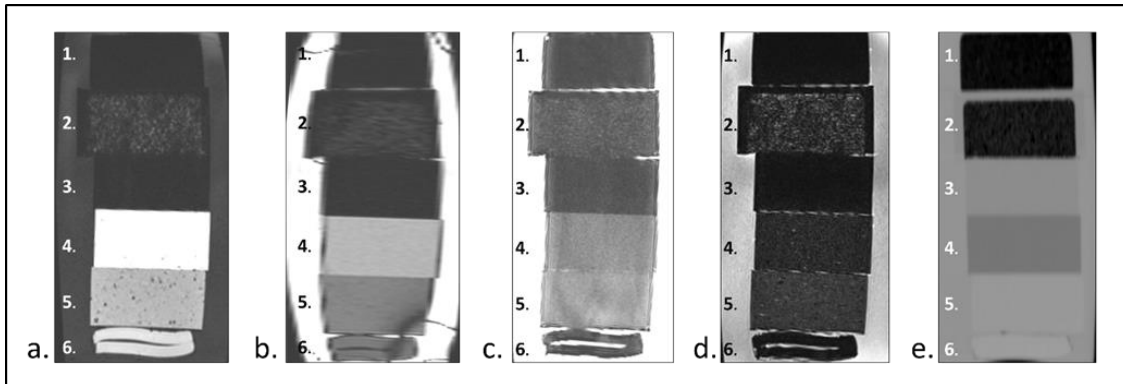
Figure 16: From top to bottom the materials shown are: 1.) compressed cork, 2.) in-house petroleum/styrofoam mixture (8.3% weight composed of mini Styrofoam balls and 91.7% weight composed of Sonneborn's Petroleum jelly), 3.) polystyrene, 4.) Clear Ballistic Gel #20, 5.) M-F Manufacturing 100% liquid PVC plastic, and 6.) Superflab. Four different MR sequences (a-d) and a CT scan (e) were performed on these materials to visually determine their contrast between water and IROC-Houston's conventional materials. The MR sequences shown in this figure were a (a.) T1-weighted, (b.), TRUFI, (c.) T2-weighted, and (d.) fluid-attenuated T2-weighted scans. The HU measured from the CT image for compressed cork, in-house petroleum/styrofoam mixture, polystyrene, Clear Ballistic Gel #20, Liquid plastic, and Superflab were, respectively, -800, -685, -33, -160, 20 and 51.

2.4.1.2 CT properties

The testing materials' (listed in Table 4) HU was measured from images acquired on GE's Lightspeed CT simulator. In general, homogeneous plastic, nylon, epoxy-based materials most resembled soft tissue and their HU's, ranging from, -29 to 65, 82 to 161, 63 to 72, respectively. Urethane based materials showed a larger HU range of -45 to 78. Gelatin based materials resembled more fatty-like tissues with HU's ranging from -164 to -175 whereas homogenous silicone materials resembled more contrast-enhanced soft tissue with HU's ranging from 185 to 319. In-house mixtures, that incorporated either silicone or hydrocarbon-based materials, visually and numerically simulated lung-like materials with HU's that ranged from, -978 to -117 and -667 to -593, respectively. Similar to MR, the concentration of the Styrofoam balls directly affect their attenuation coefficient. Mixtures with greater Styrofoam ball concentrations had more air pockets

which, enable the synthetic materials to better visually resembled lung tissue and had lower HU values.

The four selected MR-visible materials were collectively imaged on GE's Lightspeed CT simulator and are displayed in Figure 16e. Among the four selected MR-visible materials 100% Liquid PVC Plastic, and Superflab numerically represented soft tissue with HU of -10.4, and 59.9, respectively. Visually, the 100% Liquid PVC Plastic and Superflab materials had similar contrast as water, whereas Gel #20, showed a greater contrast relative to water and had a lower HU value of -170. Clear Ballistics' Gel #20 could potentially be used as either a fat or a tumor equivalent material since it did have lower HU value than water. Small fluctuations between mini Styrofoam balls and surrounding based materials in the heterogeneous mixtures created random signals that resemble high and low contrast areas. These random signals seen among in-house heterogeneous mixtures on a MR image were also comparable to random signal seen in lung tissue on a CT image. The in-house mixture with compositions of 8.3% of Styrofoam balls and 91.7% of petroleum jelly (which was previously selected as a potential synthetic lung substitute in MR) numerically resembled synthetic lung tissue with a HU of -685.

2.4.1.3 Dosimetric properties

The selected MR/CT visible materials (in-house 91.7%/8.3% petroleum jelly/styrofoam mixture, Clear Ballistic Gel #20, and Liquid PVC Plastic) were further dosimetrically investigated. Since Superflab is currently used in the clinic as a tissue equivalent material, it was excluded from dosimetric measurement. Each selected material was irradiated under three different field sizes, then corresponding PDD curves

were generated using the data from the TPS and radiochromic film. From a depth of 1.5 cm to 17 cm, the deviations between the film PDD and TPS PDD curves were determined for 10 x 10 cm^2, 6 x 6 cm^2, and 3 x 3 cm^2 field sizes. The greatest deviation between film and TPS PDD curves was found for the smallest field size for all materials. At a field size of 3 x 3 cm^2 the maximum deviation was: 12.2% at 17.0 cm for compressed cork, 10.8% at 16.5 cm for the in-house petroleum jelly styrofoam mixture, 7.1% at 16.5 cm for polystyrene, 4.1% at 12.5 cm for Gel #20, and 4.6% at 17.0 cm for 100% Liquid PVC Plastic (Table 6). While the greatest deviation between film and TPS PDD were shown for the 3 x 3 cm^2 field size, the average deviation for the 3 x 3 cm^2 field size for all of the materials, was less than 6%. The mean deviation between film PDD and TPS PDD for the selected materials for the 10 x 10 cm^2 and 6 x 6 cm^2 field sizes were all less than 1.9%, and 2.8%, respectively. Quantitatively, the mean deviation for a 3 x 3 cm^2 field size the mean deviation for compressed cork, the in-house petroleum jelly styrofoam mixture, polystyrene, Gel #20, and Liquid PVC Plastics were: 3.8 ± 3.60 cm, 5.9 ± 2.75 cm, 1.9 ± 2.02 cm, 1.5 ± 1.15 cm and 2.0 ± 1.13 cm, respectively. At a field size of 3 x 3 cm^2 the maximum deviation was: 12.2% at 17.0 cm for compressed cork, 10.8% at 16.5 cm for, 7.1% at 16.5 cm for polystyrene, 4.1% at 12.5 cm for Gel #20, and 4.6% at 17.0 cm for 100% Liquid PVC Plastic (Table 6).

Materials	10 x 10 cm^2			6 x 6 cm^2			3 x 3 cm^2		
	Max Deviation [%]	Depth [cm]	Mean Deviation [%]	Max Deviation [%]	Depth [cm]	Mean Deviation [%]	Max Deviation [%]	Depth [cm]	Mean Deviation [%]
Compress Cork	4.3	8.5	1.9 (± 1.12)	5.1	15.5	2.0 (± 1.24)	12.2	17.0	3.8 (± 3.60)
Petroleum Styrofoam Mix	7.7	15.0	1.9 (± 2.04)	7.2	13.5	2.8 (± 2.26)	10.8	16.5	5.9 (± 2.75)
Polystyrene	5.7	17.0	1.8 (± 1.67)	2.5	16.0	1.1 (± 0.59)	7.1	16.5	1.9 (± 2.02)
Clear Ballistic Gel #20	1.9	15.0	0.6 (± 0.46)	3.3	14.5	1.2 (± 0.81)	4.1	12.5	1.5 (± 1.15)
M-F Manufacture Liquid PVC Plastic	3.7	16.5	1.2 (± 1.03)	4.5	11.0	1.7 (± 1.21)	4.6	17.0	2.0 (± 1.13)

Table 6: A measured film PDD curve and a TPS PDD curve were generated for both current IROC-Houston's phantom materials and testing materials for a large (10 x 10 cm^2), medium (6 x 6 cm^2), and small (3 x 3 cm^2) field size. For each material (compressed cork, petroleum/Styrofoam mixture, polystyrene, Clear Ballistic Gel #20, and M-F manufacture's liquid PVC plastic) the maximum deviation between the material's measured PDD and TPS PDD and the overall mean deviation between 0.5 cm to 17 cm were recorded.

In addition to quantifying the maximum deviation between the film PDD and TPS PDD for each of the selected materials, the general shape of the tested material's PDD curves were compared with PDD curves of current IROC-Houston's lung and soft tissue equivalent materials. The in-house petroleum jelly/styrofoam mixture was compared to compressed cork, which is commonly used as IROC-Houston's lung equivalent materials. Similarly, Gel #20, 100% Liquid PVC Plastic were compared to polystyrene, which is also commonly used as IROC-Houston's soft tissue equivalent materials. Collective PDD data for soft tissue and lung equivalent materials for the smallest (3 x 3 cm^2) and largest (10 x 10 cm^2) field sizes are shown in Figure 17. Overall, the general PDD curve for Gel #20, and 100% Liquid PVC Plastic agreed with the polystyrene curve

and the in-house petroleum/styrofoam mixture was in agreement with the compressed cork curve. While modest discrepancies between general curve shapes between compressed cork and the in-house heterogeneous mixture were seen in all three field sizes, the 3 x 3 cm^2 PDD curve showed a slightly higher deviation around 16 cm, where the lung-to-tissue interface was located. The PDD phantom's CT, which was used in the TPS, was not imaged with film sandwich between the two halves. Therefore, it is believed that the higher deviation between the film and TPS measure in the smallest field size was primarily due to the dose build up from the film. Additionally, the petroleum/styrofoam mixture had a slightly higher physical density than compressed cork, which translated to having a smaller charge particle disequilibrium than compressed cork.
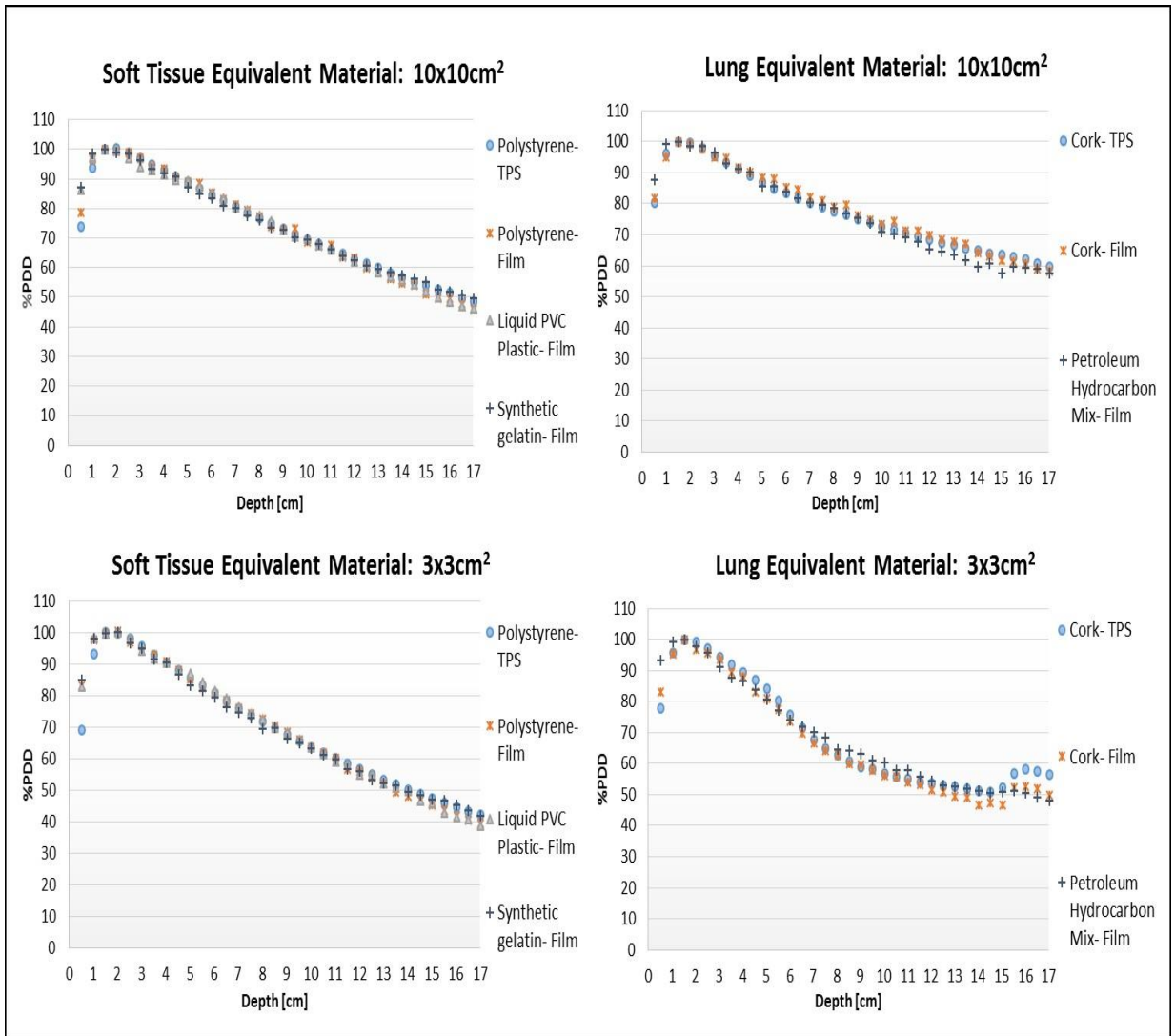
Figure 17: The four graphs are a summary of the PDD curve comparisons between IROC-Houston's current soft tissue and lung equivalent materials and testing materials for a large (10 x 10 cm²) and small (3 x 3 cm²) field size. The interfaces between the testing materials and polystyrene of the PDD phantom occur between 5 cm and 15 cm. All graphs show the current tissue substitute's film (red) and treatment planning (blue) PDD curves. The testing materials were then compared to current tissue's film and TPS PDD curves. The greatest curve deviation occurs for the lung equivalent material for the small field size.

2.5 DISCUSSION

The materials selected for MRgRT end-to-end QA phantoms for IROC-Houston were based off of three major criteria: practicality, reliability, and accuracy. Since IROC-Houston credentials radiotherapy modalities by regularly shipping end-to-end QA phantoms to institutions, materials selected for a MR/CT visible phantom needed to share

practical characteristics that would ensure the phantom's shape and size remain constant over time. Materials that do not require specific shipping or storage conditions (i.e., could be left in room temperature, and insensitive to light) and show relative ease in constructing abnormal shapes were considered as practical materials. Prior to testing a material's imaging and dosimetric properties, the material's melting point was first investigated. The material's melting point was used to determine whether a material could withstand extreme temperatures during shipment. The highest temperatures a package may experience for domestic and international shipments are, respectively, 37.1 °C and 45.5 °C[61]. Therefore, it was important that potential candidates had melting points greater than 45.5 °C. Specifically, the melting points for: Superflab, in-house petroleum jelly styrofoam mixture, Gel #20, and Liquid PVC Plastics were: 93.3 °C, 58.0 °C, 92.2 °C, and 121.1 °C, respectively. The material's selection process was also judged based off of the material's reliability. Since IROC-Houston's QA phantoms are used for many years, the material's shape and consistency must remain constant over time (i.e., the materials must not deteriorate or dehydrate over time). The materials listed in Table 4 were tested for their reliability by sitting in room temperature for 3 months. All materials except for Gel #4 and SuperStuff showed no forms of degradation. In addition to the practicality and reliability requirements, the materials selected for a MRgRT phantom had to be visible in common MR sequences, show comparable HU, and dosimetrically mimic their respective organ site.

Previously reported MR/CT visible materials in the literature did not meet IROC-Houston's criteria since most of these materials shared short shelf lives and required refrigeration storage[56-58]. We tested over 80 materials, which could potentially be used to manufacture IROC-Houston's MRgRT anthropomorphic phantoms. Most of the test

materials shared comparable HU values as human tissue but were not visible on both T1 and T2 weighted MR images. Materials that were classified as either epoxy, urethane, or nylon based sometimes showed contrast in T1-weighted images, but were consistently not visible in T2-weighted images. Either Polytek's silicone-based gels or Sonneborn's petroleum jelly were mixed with miniature Styrofoam balls in attempts to create various lung equivalent materials. Styrofoam balls were used to more realistically resemble a lung's heterogeneous appearance as viewed in MR and CT, and to lower the HU value. As we increased the concentration of Styrofoam balls it created a more realistic lung attenuation coefficient, but consequently, became less visible in MR images. The in-house mixture of 8.3% Styrofoam balls and 91.7% petroleum jelly was selected as the most optimal material for a dual modality since it was a good compromised between MR image visibility and typical lung attenuation data.

Other promising MR/CT visible materials were Smooth-On's Dragon Skin 30, Smooth-On's EcoFlex 50, and in-house mixtures composed of different concentration of Polytek's Gel 00 and miniature styrofoam balls. These materials were further investigated for their dosimetric properties but are not displayed in Figure 16 since these materials: 1) had higher physical density than their respective organ sites, and 2) did not have good dosimetric properties.

The selected testing materials visually showed different contrast among the four MR scans. However, amongst the scans, TRUFI showed the smallest contrast between the selected MR visible materials. All materials were imaged using a magnetic field of 1.5T. Using a smaller magnetic field (i.e., 0.35T) would generate a smaller net magnetic moment, which would consequently lower SNR. Lowering the magnetic field strength could change the material's T1 and T2 relaxation times which would consequently

affecting the MR contrast. In order to predict the contrast in a lower magnetic field, the material's T1 and T2 relaxations times would need to be calculated.

The measured PDD curves for the selected materials were comparable with their predicted PDD curves. The general PDD shape of IROC-Houston's typical soft tissue substitute, polystyrene, was most comparable to measured PDD curves of Gel #20, and 100% Liquid PVC Plastic. Similarly, the general PDD curve shape of IROC-Houston's conventional lung equivalent material, compress cork, was comparable to the in-house styrofoam/petroleum jelly mixture's measured PDD curve. Soft tissue equivalent materials showed a closer PDD curve agreement than lung equivalent materials. While all PDDs showed expected curve shapes, small differences were only noted for the smallest field size (3 x 3 cm^2) between the testing materials' measured and predicted PDD curves.

2.6   CONCLUSION

It was determined that four testing materials were visible and distinguishable in both MR and CT and dosimetrically represent human tissue. The in-house 91.7% petroleum jelly/ 8.3% styrofoam ball mixture resembled lung tissue since its HU was -685, dosimetrically showed expect lung-equivalent PDD curves, and visually showed random signal in both modalities. Superflab is currently used in the clinics as a tissue equivalent bolus, so it was only visually examined. It was determined as a potential material to use in a MR/CT visible phantom, since Superflab was visible in both imaging modalities. Lastly, Gel #20, and 100% Liquid PVC Plastic were determined to dosimetrically represent soft tissue and were easily view in both MR and CT modalities

and was therefore determined that both Gel #20 and 100% Liquid PVC Plastic are possible tumor equivalent substitutes for MRgRT end to end QA phantoms.

Chapter 3:   Characterize and validate radiation detectors under the presence of a magnetic field

A substantial portion of this chapter is written or based on the following publication:

A. Steinmann, D. O'Brien, R. Stafford, L. Court, Z. Wen, G. Sawakuchi, D. Fuller, D. Followill, "Characterization and validation of TLD and Radiochromic EBT3 film under the presence of 1.5T, 0.35T and 0T magnetic field strengths in MR/CT visible materials," *Medical Physics.* [In review] (2018). © John Wiley and Sons.

The permission for reuse of this material was obtained from John Wiley and Sons.

3.1   ABSTRACT

Purpose: The aim of this study was to characterize and validate thermoluminescent dosimeters (TLD) and radiochromic EBT3 film inside MR/CT visible geometric head and lung phantoms in the presence of: 0T, 0.35T and 1.5T magnetic fields.

Methods: TLD reproducibility studies were examined by irradiating IROC-Houston's TLD acrylic block five times under 0T and 1.5T configurations of Elekta's Unity system and three times under 0T and 0.35T configurations of ViewRay's MRIdian Cobalt-60 (^{60}Co) system. Both systems were irradiated with an equivalent 10 x 10 cm^2 field size, and a prescribed dose of 3 Gy to the maximum depth deposition (dmax).

EBT3 film and TLDs were characterized using two geometrical Magnetic Resonance (MR) guided Radiation Therapy (MRgRT) head and lung phantoms. Each geometrical phantom had eight quadrants that combined to create a centrally located rectangular tumor (3x3x5cm^3) surrounded by tissue to form a 15x15x15cm^3 cubic phantom. Liquid PVC plastic and Superflab were used to simulate the tumor and surrounding tissue in the head phantom, respectively. Synthetic ballistic gel and a

heterogeneous in-house mixture were used to construct the tumor and surrounding tissue in the lung phantom, respectively. EBT3 and double-loaded TLDs were used in the phantoms to compare beam profiles and point dose measurements with and without magnetic fields. GEANT4 Monte Carlo simulations were performed to validate the detectors for both Unity 0T/1.5T and MRIdian 0T/0.35T configurations.

Results: Average TLD block measurements which, compared the magnetic field effects (magnetic field vs. 0T) on the Unity and MRIdian systems, were 0.5% and 0.6%, respectively. The average ratios between magnetic field effects for the geometric lung and head phantoms under the Unity system were -0.2% and 1.6% and for the MRIdian system were 0.2% and -0.3%, respectively. Beam profiles generated with both systems agreed with Monte Carlo measurements and previous literature findings.

Conclusions: TLDs and EBT3 film dosimeters can be used in MR/CT visible tissue equivalent phantoms that will experience a magnetic field environment.

3.2   INTRODUCTION

While magnetic fields from both MRIdian (ViewRay, Oakwood Village, Ohio) and Unity (Elekta, Crawley, United Kingdom and Philips, Amsterdam, Netherlands) systems do not directly affect their primary photon beam, their secondary electrons are influenced by the magnetic field via the Lorentz force[62]. A magnetic field will influence the electron's trajectory and will consequently affect the dose deposited in a medium. In general, the magnetic field will cause an increase in penumbra, a reduction of buildup and an asymmetric dose profile shift laterally[32; 62]. Previous studies from Raaymakers et al. 2004 used GEANT4 to simulate a homogenous water phantom irradiated with a 6 MV beam perpendicular to a 0T and a 1.5T magnetic field[62]. In this study, beam profiles generated under a 1.5T magnetic field shifted 0.7 mm from the 50% isodose line whereas beam profiles generated without a magnetic field did not shift[62].

Magnetic fields can cause irregular dose deposition in heterogeneous materials due to the secondary electron's helical trajectories. At tissue-air interfaces, the electrons traveling out of the tissue medium into air will curve back into the medium and deposit additional dose laterally[33]. This phenomenon, known as the electron return effect (ERE), is dependent on the magnetic field strength and electron energy[32]. The ERE in tissue-air interfaces previously has been shown to increase dose up to 40% along the central axis[63]. Irregular electron dose deposition, induced from the presence of a magnetic field, could potentially compromise the accuracy of radiation detectors typically used in radiotherapy[32; 37]. Therefore, typical radiation dosimeters must be analyzed and characterized in the presence of a magnetic field prior to being used to measure dose in the clinic.

TLD-100s (ThermoFisher Scientific, Waltham, MA, USA) frequently are used by the Imaging and Radiation Oncology Core Quality Assurance (QA) Center in Houston (IROC-Houston) to measure the delivered dose in anthropomorphic QA phantoms. Previous studies have started to characterize TLDs in the presence of a magnetic field[64-66]. Mathis et al. 2014 studied the effects of powder-form TLDs and radiochromic EBT3 film under the presence and absence of a 1.5T magnetic field when exposed to a range (200cGy to 600cGy) of radiation dose[65]. In this study, the TLDs and film irradiated with and without magnetic fields agreed within a 5% criterion[65]. However, the Mathis et al. study irradiated TLDs and film using two different machines (a conventional linear accelerator and an MR-Linac prototype at UMC-Utrecht). Comparing radiation measurements on two different systems introduced additional uncertainties such as fluctuations in machine output. Wen et al. 2015 studied the directional dependence of single-loaded TLD capsules using IROC-Houston's output verification acrylic TLD block[66]. It was noted that the TLD capsules irradiated parallel to a 1.5T magnetic field experienced a 2.3% higher output compared to TLD capsules irradiated perpendicular to a 1.5T magnetic field[66]. This small difference was most likely due to the air gap within the single-loaded TLD capsule itself. To the authors' knowledge, no studies have characterized double-loaded TLDs (no air gap) perpendicular to a radiation beam. Double-loaded TLDs have twice the amount of LiF:M,Ti than in single-loaded TLDs, thus, removing the air spacing that are normally found in single-loaded TLDs.

IROC-Houston's end-to-end phantoms also use radiochromic EBT3 film (Ashland Inc., Wayne, NJ, USA) to measure the planar dose distribution near the tumor and organs at risk. Studies have shown that different radiochromic film prototypes (EBT3 and EBT2) respond differently when irradiated in the presence of a magnetic field[67-70].

The protective polyester layers in EBT2 film change after a magnetic field exposure causing an under response that varies with dose[67; 68]. Preliminary studies showed that the EBT3 film's dose distribution did not change in a magnetic field likely due to EBT3 having a different protective layer than EBT2[69-71]. EBT3 films preliminarily were studied in 0.35T and 1.5T magnetic field environments. However, there was not a single comprehensive study used the same experiment methodology to compare the film's response to a magnetic field in both MRIdian and Unity systems. Additionally, these previous studies only compared the film's relative signal and were not validated with Monte Carlo measurements[62]. To the authors' knowledge, no complete comprehensive study has characterized and validated TLDs and EBT3 film under the presence of 0.35T and 1.5T magnetic fields for MRIdian and Unity systems, respectively.

To develop appropriate MRgRT tissue equivalent end-to-end QA phantoms, radiation detectors used in these phantoms must be characterized and validated under the presence of a magnetic field first. Since heterogeneous interferences and density can contribute to the ERE, dosimeters must be characterized under the same material conditions for which they were designed. The purpose of this study was to characterize and validate double-loaded TLDs and radiochromic EBT3 film, used in IROC-Houston's phantoms, under the presence and absence of a 0.35T and 1.5T magnetic fields for the MRgRT systems.

3.3   MATERIAL AND METHODS

TLD's dose response and reproducibility were characterized first using a simple homogenous acrylic block. Finally, both detectors were characterized in MRgRT phantom slabs and validated using Monte Carlo calculations. Both TLD acrylic block

reproducibility studies and geometrical slab phantom studies were conducted on a Elekta's Unity system (Elekta, Crawley, United Kingdom and Philips, Amsterdam, Netherlands) and a ViewRay's MRIdian ^{60}Co system (ViewRay, Oakwood Village, Ohio).

3.3.1 TLD Acrylic Block Reproducibility Studies

IROC-Houston's TLD acrylic blocks are used to verify the output for megavoltage beams and are designed with three small cylindrical holes that perfectly fit TLD capsules. Once a TLD is inserted into the acrylic block, each TLD capsule's end will be surrounded by an air channel. The dose deposition of small tissue-air interfaces will be affected by a magnetic field due to the secondary electron's curving back into the tissue-air interface[32; 62]. This ERE phenomenon also would occur in the acrylic-air channels in the acrylic block, consequently, affecting the TLD dose measurement. To minimize any extra dose being deposited in the acrylic-air interfaces, six tight-fitting acrylic plugs were inserted into all air passages and double-loaded TLDs were used instead of single-loaded TLDs. A single acrylic TLD block was reloaded and irradiated five separate times for two magnetic field configurations (0T and 1.5T) on the Unity system and three separate times for a 0T and a 0.35T magnetic field configuration on the MRIdian ^{60}Co system. The setup configurations for both MRgRT systems are shown in Figure 18. During the Unity system irradiations, the acrylic TLD block was placed above 14.5 cm of solid water (Sun Nuclear, Melbourne, FL) to achieve the 143.5 cm SAD isocenter and a gantry angle of 0°. Additionally, these blocks were irradiated using a 10 x 10 cm^2 field size and were prescribed 300cGy at d$_{max}$ (1.3cm at 0T and 1.7cm at 1.5T). During the MRIdian system irradiations, the TLD blocks were placed at 80 SSD, and

were irradiated using an equivalent 10x10 cm^2 field size with a prescription of 300cGy delivered at d$_{max}$ (0.5cm).
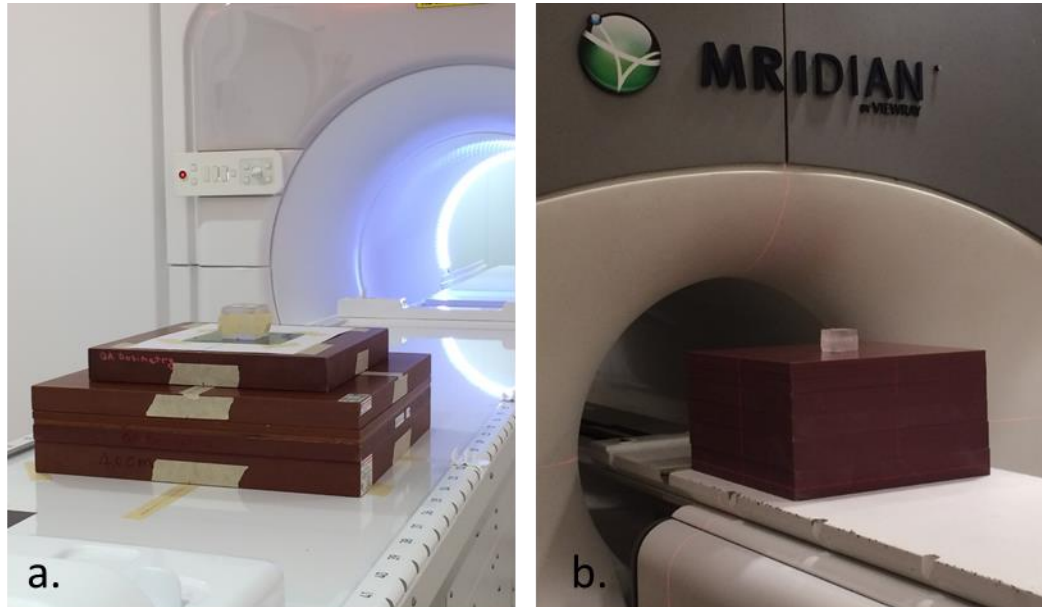
Figure 18: TLD blocks were irradiated at isocenter on Elekta's Unity system at 0T and 1.5T magnetic field strengths (a) and on ViewRay's MRIdian system at 0T and 0.35T (b).

3.3.2 Geometrical Phantom Studies

Radiochromic EBT3 film and TLDs were characterized using two geometrical head and lung phantoms slabs. These phantoms were developed using tissue equivalent and MR/CT visible materials which were described in the Steinmann et al. 2018 study[72]. Geometrical phantom slabs were constructed from eight 7.5 x 7.5 x 7.5 cm^3 quadrants that had a rectangular (3.0 x 3.0 x 5.0 cm^3) tumor centrally located around surrounded tissue to form two 15 x 15 x 15 cm^3 cubic phantoms (Figure 19). A 3.0 cm thick acrylic sleeve was placed around the entire cubic phantom to ensure that all eight segments were secured tightly. Having a tight fit was important since it minimized any air gaps between the quadrants. The geometrical phantoms were constructed using four different MR/CT

visible tissue equivalent materials. Clear Ballistic Gel #20 (Clear Ballistic, Fort Smith, AR, USA) and SuperFlab Bolus (Radiation Products Design Incorporation, Albertville, MN, USA) were used as tumor and surrounding soft tissue materials for the geometrical head phantom, respectively. The geometrical lung phantom was constructed using 100% liquid PVC plastic (M-F Manufacturing Company, Fort Worth, TX, USA) for the tumor material and an in-house mixture containing 8.3% wt. of Styrofoam balls with diameters ranging from 2-4 mm (Steve Spangler Science, Englewood, CO, USA) and 91.7% wt. of petroleum jelly (Sonneborn, Parsippany, NJ, USA) for the surrounding lung tissue. As shown in Figure 19, EBT3 film was inserted in all three planes and two double-loaded TLD powder capsules were inserted near the synthetic tumor's center. The geometrical phantoms were positioned on the treatment couch so that the TLDs were perpendicular to the magnetic field.
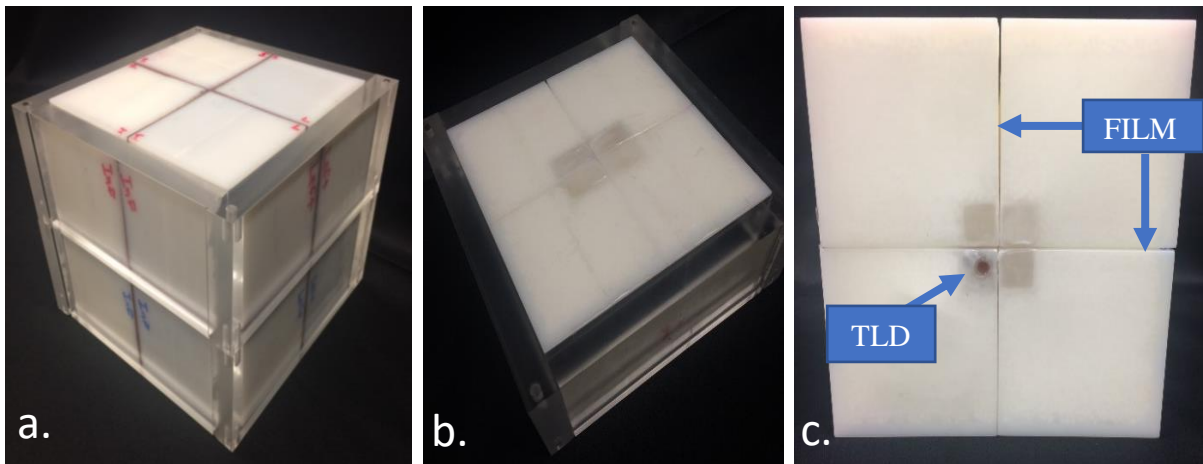
Figure 19: The geometrical lung and head phantoms were constructed out of tissue equivalent and MR/CT visible materials (figure 19a shows the lung phantom). As shown in figure 19c, radiochromic films were placed in all three fields and two TLDs were placed inside the tumor.

Solid water was positioned posteriorly and anteriorly to the geometrical phantom. Solid water positioned anteriorly was fixed for both MRgRT setups and was used to

secure the segments together. Solid water positioned posteriorly to the geometrical phantom allowed the tumor's center to align with the isocenter. Since the radiation isocenters were different in the Unity and MRIdian systems, the amount of solid water varied posteriorly to the phantom. The geometrical phantoms setups for MRIdian and Unity systems are shown in Figure 20. Under 0T and 1.5T conditions, the geometrical head and lung phantoms were irradiated five times on the Unity system. The irradiation parameters on the Unity system were: 10 x 10 cm^2 field size, 131 SAD and prescription dose of 600cGy delivered at d$_{max}$. Under 0T and 0.35T conditions, the two phantoms were irradiated three times on the MRIdian ^{60}Co system with a prescribed dose of 600cGy at 0.5 cm depth, an 80 SSD and an equivalent 10x10 cm^2 field size. Repeating the irradiations five times on the Unity system and three times on the MRIdian ^{60}Co system allowed a total of 20 and 12 TLD readings, respectively. A total of ten axial films were captured on the Unity system; five axial films were irradiated with 0T and the remaining five films were irradiated under 1.5T configuration. A total of six axial films were captured on the MRIdian ^{60}Co system; three were irradiated with 0T and the remaining three were irradiated with 0.35T. Individual films from each setup were used to create an average beam profile.
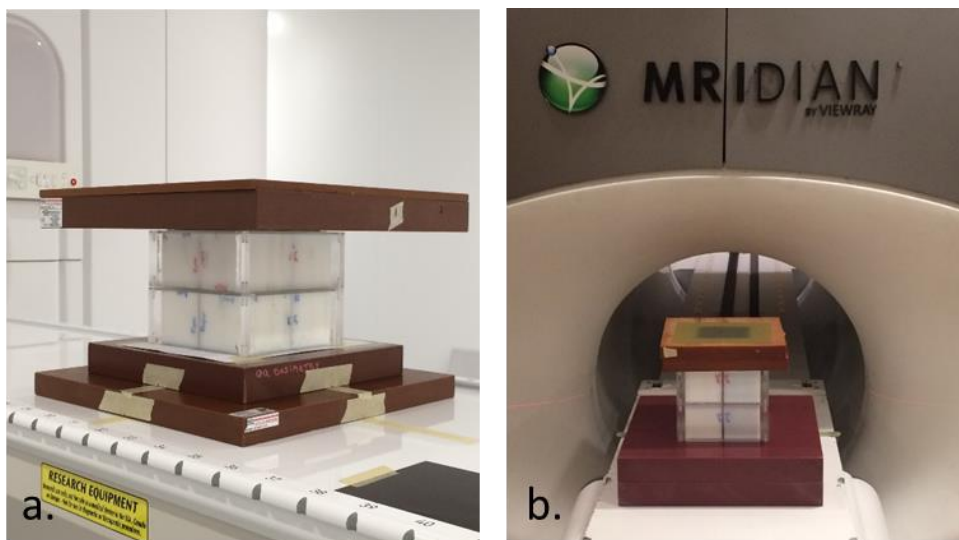
Figure 20: Head and Lung geometrical slab phantom setups for irradiation using Elekta's Unity (figure 20a) and ViewRay's MRIdian (figure 20b) systems

TLDs and radiochromic EBT3 film were read and analyzed using the same standard analysis procedures as IROC-Houston[42; 60]. TLDs were read by weighing the amount of lithium fluoride (LiF) powder on a Mettler AT261 DeltaRange (Mettler Toledo, Greifensee, Switzerland) scale and measuring the light output using a Harshaw 3500 TLD reader (ThermoFisher Scientific, Waltham, MA, USA). TLD readings in the lung and head configurations were collectively averaged and were compared with and without a magnetic field for both MRgRT systems. Film was processed by converting the optical density into dose using IROC-Houston's photoelectron CCD microdensitometer (Photoelectron Corporation, North Billerica, MA, USA). IROC-Houston's in-house MATLAB software generated dose distributions and profiles.

Measured beam profiles on MRIdian and Unity systems were validated with Monte Carlo calculations using GEANT4 (v9.6.p04). GEANT4 was chosen to perform validation measurements since it was a freely available software and previous studies used GEANT4 to simulate a radiation beam exposed to a magnetic field[35; 37; 62; 73-76]. The

GEANT4 application used for this study was developed at MD Anderson Cancer Center and was described in detail by O'Brien et al. 2016[35]. In short, this application simulated either a 7 MV or ^{60}Co beam incident to a virtual phantom. The 7 MV beam model was provided by Elekta and was developed specifically for the Unity system as a point-source model defined at isocenter (143.5 cm from the target) with a field size of 10x10 cm^2 [35; 37]. A ^{60}Co spectrum was used from the International Atomic Energy Agency (IAEA) phase-space database to simulate a ViewRay configuration. This phase-space data was based on of Mora et al.'s 1999 ^{60}Co beam model with a 2cm source capsule[77].

A virtual head and lung phantom was created in GEANT4. The materials in these virtual phantoms could be defined several ways in GEANT4. Some generic materials (i.e., water, air) were predefined in GEANT4's material database while others could be defined manually if the chemical composition and density were known. The tissue equivalent MR/CT visible materials used to construct the geometrical slab phantoms were not available in GEANT4's material database; so, the chemical composition and density were reported. The four materials used in the geometrical phantoms were sent to Intertek Pharmaceutical Services (Whitehouse, NJ, USA) to determine the materials' carbon, hydrogen, nitrogen, oxygen and chloride content. The Intertek Pharmaceutical Services used a Perkin-Elmer 2400 elemental analyzer to determine the elemental composition of carbon, hydrogen, nitrogen and oxygen and a Calorimetric Titration to determine the chloride content. The results provided from the Intertek Pharmaceutical Services are shown in Table 7.

Tested Material	Material Application	Elemental Composition				
		Carbon	Hydrogen	Nitrogen	Oxygen	Chloride
Synthetic Gel #20	H&N Tumor	84.7 %	15.3%	<0.05%	<0.05%	-
Superflab	Surrounding H&N Soft Tissue	68.8%	11.0%	<0.05%	12.4%	7.8%
Liquid PVC Plastic	Lung Tumor	66.2%	11.9%	<0.05%	12.6%	9.3%
In-house Petroleum/styrofoam mixture	Surrounding Lung Tissue	87.2%	12.8%	0.38%	-	-

Table 7: The percent elemental composition of the four MR/CT visible tissue equivalent materials used in the head and lung geometrical slab phantoms.

The virtual phantoms had the same geometry as the physical phantoms. The virtual phantoms were designed with a centrally located rectangular 5.0 x 3.0 x 3.0 cm^3 tumor inside a 15 x 15 x 15 cm^3 cubic phantom and 5.0 cm of solid water anteriorly above the phantom. Both head and lung geometrical slab phantoms were simulated with 0T and 1.5T magnetic fields for a 7 MV beam, and 0T and 0.35T magnetic fields for a ^{60}Co beam. Four beam profiles were generated in each lung and head phantom for both virtual and physical environments. For each phantom configuration, two beam profiles were created from a ^{60}Co beam under 0T and 0.35T magnetic field strengths and the other two beam profiles were created from a 7 MV beam under 0T and 1.5T magnetic field strengths.

3.4 RESULTS & DUSCUSSION

3.4.1 *TLD Block Reproducibility Studies*

Each block had three double-loaded TLD capsules aligned perpendicular to the magnetic field. Three double-loaded TLDs, in a single acrylic block, created six TLD readings per irradiation. The average measured TLD doses in the presence or absence of

a magnetic field are listed in Table 8 for Elekta's Unity and ViewRay's MRIdian MRgRT systems. The Unity system's average TLD doses for 0T and 1.5T magnetic field strengths were 334.9 cGy ($\pm$0.5%) and 333.1 cGy ($\pm$1.4%), respectively, whereas the MRIdian system's average doses for 0T and 0.35T magnetic field strengths were 273.4 cGy ($\pm$0.9%) and 275.1 cGy ($\pm$1.0%), respectively. The average ratio between measurements with and without magnetic fields of the Unity and MRIdian systems were 0.995 and 1.006, respectively. The standard deviations of the average TLD doses for all conditions were small ($<$1.4%) and showed excellent reproducibility in the TLD readings.

A two-sided, unpaired T-test was used to determine whether there was a statistical significance between TLDs exposed with and without magnetic fields. With a 95% confidence interval, both ViewRay ($p>0.08$) and Unity ($p> 0.06$) p-values were greater than 0.05, thus suggesting with a 95% confidence, that there was not a statistical significance between TLDs irradiated with and without magnetic field. Since the p-values were close to 0.05, a followed up was done with a two one-sided equivalence test (TOST) to determine whether TLDs irradiated with a magnetic field were statistically equivalent to TLDs irradiated without a magnetic field. The delta used for the TOST allowed the differences in means to be within 1%. The TOST test showed p-values <0.05 (Unity: $p<0.04$ and MRIdian: $p<0.02$) on both MRgRT configurations. Therefore, with 95% confidence, the TOST test indicated that TLDs irradiated with and without magnetic fields on the same treatment system were statistically equivalent.

Acrylic TLD Blocks	Unity			MRIdian		
	0.0T [cGy]	1.5T [cGy]	**Ratio [1.5T/0T]**	0.0T [cGy]	0.35T [cGy]	**Ratio [0.35T/0T]**
	334.9 (±0.5%) n=5	333.1 (±1.4%) n=5	**0.995**	273.1 (±0.9%) n=3	275.1 (±1.0%) n=3	**1.006**

Table 8: The acrylic block TLD irradiations for both MRgRT Unity and MRIdian systems in the presence and absence of the magnetic field. All standard error of means were less than 1.4%. (Note: n corresponds to the number of times the acrylic block was irradiated under a specific condition.)

With MRgRT systems recently installed in the radiation oncology centers and recently used in NCI supported clinical trials, future large multi-institutional clinical studies will be conducted on these systems. IROC-Houston has the responsibility to ensure that these systems can treat patients in a comparable and accurate manner, which is accomplished through IROC-Houston's end-to-end anthropomorphic QA phantoms by credentialing institutions wishing to participate in NCI sponsored clinical trials. Institutions' performances are analyzed by comparing measured TLD and radiochromic film to expected treatment plans. Double-loaded TLDs are equipped with 22 mg of powder LiF compared to 11 mg of LiF found in single-loaded TLDs. The extra powder effectively eliminates any air gaps within the capsules and allows for two reading measurements. Double-loaded TLDs were used to mitigate any potential ERE effects due to the absence of any air gaps. Dose measurements with double-loaded TLDs in the acrylic blocks and geometrical slab phantoms were shown not to be affected by ERE in both MRgRT systems when comparing doses with and without magnetic fields.

Our results agreed with previous studies, showing that there is not a statistical difference between TLDs irradiated with and without magnetic fields for both ViewRay and Unity systems. Furthermore, our studies showed smaller differences in the ratios

between TLDs irradiated in 0T and 1.5T environments than shown in previous studies. Specifically, we found TLDs to be within 0.6% compared to a previous study that found TLDs to be within 5%[65]. One reason our results had greater agreement was attributed to the TLD readout process. IROC-Houston has an established TLD readout process that allows TLDs to be measured within 2.3% certainty (at 1 standard deviation)[42]. This study used standardized double-loaded TLD capsules, whereas the previous study self-packaged LiF and self-measured the TLD dose. If a user had less experience, TLD uncertainties could be as great as 4.6% (at 1 standard deviation)[78]. Additionally, the previous study examined the magnetic effect on TLDs by comparing the TLD response on two different systems: a conventional 6 MV linear accelerator (B=0 T) and a 6 MV MR-Linac (B= 1.5T)[65]. Directly comparing TLDs irradiated with and without magnetic fields on two different systems will introduce greater uncertainties. This work had the unique opportunity to irradiate the TLD acrylic blocks and geometrical phantoms with and without magnetic field using the same machine for both MRIdian and Unity treatments.

While this work was performed on the same unit, the window of opportunity to irradiate the phantoms with and with a magnetic field was extremely limited. The magnet on an MRgRT unit was ramped down rarely and were usually ramped down to perform upgrades on the system. Due to the time constraints, the phantoms and TLD blocks were only irradiated three and five times on the MRIdian and Unity MRgRT systems, respectively, yet the phantoms were irradiated on a single system and had direct comparisons between irradiations with and without a magnetic field. The output of the machines, when irradiated with and without magnetic fields, were assumed to have

negligible fluctuations. The Unity system, based on a series of output measurements, had less than a 0.7% fluctuation in the output over time[35].

3.4.2   Geometrical Slab Phantom Studies

Radiochromic EBT3 film and double-loaded TLDs were irradiated in both the head and lung geometrical phantoms. TLDs were read in-house using IROC-Houston's standard reading procedure. The measured TLD doses for each phantom type, i.e. head and lung, were averaged and are shown in Table 9 for the two MRgRT systems. The average Unity system TLD doses for 0T and 1.5T magnetic fields were 491.9 cGy ($\pm$1.5%) and 492.9 cGy ($\pm$1.3%) for the geometrical lung phantom and 453.1 cGy ($\pm$0.7%) and 441.6 cGy ($\pm$1.6%) for the geometrical head phantom. The average measured TLDs ratios between without/with magnetic fields in the Unity system configuration for lung and head phantoms were, respectively 1.002 and 0.984. The ratio of 0.984 comparing 1.5T dose measurements to those without any magnetic field was corrected due reconstructing the geometrical head phantom's quadrants between the 0T measurements and the 1.5T measurements. After 0T measurements, it was discovered that the Superflab had interacted with the high-impact polystyrene (HIPS) barrier used to encapsulate the gel materials it, so, the HIPS was replaced with solid water. After the 1.5T measurements it was realized that the geometrical head phantom's modified solid water exterior thickness was thicker than the original HIPS and resulted in a 1.008 correction to the original values. For the MRIdian ^{60}Co system, the average TLD doses for 0T and 0.35T magnetic field strengths were 296.4 cGy ($\pm$1.1%) and 295.7 cGy ($\pm$1.1%) for the geometrical lung phantom and 271.7 cGy ($\pm$1.1%) and 272.4 cGy ($\pm$1.2%) for the geometrical head phantom, respectively. The average ratios of measured

TLD average doses for the MRIdian system comparing with to without magnetic fields for the lung and head phantoms were 0.998 and 1.003, respectively.

The ratios between TLD irradiated with and without magnetic fields on a single MRgRT system were all within 1.6%, which is well within IROC-Houston's 2.3% TLD uncertainty. The TLD results agreed with previous studies using a thimble ion chamber (Exradin A1SL) that showed a 1.26% higher dose output in the 1.5T than in a 0T magnetic field environment[79]. TLDs agreeing within 1.6% would suggested that the ERE effect is not affecting double-loaded TLDs dosimetry in either homogenous or heterogeneous configurations. If the magnetic field influenced the TLD dose, it was within the TLD's inherent dose measurement 2.3% uncertainty and could not be delineated physically from the TLD reading uncertainty[42]. Therefore, these results would conclude that double-loaded TLDs were sufficient dosimeters to measure dose in 0.35T to 1.5T environments.

Miniature Phantom	Unity			MRIdian		
	0.0T [cGy]	1.5T [cGy]	Ratio [1.5T/0T]	0.0T [cGy]	0.35T [cGy]	Ratio [0.35T/0T]
Lung	491.9 (± 1.5%)	492.9 (± 1.3%)	1.002	296.4 (± 1.1%)	295.7 (±1.1%)	0.998
Head	453.1 (±0.7%)	446.1 (± 1.6%)	0.984*	271.7 (± 1.1%)	272.4 (± 1.2%)	1.003

*Table 9: Geometrical lung and head phantoms measured doses with and without magnetic field from a total of five and three times irradiations on the Unity and MRIdian systems, respectively. All standard errors of the means were less than 1.6%. *Corrected by 1.008 for the increased barrier thickness.*

Radiochromic EBT3 films were used to measure beam profiles centrally located inside the geometrical phantoms. The right/left axial beam profiles were analyzed due to the ERE affecting the lateral planes in both ViewRay and Elekta systems. The measured

and simulated beam profiles for the head and lung geometrical phantoms in the presence and absence of a magnetic field were compared and are shown in Figure 21 and Figure 22 for the Unity and MRIdian systems, respectively. Figure 21b shows a disagreement in the shoulder region between the two profiles due to an accumulation of petroleum gel without styrofoam beads that was not simulated in the GEANT4 Monte Carlo. Monaco treatment planning software was used as a different dose calculation method to validate the geometrical lung's 1.5T film measurement. Under all conditions the two curves (simulated vs. measured) fall within the measurement uncertainty as evidenced by the error bars. The absolute differences between measured and calculated beam profiles were compared at the 80%, 50% and 20% dose levels along the edge of each set of profiles. The differences are shown in Table 10 for the Unity MRgRT system with the exception of the shoulder region (80% dose level) of the Unity lung phantom comparisons as explained above. The maximum average difference between the measured and calculated profiles was less than 2.2 mm.
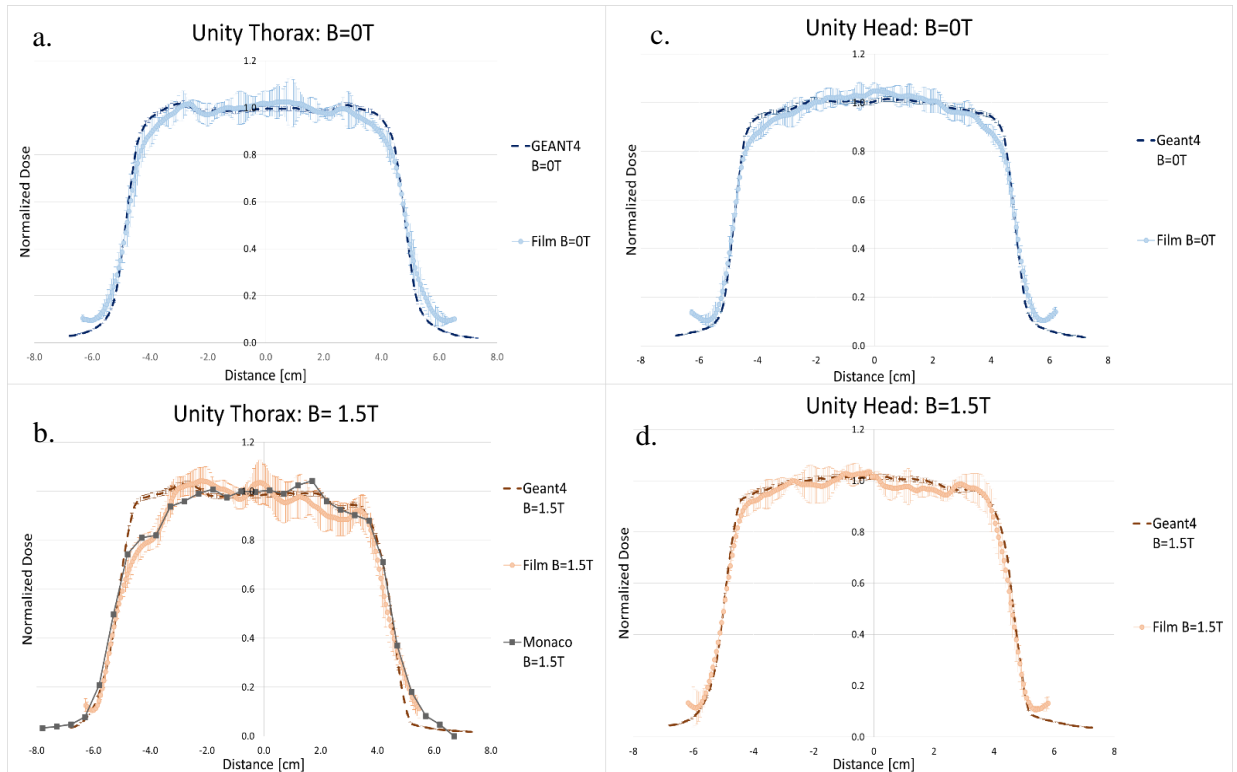
Figure 21: Beam profiles comparing GEANT4 Monte Carlo measurements and EBT3 film for the geometrical lung (a-b) and head (c-d) phantoms that were irradiated on Unity's 7 MV beam under 0T(a and c) and 1.5T (b and d) magnetic field strengths. The error bars were calculated using the standard error of mean.

Normalized Dose	Lung		Head	
	Unity B= 0T DTA [mm]	**Unity B= 1.5T** DTA [mm]	**Unity B= 0T** DTA [mm]	**Unity B= 1.5T** DTA [mm]
80%	1.1 ± 0.7	-	1.2 ± 0.8	0.9 ± 0.7
50%	0.5 ± 0.3	1.3 ± 0.7	0.3 ± 0.3	0.5 ± 0.4
20%	2.2 ± 1.0	1.2 ± 0.3	1.4 ± 0.5	0.3 ± 0.3

Table 10: Measure distance at 80% and 50% on both left and right side of the beam profiles were used to calculate absolute differences between measured and simulated beam profiles on the Unity's 0T and 1.5T for both head and lung phantoms. Average absolute differences between both left and right sides of the curves were recorded

Virtual beam profiles were generated by modifying the Monte Carlo code used in the O'Brien et al. 2016 study[35]. These modifications included: 1) adding a virtual geometrical phantom and 2) defining the chemical compositions of the MR/CT visible tissue equivalent materials used in the geometrical phantoms. The most accessible and

practical way to define the materials in GEANT4 was to describe their chemical composition and density. The material safety data sheets and patents of each material used in the geometrical phantoms gave a general idea of the elements used in each material. Tests performed by Intertek Pharmaceutical Services measured the percentage of specific elements thought to be used in each material. It should be noted that there are uncertainties in estimating the elements in the materials. It was thought that the materials only had oxygen, nitrogen, hydrogen, carbon and chloride elements, and thus only those elements were examined. Each elemental composition test added an uncertainty of up to 0.4%. Since only five elements were assessed, there were additional uncertainties as to other possible elements present in the materials which were not defined in the Monte Carlo.
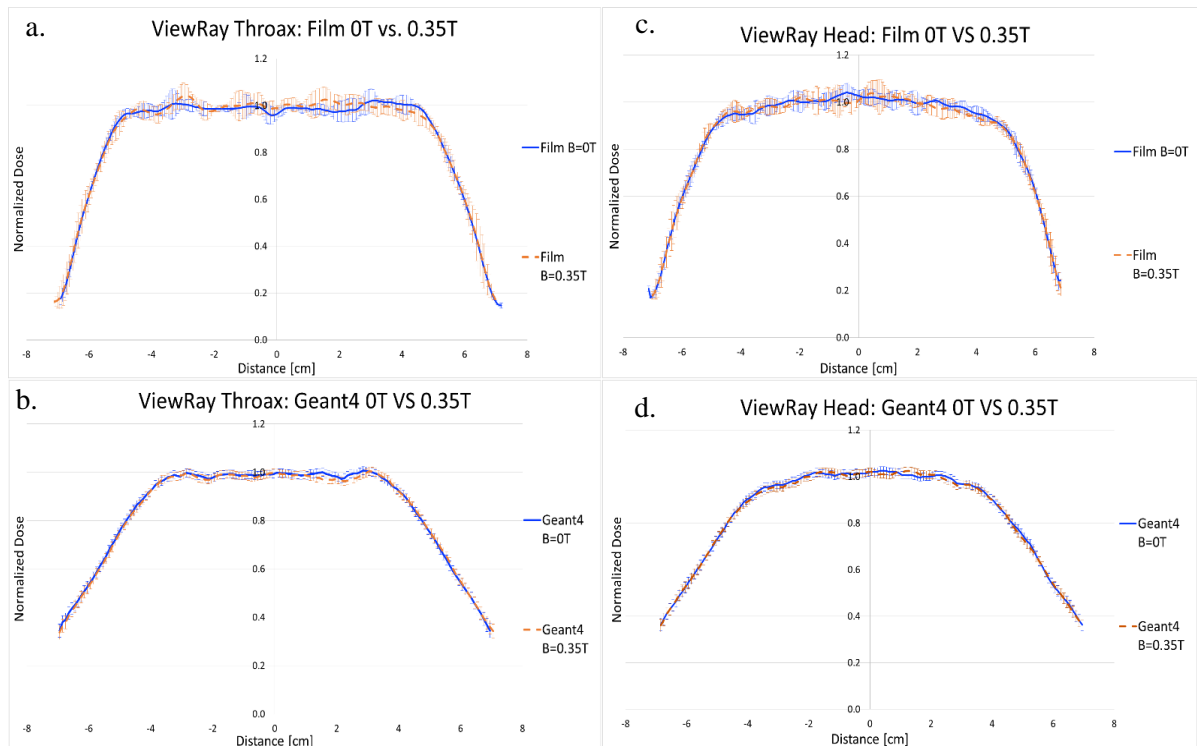
Figure 22: Beam profiles comparing 0T and 0.35T for the geometrical lung (a-b) and head (c-d) phantoms that were irradiated on MRIdian's ^{60}Co beam (a and c) and Monte Carlo generated beam profiles using Geant4 (b and d). The error bars were calculated using the standard error of mean.

Normalized Dose	Lung		Head	
	Geant4: B= 0T VS B=0.35T DTA [mm]	Film: B=0T VS B=0.35T DTA [mm]	Geant4: B= 0T VS B=0.35T DTA [mm]	Film: B=0T VS B=0.35T DTA [mm]
80%	0.4 ± 0.3	0.6 ± 0.3	0.1 ± 0.1	0.5 ± 0.5
50%	0.4 ± 0.2	0.4 ± 0.3	0.2 ± 0.1	0.4 ± 0.2
20%	-	0.6 ± 0.3	-	0.4 ± 0.2

Table 11: Measured distance at 80% ,50% and 20% on both left and right sides of the beam profiles were used to calculate absolute differences between MRIdian's 0T and 0.35T configurations for Monte Carlo (Geant4) and measured films. The average differences between the beam profiles were measured for both lung and head phantoms.

Figure 22 displays measured and generated beam profiles for lung and head configurations using the MRIdian system. The absolute differences between 0T and 0.35T beam profiles generated on Monte Carlo were compared to the absolute differences between 0T and 0.35T beam profiles measured on film. The absolute differences were compared at 80%, 50% and 20% for each profile set. Table 11 displays the average differences using the MRIdian configuration. The maximum average difference between 0T and 0.35T was 0.6 mm for film and 0.4 mm for Monte Carlo. Under all conditions, the two curves fall within the measurement uncertainty as evidenced by the shown standard deviation. Despite the disagreement seen in the penumbra between measured and Monte Carlo generated beam profiles, both curves showed that low magnetic fields (i.e., 0.35T) did not shift the beam profiles and showed the same beam profile shape as 0T configurations. This result would suggest, at first order, the 0.35T magnetic field environment does not influence the dose deposition on the EBT3 film.

The MRIdian system was simulated using an open-source head model, provided from the International Atomic Energy Agency. This phase-space data simulated a ^{60}Co capsule with a finite width of 2 cm[77]. GEANT4 did not accurately simulate a true MRIdian ^{60}Co system since the phase space file only accounted for a single multi leaf

collimator (MLC) and a common finite source width. The treatment head of an MRIdian ^{60}Co system has two sets of MLCs that were used to focus the radiation beam to create a steep penumbra. Having two sets of MLCs allowed a ^{60}Co system to better resemble a penumbra traditionally seen on a 6 MV linear accelerator. However, the MRIdian ^{60}Co system did not have the same penumbra slope as a 6 MV beam. The phase-space file used to simulate a ^{60}Co beam had a typical ^{60}Co treatment head configuration including a single MCL set. The head configuration could not be altered to better resemble an MRIdian head configuration due to using a phase-space data with fixed parameters. This factor created additional uncertainties to the penumbra on the simulated beam profiles of the MRIdian system since only a single MLC set was simulated. Film validation was performed by computing the distance to agreement (DTA) between 0T and 0.35 T beam profiles on film and the DTA between 0T and 0.35T on Monte Carlo simulated beam profiles.

Two geometrical phantoms were irradiated using EBT3 film on a Unity and MRIdian system. Monte Carlo generated beam profiles were used to validate EBT3 film irradiated with and without magnetic fields for Unity and MRIdian MRgRT systems. Using a 1.5T magnetic field parameter, Monte Carlo accurately resembled film measurements in a 1.5T environment, thus suggesting that a high field does not affect EBT3 readings. Higher magnetic fields (i.e., 1.5T) are more likely to have a greater effect on radiation dosimeters than on low magnetic field environments (i.e., 0.35T), thus suggesting that EBT3 film also would not affect a lower (i.e. 0.35T) magnetic field environment. This assumption was proven to be true when comparing the average DTA between 0T and 0.35T setups for both film and Monte Carlo measurements.

3.5 CONCLUSION

TLDs irradiated with and without magnetic fields showed high reproducibility in both MRgRT systems. Both Unity and MRIdian systems showed less than 0.6% difference in the acrylic block study. Under a homogenous acrylic block setting, the TLD dose indicates a negligible effect from the presence of a magnetic field in MRgRT systems with 0.35T and 1.5T magnetic fields. Furthermore, TLD's and radiochromic film's responses are reproducible in MRIdian and Unity systems when using more complex conditions (i.e., lung and head geometrical slab phantom configurations). The ratio between TLD doses with and without a magnetic field agreed within 1.6% for geometrical phantoms irradiated in both MRgRT system. Beam profiles generated from radiochromic film irradiated in the lung and head geometrical phantoms on the Unity system agreed very well with the general shape of beam profiles generated from a Monte Carlo simulation. Beam profiles generated on the MRIdian configurations did not match beam profiles generated on Monte Carlo due to the limitations of using a phase-space with fixed parameters that simulated a single MLC set. The beam profiles generated on Monte Carlo with and without magnetic fields showed similar shifts as beam profiles measured in the MRIdian system. This study showed that, double-loaded TLDs and radiochromic EBT3 films can be used in phantoms that will experience a 0.35T to 1.5T magnetic field.

Chapter 4: MRgRT Head and Neck QA Phantom: Design, Construction and Feasibility Study

A substantial portion of this chapter is written or based on the following publication:

4.1 ABSTRACT

Purpose: The purpose of this paper was to design, manufacture, and evaluate a tissue equivalent, dual MR/CT visible anthropomorphic Head and Neck (H&N) phantom. This phantom was specially designed as an end-to-end quality assurance (QA) tool for magnetic resonance (MR) guided radiotherapy (MRgRT) systems participating in NCI-sponsored clinical trials.

Method: The MRgRT H&N phantom was constructed using a water-fillable acrylic shell and a custom insert that mimics an organ at risk (OAR) and target structures. The insert consists of a primary and secondary PTV manufactured of a synthetic clear ballistic gel, an acrylic OAR and surrounding tissue fabricated using melted Superflab. Radiochromic EBT3 film and TLDs were used to measure the dose distribution and absolute dose, respectively.

The phantom was commissioned by conducting an end-to-end test that included: imaging on a GE Lightspeed CT simulator, planning on Monaco treatment planning software (TPS), verifying treatment setup with MR and irradiating on Elekta's 1.5T Unity

MR linac system. The phantom was irradiated three times using the same plan to determine reproducibility. Three institutions, equipped with either ViewRay MRIdian ^{60}Co or ViewRay MRIdian Linac, were used to conduct a feasibility study by performing independent end-to-end studies. TLDs were evaluated in both commissioning and feasibility studies by comparing ratios of measured TLD to reported TPS calculated values. Radiochromic film was used to compare measured planar dose distributions to expected TPS distribution. Film was evaluated by using an in-house gamma analysis software to measure the discrepancies between film and treatment planning software (TPS).

Results: Commissioning of the MRgRT H&N phantom on the Unity system resulted in reproducible TLD doses (SD < 1.5%). The measured TLD to calculated dose ratios for the Unity system ranged from 0.94 to 0.98. The Viewray dose result comparisons had a larger range (1.03-0.94) but these depended on the TPS dose calculations from each site. Using a 7%/4mm (85% pixels passing) gamma analysis, Viewray institutions had average axial and sagittal passing rates of 97.3% and 96.2% and the unity system had average passing rates of 97.8% and 89.7%, respectively. All of the results were within IROC's 7%/4mm criterion.

Conclusions: An MRgRT H&N tissue equivalent and visible on both CT and MR was developed. There was no difference in the results noted between Unity, MRIdian Linac and MRIdian ^{60}Co systems. The MRgRT HN phantom can be used as a credentialing tool for NCI-clinical trials using MRgRT systems.

4.2   INTRODUCTION

New radiotherapy devices, referred to as MRgRT systems, integrate an MR imager with either a linear accelerator or radioactive ^{60}Co source. Globally, there are presently four different MRgRT prototypes used in the clinic. These include: the MRgRT suite (Varian, Palo Alto, California, USA and Siemens, Erlangen, Germany), the Unity (Elekta, Crawley, United Kingdom and Philips, Amsterdam, Netherlands), the MRIdian ^{60}Co (ViewRay, Oakwood Village, Ohio), and the MRIdian Linac (ViewRay, Oakwood Village, Ohio) [10-13]. In short, the MRgRT suite is a 1.5T MR-on-rails system that moves an MR unit into a linear accelerator vault to acquire images. The Unity system is equipped with a 7 MV beam mounted to a slip-ring gantry located above a modified 1.5T magnet. The MRIdian and MRIdian Linac systems are equipped with three ^{60}Co sources and a single 6 MV linear accelerator, respectively, that are centrally located within a split 0.35T magnet. Clinics within the United States either have the MRIdian ^{60}Co, the MRIdian Linac, or the Unity system.

Technologies used in an MRgRT system, compared to current image guided systems, have the potential to revolutionize radiotherapy. Unlike conventional KV or MV image guided systems, MRgRT systems offer superior soft tissue delineation while not subjecting the patient to a dose of radiation. The ability to visualize the gross tumor volume (GTV) could further reduce margins, thereby, reducing normal tissue toxicity and increasing local control. Acquiring MR images can be done more frequently since they would not contribute to additional dose. MRgRT systems can monitor treatment effectiveness since their near diagnostic-quality MR images could delineate between soft tissue and would be captured before every treatment. Advance radiotherapy techniques

can be enhanced with an MRgRT system by permitting real-time gating, target tracking and online adapted radiotherapy[80; 81]. These techniques would revolutionize radiation therapy since treatment would be based on the actual disease location at the given time radiation was delivered.

The safety and usefulness of MRgRT systems are still being investigated. The National Institutes of Health (NIH) has sponsored several short-term clinical trials that preliminarily address safety issues in acquiring daily MR images (NCT02973828) and delivering radiation using MRgRT systems (NCT03284619). Additionally, NIH-sponsored clinical trials (NCT03048760, NCT01999062) have begun to investigate how new MRgRT workflows (i.e., online adapted radiotherapy) and advanced treatment techniques (i.e., auto-contouring, MR gating) would affect the clinic. NIH has also sponsored several short-term pilot studies (NCT02264886, NCT02683200, NCT02701712, NCT02264886) to investigate the effectiveness of using an MRgRT system for various anatomical locations. While these pilot studies can preliminarily determine regions that would likely benefit from MRgRT, more extensive multi-institutional clinical trials will be needed in the future to thoroughly evaluate clinical outcomes (i.e., local control, survival rates) for a given disease site. A proposed clinical trial could examine the correlation between local control rates and MR image guidance on an MRgRT system[82]. Head and neck (H&N) region tumors would be ideal for this proposed clinical trial since CT images lack soft tissue delineation[83].

In order for radiotherapy centers to participate in large multi-institutional studies, the National Cancer Institute (NCI) requires each participating institution to be a part of the Imaging and Radiation Oncology Core (IROC) QA program which includes credentialing for advanced technologies. The Imaging and Radiation Oncology Core

quality assurance (QA) center in Houston (IROC-Houston) has been funded by the NCI since 1968 to ensure all institutions participating in National Clinical Trial Networks (NCTN) can accurately and consistently deliver radiation doses to trial patients such as from intensity modulated radiotherapy (IMRT) treatments. IROC-Houston has developed various on-site and off-site auditing tools to assure quality is maintained throughout participating institutions. Among such QA tools, IROC-Houston ships off-site anthropomorphic phantoms to credential NCTN trial participants using advanced technology treatment modalities[84]. During the credentialing process, the phantom will undergo the same treatment workflow as a patient would and an end-to-end QA examination is performed to assess the institution's ability to deliver the treatment plan.

IROC-Houston has a collection of site-specific anthropomorphic phantoms. These anatomical regions include: H&N, pelvis, brain, thorax, spine and liver. The H&N phantom is IROC-Houston's oldest and most common phantom used in the credentialing process. This custom phantom is constructed using a solid high impact polystyrene (HIPS) slab that is fitted into an anthropomorphic shaped human head. The custom insert contains an acrylic spinal cord, and two (primary and secondary) PTVs manufactured using solid water which are dosimetrically monitored with radiochromic film and thermoluminescent detectors (TLD)[60]. The spinal cord is adjacent to the primary PTV which requires each institution to create an IMRT plan with a steep dose gradient.

Integrating an MR imager within a radiotherapy system will inherently transform how treatment plans and deliveries are performed. In order to account for an MRgRT workflow, comprehensive end-to-end phantoms must be CT and MR compatible. Conventional IROC-Houston phantoms, designed for CT-only workflows, are not suited for MR workflow[72]. The aim of this study was to design, manufacture, and evaluate a

tissue equivalent MR/CT visible anthropomorphic H&N phantom, that met IROC-Houston's phantom requirements and could be used as a QA tool to credential MRgRT systems participating in NCI-sponsored NCTN clinical trials.

4.3   MATERIAL AND METHODS

The MRgRT H&N phantom was designed to meet IROC-Houston's radiotherapy, diagnostic and practicality criteria. Materials used in the MRgRT H&N phantom were carefully selected based on findings in the Steinmann et al. 2018 study[72]. To meet radiotherapy and diagnostic requirements, the entire phantom was designed to dosimetrically represent human tissues (i.e., spinal cord, soft tissue) by using materials that were dosimetrically tissue equivalent and visible on MR and CT imagers. To meet practicality criteria, materials were carefully selected so that they required minimal maintenance, did not morph over time, did not require preservatives, and had high melting points to withstand any harsh shipping conditions. Once the H&N insert was constructed, the phantom was reproduced on a 1.5T Unity system and then sent out to three institutions to conduct a miniature end-to-end feasibility study.

4.3.1   Phantom Design

The MRgRT H&N phantom consisted of a water-fillable acrylic shell (The Phantom Laboratory, Salem, New York, USA) and a custom designed H&N insert. Externally the hollow acrylic shell was morphed to resemble a human head, but internally consisted of a rectangular concavity that tightly held a MR/CT compatible insert. The hollow anthropomorphic MRgRT H&N phantom next to its 7.5 cm x 10.5 cm x 13 cm custom insert is seen in Figure 23. The custom H&N insert was designed based on a

Radiation Therapy Oncology Group (RTOG) oropharyngeal protocol (H-0022) which consisted of two PTVs (primary and secondary) and an OAR[60].
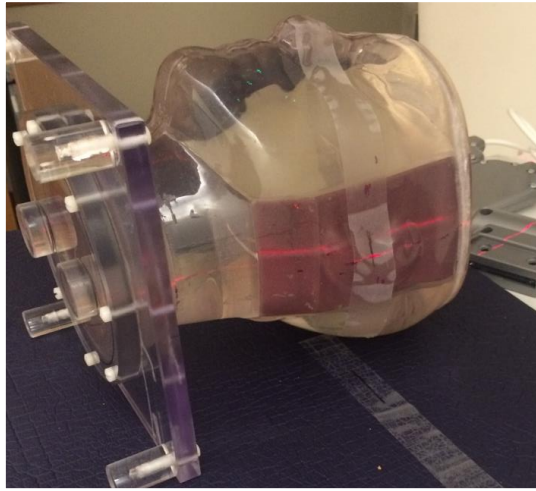
Figure 23: The MRgRT H&N Phantom. The phantom consists of a water-fillable anthropomorphic shell and a MR/CT compatible insert.

Figure 24 displays a CT axial view of the H&N insert. Internally, the insert consists of: 1) a moon-shaped cylindrical primary PTV, 2) a cylindrical secondary PTV and 3) a cylindrical spinal cord that simulated an OAR. The primary PTV is adjacent to the OAR and the secondary PTV is located at a distance. Inferior and superior pieces of the two-part insert were secured together from two high impacted polystyrene (HIPS) plastic screws. The MRgRT H&N insert used radiochromic EBT3 film and double-loaded TLDs as portable dosimeters. A total of three radiochromic films were placed into the insert to capture axial and sagittal planes. A sagittal film was placed in between the primary PTV and OAR for each superior and inferior piece and an axial film was inserted in between the two pieces. Radiochromic films were pinpricked on the outer parameters to allow for film registration. At the insert's center, eight double-loaded TLD capsules were placed into the insert. Half of the TLDs were inserted into the inferior portion and, the other half were inserted in the same position on the superior piece.
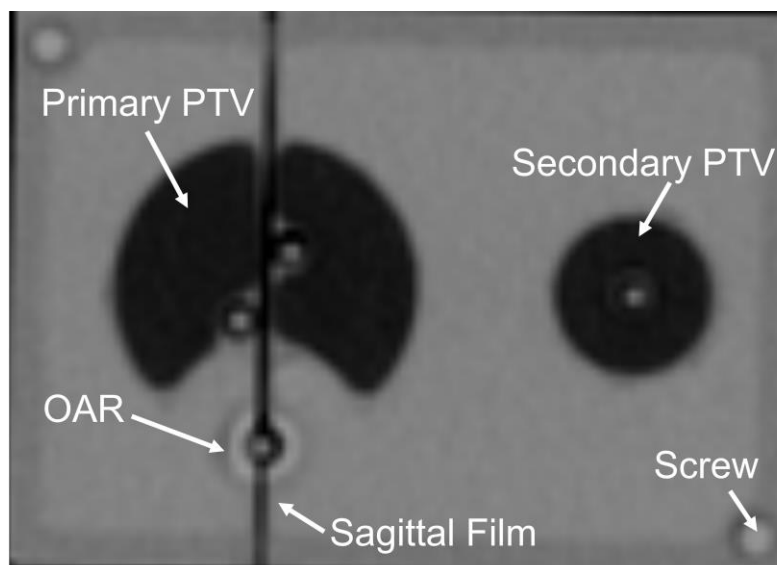
Figure 24: A CT image of the MRgRT H&N insert.

Clear Ballistic Gel #20 (Clear Ballistics, Fort Smith, Arkansas, USA) was used to create the PTV structures. The primary and secondary PTV had dimensions of 5.0 cm in length and had diameters of 4.0 cm and 2.0 cm, respectively. The primary and secondary PTV held a total of four and two TLDs, respectively. The primary PTV had TLDs located anteriorly and posteriorly from the center whereas TLDs were held in the center of the secondary PTV. The OAR was constructed using acrylic (Professional Plastics, Fullerton, California, USA) which extended 13 cm in length and was 1 cm in diameter. The OAR held a total of two TLDs. Each TLD was located in the center of the spinal cord structure in each insert piece. Table 12 summarizes the materials used in each structure as well as the dimension and total TLDs used. All structures were surrounded by melted Superflab which was encapsulated in solid water to create a rigid rectangular structure. Both Superflab and Clear Ballistic Gel #20 were melted at, respectively, 121.1°C and 148.9°C then poured into a solid water mold. The molds were moved to a vacuum chamber until the melted materials had solidified at room temperature.

Structure	Material	Diameter (cm)	Length (cm)	Total TLDs Used[*]
Primary PTV	Clear Ballistic Gel #20[a]	4	5	4
Secondary PTV	Clear Ballistic Gel #20[a]	2	5	2
OAR	Acrylic[b]	1	13	2

a: Clear Ballistics, Fort Smith, Arkansas, USA, b: Professional Plastics, Fullerton, California, USA,

Table 12: The materials used to manufacture a MRgRT H&N insert, dimensions of each and total number of TLD used in each structure (*half of the TLDs were inserted into the inferior part and the other half inserted into the superior part of the MRgRT H&N insert).

4.3.2 Phantom Imaging

The MRgRT H&N phantom was imaged on a CT simulator, MRIdian ^{60}Co, and Unity system. The phantom was first scanned using a brain protocol on a GE Lightspeed CT simulator (General Electric Company, New York, New York, USA) with scanning parameters of: DFOV= 500.0 mm, 120 kVp, 275 mA, and slice thickness=3mm. ViewRay's 0.35T MRIdian ^{60}Co system captured a single MR image of the MRgRT H&N phantom using a TrueFISP (true fast imaging with steady-state free precession) sequence with scanning parameters of: FA=60°, TR=3.33 ms, TE=1.43 ms, NEX=1. A T1-weighted image was produced from Elekta's 1.5T Unity system and had scanning parameters of: FA=8°, TR=8.0 ms, TE=3.6 ms, ETL=136, NEX=1. Table 13 summarizes the MR scanning parameters on both the MRIdian and Unity systems.

Parameters	MRIdian	Unity
MR Scanning Sequence	True Fast Imaging with Steady-state free Precession (TrueFISP)*	T1-Weighted Gradient
FA	60°	8°
TR (ms)	3.33	8.0
TE (ms)	1.43	3.6
ETL	-	136
NEX	1	1

Table 13: MR images were captured on both MRIdian and Unity systems. The ViewRay system acquired a TRUFI image and the Unity system acquired both T1- weighted and T2-weighted image. * TRUFI and TrueFISP are the same sequence, but under different manufactures have different names.

4.3.3 Dose Prescription

The prescription dose was based on the dosimetric requirements set for IROC-Houston's conventional H&N phantom. The dosimetric criteria is illustrated in Table 14. The primary and secondary PTV prescriptions required at least 95% coverage of 6.6 Gy and 5.4 Gy, respectively. Less than 93% of the prescribed dose, for both PTV sites, received less than 1% of the PTV. The OAR was restricted to receive a maximum dose of 4.5 Gy and the normal tissue structure was restricted to receive less than 110% (i.e., 7.3 Gy) of the prescribed dose.

MRgRT H&N Structure	Dose Prescription
Primary PTV	$D_{95} \geq 6.6$ Gy $D_{99} \geq 6.1$ Gy
Secondary PTV	$D_{95} \geq 5.4$ Gy $D_{99} \geq 5.0$ Gy
OAR	$D_{Max} < 4.5$ Gy
Normal Tissue	$D_{Max} \leq 7.3$ Gy

Table 14: During both reproducibility and feasibility studies, treatment plans were based on the same dose constraints.

4.3.4 Treatment Delivery

Reproducibility and feasibility studies were conducted on the MRgRT H&N phantom. During the reproducibility study, the MRgRT H&N phantom was irradiated three times on a single Unity system and then sent out to three other MRgRT sites to conduct a multi-institutional feasibility study. During this miniature feasibility study the phantom was irradiated using two different MRIdian ^{60}Co systems and irradiated once on an MRIdian Linac system. The MRgRT H&N phantom was evaluated based on an end-to-end test for both reproducibility and feasibility studies using the TLD and EBT3 radiation dosimeters.

TLDs were read in-house using the same method as IROC-Houston's off-site auditing program[42]. Double-loaded TLDs (ThermoFisher Scientific, Waltham, Massachusetts, USA) were used as an absolute dosimeter and were read two weeks from irradiation date to account for fading. The exact amount of lithium fluoride power inside a double-loaded TLD capsule was weighed using a Mettler AT261 DeltaRange (Mettler Toledo, Greifensee, Switzerland) scale and light output was measured using the Harshaw M3500 TLD reader (ThermoFisher Scientific, Waltham, Massachusetts, USA). The optical density from the irradiated film was read using a photoelectron CCD microdensitometer (Photoelectron Corporation, North Billerica, Massachusetts, USA). The measured intensity read on the CCD microdensitometer was converted to dose and was post processed using an in-house MATLAB software (The MathWorks, Inc., Natick, Massachusetts, USA).

Treatment delivery was compared to the expected TPS and was analyzed by two methods. These methods included: 1) comparing the reported to measured dose for each

TLD location, 2) performing gamma analysis on axial and sagittal films and generating dose profiles for each orientation.

4.3.4.1 **Reproducibility Study**

The phantom was filled with water and imaged on a GE Lightspeed CT simulator using a brain protocol with parameters of: DFOV=500.0 mm, 120 kVp, 275 mA, and slice thickness=3mm. The CT image was transferred to Monaco TPS (Elekta, Crawley, United Kingdom) where TLDs, OAR, and PTVs were contoured and an IMRT plan created. The IMRT treatment plan used nine gantry angles and used IMRT constraints similar to Tonigan's thesis using a median complexity treatment plan[85].

The MRgRT H&N phantom was positioned on the Unity system's couch and a uniform foam coil was placed above the phantom. Figure 25 displays the treatment setup used for the reproducibility study. Once the phantom was positioned on the couch, the phantom was moved into the gantry. During each irradiation the phantom captured a T1-weighted MR image (with scanning parameters of: FA=8°, TR=8.0 ms, TE=3.6 ms, ETL=136, NEX=1). The MR image was fused to the CT image using Monaco's automatic image fusion tool. The fused image data set was used to re-optimize the dose distribution based on the phantom's current position. The adjusted plan was accepted and was used to treat the MRgRT H&N phantom. The maximum, minimum and mean dose were recorded on all TLD locations. For each irradiation, the treatment took around 35 minutes and reloading the phantom with new detectors took around 15 minutes. The MRgRT H&N treatment plan used to compare the treatment plan to the measured dose was exported from a universal memory thumb drive.

Figure 25: The MRgRT H&N setup at MD Anderson's Unity System. The MRgRT H&N phantom was secured in place with blue tape and a white foam coil was fastened above the phantom. The coil was used to capture an MR image and remained on during the irradiation. It should be noted that the coil was lowered close to the phantom's surface but did not directly contact the phantom.

4.3.4.2 Feasibility Study

The MRgRT H&N phantom was used to conduct a multi-institutional feasibility study. During this feasibility study, the phantom was irradiated on either an MRIdian ^{60}Co or an MRIdian Linac system. Each institution received detailed instructions which helped to create uniformity between the participating institutions. These instructions required the institutions to: 1) prepare the phantom for imaging and treatment (i.e., fill the hollow phantom with tap water and place the insert into the phantom), 2) capture a CT simulated image, 3) design an IMRT treatment plan, 4) verify treatment setup by capturing an on-board MR image and 5) deliver the expected IMRT treatment plan. Each institution was also instructed to contour the TLD capsules and record the TLD's expected minimum, maximum

and mean doses. The digital treatment plan data was sent to IROC-Houston, where the institution's treatment delivery was evaluated.

4.4   RESULTS

4.4.1   Phantom Imaging

As shown in Figure 26, the MRgRT H&N phantom was imaged using a GE CT simulator, Unity and MRIdian MRgRT system. All three images in Figure 26 clearly display distinguishable internal structures. This ability to see contrast between the disease site and surrounding tissue allows institutions to real-time visualize the phantom during treatment. The insert's rigid exterior and OAR are made of solid water and acrylic, respectively. These materials lack hydrogen content and appear black on the MR image. The OAR is visualized through the contrast between the absences of signal surrounded by MR-visible surrounding tissue. In comparison to the MRIdian ^{60}Co system, the Unity system captures a higher spatial resolution image. MRgRT systems show different contrasts within the insert. These variations in contrast and spatial resolution are attributed to the different MR scanning sequences and magnetic fields, respectively. A T1-weighted imaging sequence was applied to the 1.5T Unity system whereas a TrueFISP sequence was applied to the 0.35T MRIdian system. The MR image from the Unity system captures greater susceptibility artifacts compared to the MRIdian image.

| GE CT Simulator | Elekta/Philips Unity | ViewRay MRIdian |
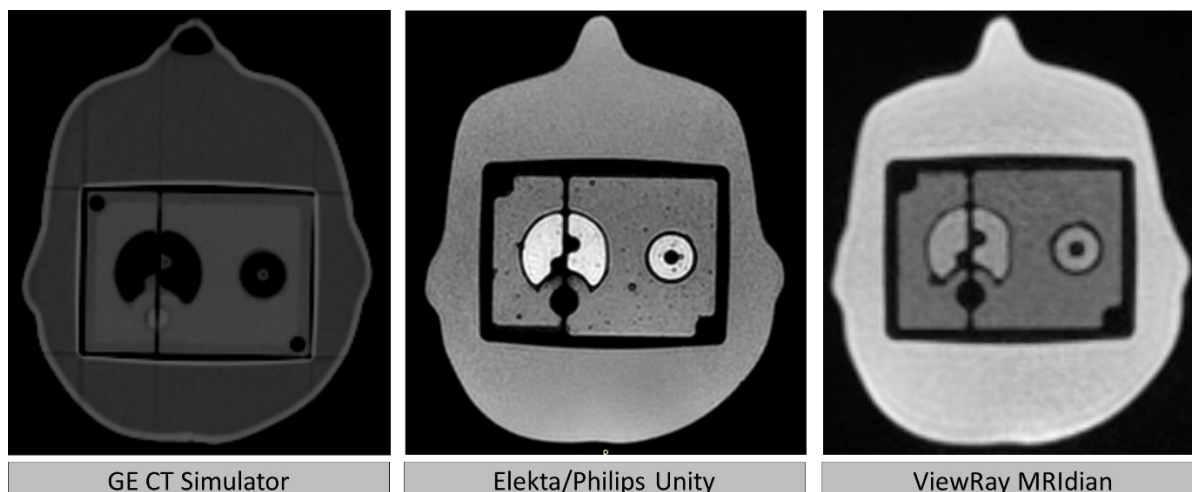
Figure 26: The MRgRT H&N phantom was filled with water and scanned on: (a) GE CT simulator, (b) Unity system's 1.5T MRI with a T1 sequence and (c) ViewRay's MRIdian Co-60 0.35T system with a TRUFI sequence. All images clearly show the OAR, primary and secondary PTV.

4.4.2   Treatment Delivery

Measured TLD readings were compared to the TPS. Ratios between measured TLD dose to reported dose are shown in

Table 15 and

Table 16 for the commissioning and feasibility study, respectively. TLDs that fall within 7% (i.e. 0.93 to 1.07) of the reported dose were considered to be within IROC's acceptance criteria. For the commissioning study, the average ratio between measured and reported values for the primary PTV's superior anterior, inferior anterior, superior posterior, and inferior posterior TLD locations were: 0.98, 0.96, 0.94, 0.96 and for the secondary PTV's superior and inferior were: 0.96 and 0.96, respectively. The first row in Table 15 and Table 16 displays the average results in the reproducibility study. The average ratios between measured TLD and reported doses in the feasibility study were: 1.00, 0.99, 0.98, and 0.99 for the primary PTV's superior anterior, inferior anterior, superior posterior and inferior posterior locations, respectively. For both studies, the

ratios between measured TLD readings to treatment planning readings were all within

IROC's acceptable criteria region.

TLD Location	Reproducibility Test			Average	Coefficient of variance
	Unity 1-a	Unity 1-b	Unity 1-c		
PTV Sup. Anterior	0.97	0.98	0.98	0.98	0.7%
PTV Inf. Anterior	0.97	0.95	0.96	0.96	1.5%
PTV Sup. Posterior	0.94	0.94	0.94	0.94	0.4%
PTV Inf. Posterior	0.94	0.95	0.94	0.95	0.9%
Secondary PTV: Sup.	0.97	0.95	0.96	0.96	1.1%
Secondary PTV: Inf.	0.96	0.95	0.96	0.96	0.4%

Table 15: Reproducibility results of four TLD positions in the Primary PTV. The left column represents TLD locations for the doses calculated from Monaco's treatment planning software. The middle three columns represent the average TLD measured for each location. The average ratios between measured and calculated dose and the coefficient of variance are displayed in the right column. The TLD measurements were all within 6% of the reported TLD dose.

Institution	Energy	Superior Anterior	Inferior Anterior	Superior Posterior	Inferior Posterior
Unity 1	7 MV	0.98	0.96	0.94	0.95
ViewRay 2	6 MV	1.01	1.01	1.02	1
ViewRay 3	Co-60	1.03	1.03	1.02	1.01
ViewRay 4	Co-60	0.98	0.97	0.95	0.99
Average	--	1.00	0.99	0.98	0.99

Table 16: Feasibility study results for four TLD positions in the primary PTV. Results are the ratio between measured TLD dose and reported dose from the treatment planning software.

Axial and sagittal films were evaluated using a gamma analysis[86]. Films were

said to pass if more than 85% of the pixels passed a 7%/4mm criterion. Table 17 and

Table 18 display the percentage of pixels passing the gamma criterion for axial and

sagittal film planes in the reproducibility and feasibility study, respectively. The

commissioning study's three irradiations had individual passing rates of 96.4%, 98.1%,

and 99.1% for axial films and 89.9%, 89.9% and 89.2% for sagittal films. The average

percent of pixels passing in the reproducibility study were 97.8% and 89.7% for axial and sagittal film planes, respectively. For the three feasibility study irradiations on the MRIdian units, the axial film had individual passing rates of: 97.8%, 97.6%, and 96.7%, and for the sagittal films had respectively passing rates of: 89.7%, 95.7%, and 95.6%. On the feasibility study, all axial and sagittal films passed IROC's gamma criteria with an average pixel passing of 97.6% and 92.3%, respectively. During the gamma analysis three dose profiles were generated in anterior-posterior, left-right, and superior-inferior orientation. The typical dose profiles generated from these studies are shown in Figure 27. From a qualitative perspective, film dose profiles and calculated dose profiles were in excellent agreement with all studies.

Institution	% Pixel Passing [±7%/4mm]	
	Axial	Sagittal
Unity 1-a	96.4%	89.9%
Unity 1-b	98.1%	89.9%
Unity 1-c	99.1%	89.2%
Average	97.8%	89.7%

Table 17: The MRgRT H&N phantom was irradiated three times on a 1.5T Unity MR Linac system. Axial and sagittal planes were evaluated based on 7%/4mm gamma criteria.

Institution	Energy	% Pixel Passing [±7%/4mm]	
		Axial	Sagittal
Unity 1	7 MV	97.8%	89.7%
ViewRay 2	6 MV	97.9%	95.7%
ViewRay 3	Co-60	96.7%	96.6%
ViewRay 4[*]	Co-60	-	-
Average	-	97.6%	96.2%

*Table 18: Five different MRgRT systems treatments were evaluated based on the 7% dose and 4mm distance to agreement gamma criteria for both axial and sagittal planes. This table displays the percentage of pixels passing the gamma criteria. *Data unavailable from institution for analysis.*

a. **Institution 3 (MRIdian ^{60}Co): Anterior-Posterior Profile**
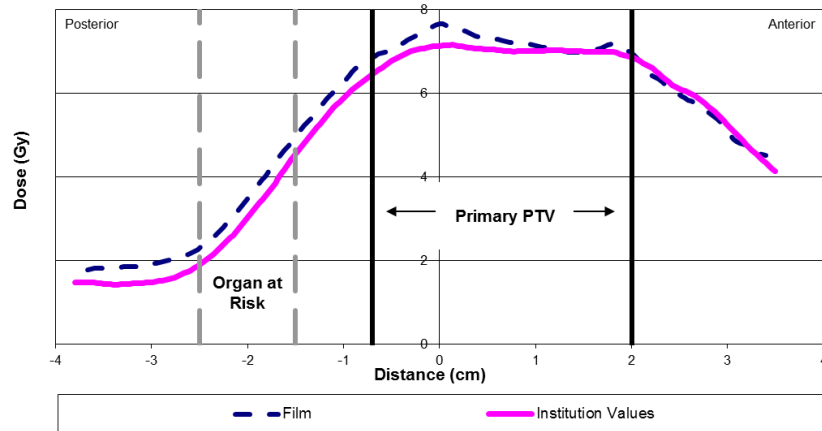
b. **Institution 3 (MRIdian ^{60}Co): Left-Right Profile**
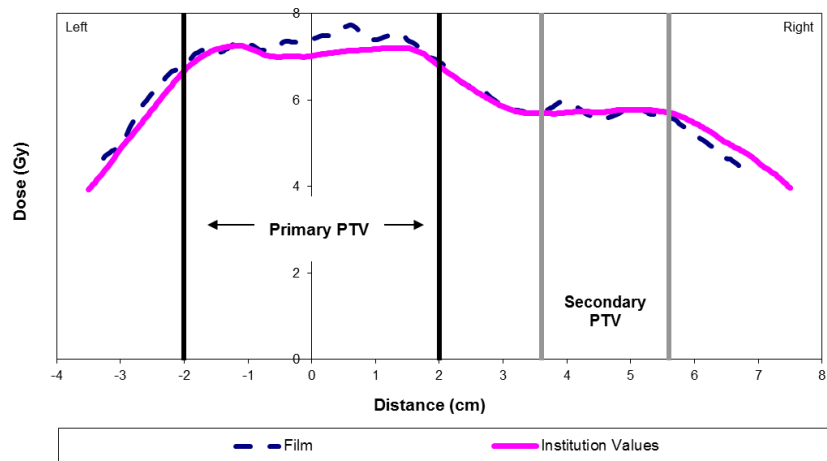
c. **Institution 3 (MRIdian ^{60}Co): Superior-Inferior Profile**
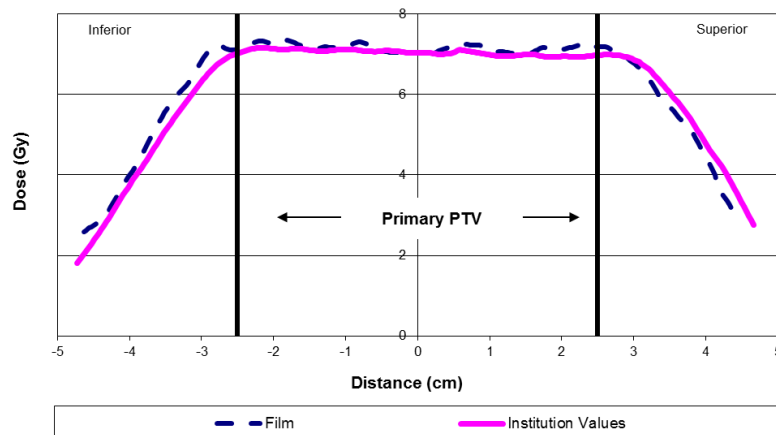
Figure 27: Dose profiles generated in the (a) anterior-posterior, (b) left-right, and (c) superior-inferior direction. These graphs compare dose profiles generated on film to those generated from the treatment planning. These graphs were generated from institution 3, but resemble the typical dose profiles generated from both feasibility and commissioning studies.

4.5 DISCUSSION

The MRgRT H&N phantom was designed as a tool to credential institutions wishing to use an MRgRT system to participate in NCI-sponsored clinical trials. IROC-Houston's conventional phantoms were originally designed for CT-only workflow and constructed of solid materials that were tissue equivalent and visible on CT but were not visible on MR[72]. The lack of MR signal in IROC-Houston's traditional H&N phantom created a solid black MR image and caused internal structures to be indistinguishable. In order to use an H&N phantom in all aspects of the MRgRT treatment workflow, it was critical that the phantom be tissue equivalent and visible in both CT and MR. Having a multi-modality phantom would truly simulate an MRgRT end-to-end workflow. Therefore, IROC-Houston's conventional H&N phantom was an insufficient end-to-end tool for MRgRT systems since it was not MR visible.

Several studies have attempted to manufacture phantoms that are MR and CT compatible, but these do not fit IROC-Houston's requirements. These requirements include: 1) materials must be dosimetric equivalent to tissue, 2) materials must be MR/CT visible, 3) portable radiation dosimeters are easy to install into the insert, 4) phantom insert must be durable, and 5) the phantom requires minimal maintenance (i.e., can be stored at room temperature). Some studies have created H&N phantoms using materials that either had short shelf-lives, required additional additives to prevent micro-organism infestation or required special storage conditions (i.e., refrigerators)[57; 87]. Some studies attempted to construct a dual MR/CT H&N phantom by adding MR visible markers to phantoms that are traditionally used in CT-only workflow[88; 89]. Other MR/CT compatible

H&N phantoms are simplistic and were designed to address different challenges in MR-only workflows[90]. These phantoms were not designed to perform end-to-end tests, but instead they were designed to quantify MR distortion and study the ability to create synthetic electron density from a MR image. Therefore, there is not an end-to-end MRgRT H&N phantom which supports portable dosimeters and have complex multi-contrast internal structures.

The MRgRT H&N insert was constructed from gel-based materials. Gel-based materials, compared to solid materials, were more difficult to manufacture and required extra construction time since these materials could not precisely be sculpted into a complex internal structure. The construction process to create precise structures using gel-based materials included: 1) melting Superflab (121.1 °C) and Clear Ballistic Gel #20 (148.9 °C), 2) pouring melted materials into custom made molds and 3) storing materials in an air-tight vacuum until solidified. The vacuum chamber was used to eliminate air bubbles created during the pouring process and the molds were used to create precise and reproducible structures. To increase rigidity and to sustain shape during rough shipping conditions, solid water was used to encapsulate internal structures and to create an exterior insert shell.

IROC-Houston's conventional phantoms are also equipped with several film pin prick registration locations. The purpose of these small pinpricked areas is to identify the film's location relative to the phantom's location. Film pin pricks are created in IROC-Houston's conventional H&N phantom by inserting a fine needle into a small drilled hole near the internal structures. This method was not feasible in the MRgRT H&N insert since a fine needle could pierce through any direction inside the gel material; thus, creating greater film registration uncertainties. Additionally, piercing a needle through

gel material could damage the internal parts of the insert. To prevent additional uncertainties and increase the insert's longevity, small holes were not created in the gel material. Rather, the insert was designed with wider exterior walls and small holes were drilled into the solid water exterior shell.

IROC-Houston is responsible for ensuring multi-institutions are delivering consistent treatments. One method by which IROC-Houston evaluates this consistency is by sending anthropomorphic phantoms with detail dose prescription instructions to institutions. With the goal of using the MRgRT H&N phantom to examine an institution's ability to deliver radiation consistently among other institutions, it was important that this phantom also use the same instructions and evaluation metrics as IROC-Houston's conventional H&N phantom. During both commissioning and feasibility studies, institutions were required to use a specific dose prescription and to use on-board MR imagers to verify treatment setup. Additionally, IROC-Houston allowed institutions to use other MR workflow components as needed. Thus, institutions were free to incorporate MR-based treatment planning and real-time MR image guidance. While most institutions used CT-only to create an IMRT plan, one institution (ViewRay 4) chose to use the electron density captured on a CT image and then plan based on the MR image.

Unlike MRIdian systems, the Unity system was not equipped with lasers inside the vault. In fact, the Unity system solely relied on capturing an MR image to account for any setup discrepancies between each irradiation. Part of the Unity system's workflow required a re-optimization based on the current setup position. The commissioning test encompassed all parts of the workflow including MR setup verification methods. During each irradiation the treatment couch was moved outside the bore and the insert was removed from the phantom to load new unirradiated detectors

into the insert. Once unirradiated TLDs and film sheets were reloaded into the phantom, the H&N insert was screwed into the phantom and the treatment couch was moved back inside the bore. During this process, the phantom could have been moved in a slightly different position due to the couch movement and the insert's re-installation into the phantom. There were no lasers to verify whether the phantom was in the same position as the previous irradiation. To account for any movement, MR images were acquired before each irradiation and the treatment plan was re-optimized accordingly.

Each step in the radiation treatment process will have associated uncertainties. Since MRgRT systems have different workflows than conventional linear accelerators, they will also have different associated uncertainties. Some of the various sources of uncertainties could arise from: 1) MR/CT image fusion, 2) potential minor dosimetric effects on TLDs from an MR environment, 3) linear accelerator output consistency 4) MR geometrical accuracy and 5) re-optimization differences. While the major purpose of these studies was not to quantify the source of uncertainties, these studies were used to evaluate an institution's performance based on the entire treatment process. If an institution failed IROC-Houston's passing criterion then it was that institution's responsibility to further investigate the source of errors and implement new protocols to mitigate uncertainties from those components. Even with various uncertainties, the gamma results from them MRgRT H&N phantom demonstrated that those uncertainties played a minimal role in the overall dose delivery. These studies also demonstrated that the Unity, MRIdian ^{60}Co, and MRIdian Linac systems have the ability to consistently deliver IMRT treatments.

4.6   CONCLUSION

NCI sponsored clinical trials will further investigate the impact of using MRgRT systems for various disease sites including cancers in the H&N region. The MRgRT H&N phantom was designed to credential institutions wishing to use IMRT techniques with MRgRT systems. This phantom was designed to be used in all aspects of MRgRT treatment workflows in that it was constructed using tissue equivalent materials which could be visualized in 0.35T-1.5T MR imagers, and CT imagers. Commissioning and feasibility studies showed high reproducibility and agreement between all MRgRT systems, thus, indicating that the MRgRT H&N phantom would be a useful metric in credentialing institutions participating in NCI clinical trials. Additionally, the end-to-end test demonstrated that the Unity, MRIdian ^{60}Co, and MRIdian Linac systems workflows could deliver comparable advanced IMRT treatments in the H&N region.

Chapter 5:   MRgRT Thorax QA Phantom: Design, Construction and Feasibility Study

A substantial portion of this chapter is written or based on the following publication:

A.Steinmann, P Alvarez, H Lee, R. Stafford, L. Court, Z. Wen, G. Sawakuchi, D. Fuller, D. Followill, "MRgRT Thorax Anthropomorphic QA Phantom: Design, Development, Commissioning and Feasibility Study," *Medical Physics.* [In review] (2018). © John Wiley and Sons.

The permission for reuse of this material was obtained from John Wiley and Sons.

5.1   ABSTRACT

Purpose: To design, manufacture and evaluate a dynamic MRI/CT compatible anthropomorphic thorax phantom used to credential MR guided radiotherapy (MRgRT) systems participating in NCI-sponsored clinical trials.

Method: The anthropomorphic thorax phantom was constructed from a water-fillable acrylic shell that contained several internal structures representing radiation sensitive organs within the thoracic region. A custom MR/CT visible cylindrical insert was designed to simulate the left lung with a centrally located tumor target. The surrounding lung tissue was constructed from a heterogeneous in-house mixture using petroleum jelly and miniature (2-4mm diameter) styrofoam balls and the tumor structure was manufactured from liquid PVC plastic. An MR conditional pneumatic system was developed to allow the MRgRT insert to move in similar inhale/exhale motions. TLDs and radiochromic EBT3 film were inserted into the phantom to measure absolute point doses and dose distributions, respectively.

The MRgRT thorax phantom was evaluated through a commissioning study and a feasibility study. Comprehensive end-to-end examinations were done where the

phantom was imaged on a CT, an IMRT treatment plan was created and an MR image was captured to verify treatment setup. Then, the phantom was treated on an MRgRT system. The commissioning study evaluated the phantom's reproducibility ease by irradiating three times on an Elekta's 1.5T Unity system. The phantom was shipped to three independent institutions and was irradiated on either an MRIdian cobalt-60 (^{60}Co) or an MRIdian linear accelerator system. Treatment evaluations used TLDs and radiochromic film to compare the planned treatment reported on the treatment planning software against the measured dose on the dosimeters.

Results: The commissioning of the phantom on the Unity system resulted in reproducible TLD doses (SD < 1.5%). The measured TLD to calculated dose ratios from the commissioning and feasibility studies ranged from 0.93 to 1.01 and 0.96 to 1.03, respectively. Using a 7%/5mm gamma analysis criteria, the commissioning and feasibility studies resulted in an average passing rate of 93.3% and 96.8%, respectively. No difference was noted in the results between the MRIdian ^{60}Co and 6 MV delivery to the phantom and all treatment evaluations were within IROC-Houston's acceptable criterion.

Conclusions: The motion enabled anthropomorphic MRgRT thorax phantom, CT/MR visible and tissue equivalent, was constructed to simulate a lung cancer patient and was evaluated as an appropriate NIH credentialing tool used for MRgRT systems.

5.2   INTRODUCTION

Magnetic resonance (MR) guided radiotherapy (MRgRT) systems integrate MR imagers with either a radioactive ^{60}Co source or a linear accelerator. Within the United States there are three different MRgRT clinical models, which include the MRIdian ^{60}Co (ViewRay, Oakwood Village, Ohio), the MRIdian Linac (ViewRay, Oakwood Village, Ohio), and the Unity (Elekta, Crawley, United Kingdom and Philips, Amsterdam, Netherlands) [10-13]. All of these MRgRT systems are equipped with an on-board MR imager which has a magnetic field ranging from 0.35T to 1.5T. The MRIdian ^{60}Co system was the first system to treat patients in the United States and is equipped with three ^{60}Co head sources that are centrally located between a split 0.35T superconducting magnet. The MRIdian Linac is an upgraded prototype of the MRIdian ^{60}Co system and is equipped with a single 6 MV linear accelerator in between a 0.35T split magnet. The Unity system is equipped with a single 7 MV linear accelerator mounted above a modified 1.5T magnet.

MRgRT systems utilizing on-board MR imagers during treatment could potentially revolutionize radiation therapy. Some of the most promising advancements are: gating, target tracking and online adapted radiotherapy (ART) techniques[80; 81; 91]. Inherently, MR imagers do not contribute to patient dose. This means a patient's tumor could be tracked during the entire treatment through a series of cine MR images without increasing the patient's absorbed dose. If a target structure moves outside a desired treatment boundary, the MRgRT system can theoretically recognize this variation and momentarily stop delivering radiation until the target moved backed into the desire location[91]. MR gating techniques would most benefit tumor sites located on anatomical structures that regularly move (i.e., lungs, pancreases, GI track). In addition to tumor

tracking, these MRgRT systems could potentially perform online ART by capturing an MR image prior to every treatment and recalculating a new treatment plan based on the disease site's response to radiation, location, and size. Online ART and MR-based tracking could help create even more patient-specific radiation treatments by modifying tumor margins before every treatment. As a result, these techniques can potentially improve local tumor control and reduce normal tissue toxicity.

Clinical outcomes and applications are still being explored since the first MRgRT system to treat a patient in the United States was in 2014[92]. To preliminarily address MRgRT safety concerns, the National Institutes of Health (NIH) has sponsored two clinical trials that focused on the safety aspects of capturing MR images (NCT02973828) and delivering radiation (NCT03284619). With on-board MR imagers having the potential to use MR cine images to track tumors, NIH has also sponsored several short-term single institutional studies that permit MRgRT systems to track and treat moving disease sites located on either a liver (NCT02683200) or a lung (NCT02264886) structure. NIH has also sponsored several limited clinical trials that used online ART techniques. Much of these clinical trials focused on disease sites located on either lung (NCT02264886/ NCT02950792) or breast (NCT01999062) anatomical structures. Many of NIH sponsored clinical trials have used tumors located in the thorax region to understand the potential applications of MRgRT systems. Larger multi-institutional National Clinical Trial Networks (NCTN) will be sponsored by the NIH to further investigate the clinical uses and outcomes of treating lung tumors on an MRgRT system.

Institutions participating in multi-institutional clinical trials must cohesively deliver the same treatment protocol as other participating institutions on the trial. NIH requires each institution to first participate in a credentialing process to demonstrate its

ability to consistently deliver intensity modulated radiation therapy (IMRT) using a strict treatment protocol. NIH has funded the Imaging and Radiation Oncology Core Quality Assurance (QA) center in Houston (IROC-Houston) to credential all institutions wishing to participate in NCTN clinical trials. During the credentialing process, IROC-Houston ships out a standardized anthropomorphic phantom and requires the institution to follow a standard treatment protocol that is provided by IROC-Houston. These instructions require the institution to capture a CT simulation, create an individual treatment plan and deliver radiation to the phantom. IROC-Houston will then evaluate the institution's end-to-end performance by comparing the treatment plan to the dose delivered on the phantom.

IROC-Houston has an assortment of site-specific anthropomorphic phantoms. Depending on the clinical trial, IROC-Houston will ship either a head and neck (H&N), thorax, spine, liver, or prostate anthropomorphic phantom to an institution for an off-site credentialing test. IROC-Houston's conventional thorax phantom is the second most common phantom used to credential institutions and is described in detail by Followill et al. 2007[59]. In short, the conventional thorax phantom is a water-fillable shell that contains several internal structures. Inside the thorax-shape external shell, the phantom is equipped with two lungs manufactured of compressed cork, an acrylic spinal cord and a nylon heart. The left ipsilateral lung was designed as an attachable insert that can connect to a motion table. The insert movement simulates patient breathing by regularly moving every three seconds. The conventional lung insert was designed with a single tumor manufactured from high impact polystyrene (HIPS) and was centrally located around surrounding lung mimicking tissue that was manufactured from compressed cork.

Integrating an MR imager with a radiotherapy system will inherently change the overall workflow. As described in the Steinmann et al. study, IROC-Houston's conventional thorax phantom was constructed with hydrogen deficient materials[72]. The lack of hydrogen creates a lack of MR signal between the tumor and surrounding tissue materials, thus, causing the two structures to be indistinguishable in a MR image. Additionally, the motion table used to simulate patient breathing is MR unsafe since it contains ferromagnetic materials. If the motion table is placed too close to the MR system, the ferromagnetic materials would become magnetized and would dangerously project into the MR system. If the motion table's rotary motor was positioned far away from the magnetic field (i.e., past the 5 G line) and was turned on, it would still affect the MR components since the induced magnet field would interfere with the acquired signal and distort the MR image. Therefore, IROC-Houston's conventional thorax phantom and motion table are completely inadequate for use in MR environments and a new MRgRT thorax phantom and motion system must be developed for MRgRT workflows so that they are safe to use in an MR system and all of their internal structures are distinguishable.

Current studies have attempted to manufacture MR/CT compatible thorax phantoms, but they do not fit IROC-Houston's off site anthropomorphic phantom requirements. IROC-Houston's phantoms must contain multiple internal structures (i.e., tumor, heart, contralateral lung, spinal cord) and use passive dosimeters. Specifically, for MRgRT workflows, the phantom materials also must be MR/CT visible, tissue equivalent, durable, and they must require minimal maintenance and storage conditions[57; 87]. To the author's knowledge, there are only three MR/CT compatible thorax phantom designs that use synthetic materials. The MRI-LINAC Dynamic thorax phantom (CIRS,

Norfolk, Virginia, USA) contains two sections: the superior part is a grid used to quantify MR geometrical distortions and the inferior part attempts to create a very simplistic phantom with a moving target. The inferior portion of the phantom has a single cylindrical-shape air cavity which is not a realistic simulation of a lung with a moving MR target. This phantom does not anatomically represent the thorax since it does not contain critical organs (i.e., spinal cord, heart, and contralateral lung). The target is attached to a rigid extended shaft that is connected to a stepper motor. The stepper motor itself contains ferromagnetic materials and is considered MR unsafe. If this stepper motor is placed too close to the bore, it could become magnetized and dangerously project into the MRgRT system. Therefore, this phantom is not ideal for IROC-Houston since it does not contain multiple internal structures and the motor is MR unsafe.

The other two MR/CT compatible thorax phantoms, which used synthetic materials, are similarly designed and contain a water-fillable acrylic shell with limited internal structures. The PET/MRI/CT Compatible Respiratory Tumour Motion Phantom (CRTMP) (Shelley Medical Imaging Technologies, London, Ontario, Canada) consist of two equally spaced cylindrical air cavities representing lungs and a fillable cylinder representing a spinal cord. Inside one of the air cavities is a fillable spherical tumor that connects to an MR safe motor. The QUASAR™ MRI[4D] motion phantom consists of two asymmetric cylindrical inserts and was not designed with other important critical structures (i.e., heart or spinal cord). Additionally, the QUASAR™ MRI[4D] phantom does not anatomically represent two lungs since the created air cavities are adjacent to each other with little separation. The center air cavity is equipped with a fillable spherical tumor that connects to an MR safe motor. Both CRTMP and QUASAR™ MRI[4D] phantoms are similarly designed with a customizable insert that mimics tumor motion

with an MR safe ceramic piezoelectric motor. These phantoms only show a single contrast (i.e., absent signal vs. water signal) in an MR image. While MR contrast agents (i.e., gadolinium) could be used to add additional contrast, the contrast has a high atomic number and would not dosimetrically resemble tissue. These phantoms did not meet IROC-Houston's requirements since they lack organ at risk (OAR) structures and are not equipped with portable dosimeters.

The aim of this study was to design, manufacture, and evaluate an MR/CT compatible, dynamic anthropomorphic thorax phantom used as an end-to-end test for MRgRT systems.

5.3   MATERIAL AND METHODS

The MRgRT thorax phantom and motion system were designed to meet IROC-Houston's radiotherapy, diagnostic imaging and practicality criteria. To meet radiotherapy and diagnostic criterion, materials used in the phantom were selected based on their ability to structurally represent human anatomy, be visible in both MR and CT images and be tissue equivalent. Practicality criteria were met in the phantom by selecting materials that maintained constant shape, required minimal maintenance, and were made with synthetic materials that did not require additives. For the practicality criteria of the motion systems, the motion parts used in the treatment vault needed to be MR safe and easily connect to the thorax phantom. Once designed and manufactured, the MRgRT thorax system was reproduced on a single Unity system and sent out to three institutions for a miniature multi-institutional feasibility study.

5.3.1 *Phantom Design*

All internal structures in the conventional thorax phantom, except the ipsilateral lung and tumor, were distinguishable in an MR image since the MR signal from water outlined their shapes. IROC-Houston's conventional thorax phantom was modified so that the entire thorax phantom could be used in an MRgRT workflow. These modifications included: 1) a new MRgRT lung insert and 2) an MR safe motion system.

The MRgRT thorax phantom was designed to resemble closely human anatomy by constructing several shapes to represent internal structures and to mimic IROC-Houston's current photon thorax phantom. The thorax phantom was manufactured with an external water-fillable PVC shell (The Phantom Laboratory, Salem, New York, USA) and contained four internal structures which geometrically represented a spinal cord, a heart and two lungs. The right contralateral lung, spinal cord and heart were immobile structures whereas the left ipsilateral lung was designed to connect to a motion system so that it could simulate patient breathing. A platform with a 15 degree inclination was connected to the exterior shell to create anterior-posterior and superior-inferior motion. Figure 28 displays the MRgRT thorax phantom compartments which include: the exterior phantom, the 15-degree platform, the attachable ipsilateral lung insert's shell and the four individual lung pieces.

Figure 28: The MRgRT Thorax Phantom. The phantom consists of a water-fillable anthropomorphic thoracic shell, an inclining 15-degree platform and an external insert shell that holds four individual MR/CT compatible insert pieces.
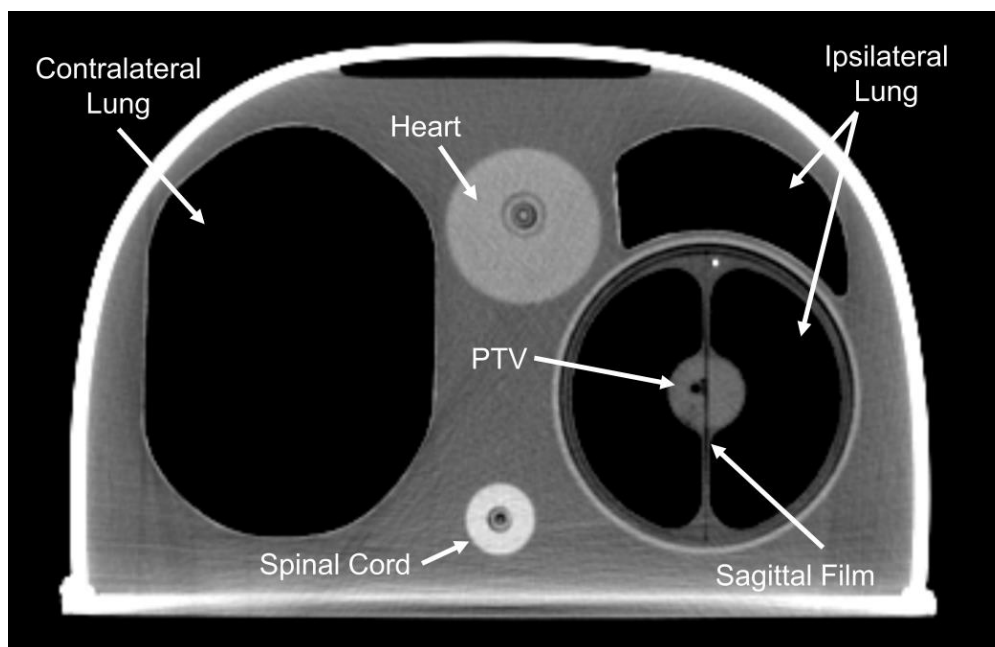
Figure 29: A CT image of the center of an MRgRT thorax phantom. Inside the acrylic shell are a contralateral lung, an ipsilateral lung, a heart, and a spinal cord structure. The PTV is located at the center of the ipsilateral lung. Sagittal and axial radiochromic films are inserted into the ipsilateral lung. Each heart and spinal cord structure holds a single TLD and the PTV holds two (superior and inferior) TLDs.

The OAR structures were manufactured using acrylic, nylon, and compressed cork for the spinal cord, heart and contralateral lung structures, respectively. The heart and spinal cord were each designed to hold a double-loaded TLD. The materials used in the MRgRT lung insert were selected from the Steinmann et al. 2018 study[72]. The ipsilateral lung had an outer diameter of 12.5 cm and a length of 19 cm and was constructed with an in-house heterogeneous mixture of 8.3% wt. of 2-4 mm styrofoam balls and 91.7% wt. of petroleum jelly. The in-house heterogeneous mixture was encapsulated in high impact polystyrene (HIPS). Centrally located in the lung insert was a prolate spheroid which represented the tumor and had a major and minor diameter of 10 cm and 5 cm, respectively. The tumor was constructed with 100% liquid PVC plastic that was encapsulated with solid water and held two double-loaded TLDs. Table 19 summarizes the internal structures' materials, dimensions, and total TLD used and Figure 29 displays an axial CT image of the internal structures.

The MRgRT lung insert was composed of four individual pieces which combined into a single unit when a HIPS shell was used to secure the pieces in place. Alignment notches were built into the individual lung pieces and the HIPS lid to create a unique reproducible orientation. The HIPS lid was also constructed with an aluminum rod which was designed to connect to part of the pneumatic system and not interfere with the target's dose delivery. The MRgRT lung insert allowed radiochromic films and TLDs to be inserted centrally to the tumor. A total of three radiochromic films were installed into the MRgRT lung insert. Two radiochromic films captured the sagittal plane by placing each film at the superior and inferior parts of the insert. A single film was placed in between

the sagittal planes to capture an axial plane. Double-loaded TLDs were installed at the centers of the superior and inferior pieces.

Structure	Material	Diameter (cm)	Length (cm)	Total TLDs Used
Primary PTV	100% Liquid PVC Plastic[a]	4	5	2[*]
Ipsilateral Lung	In-house Petroleum Jelly[b] Styrofoam ball[c] mixture[‡]	12.5	18	-
Contralateral Lung	Compressed Cork[d]	12.5	18	-
OAR: Spinal Cord	Acrylic[e]	1	13	1
OAR: Heart	Nylon[d]	8	-	1

a: M-F Manufacturing Company, Fort Worth, Texas, b: Sonneborn, Parsippany, New Jersey, USA c: Steve Spangler Science Styrofoam Beads, Englewood, Colorado, USA, d: McMaster-Carr, Elmhurst, Illinois, USA, e: Professional Plastics, Fullerton, California, USA
‡:In-house mixture that used 8.3% weight of Styrofoam balls and 91.7% weight of petroleum jelly.
*: One TLD was inserted in the superior piece and the other TLD was inserted into the inferior piece.

Table 19: The materials used to manufacture the MRgRT thorax phantom.

5.3.2 Pneumatic Motion System Design

IROC-Houston's conventional photon lung phantom is moved physically to mimic breathing patterns by attaching a programmable stepper motor/bi-slider system to a motion platform on which the phantom rests. The stepper motor system components are classified as MR unsafe materials since they contain ferromagnetic materials. A pneumatic system was designed as an alternative way to represent breathing motion inside an MR environment. The schematic of the pneumatic system used for the MRgRT thorax phantom is shown in Figure 30. A compacted 1.5 L air compressor (Model#: D55140, DeWalt, Baltimore, Maryland, USA) was used to constantly supply air to a 3-way valve (Part#: S20U30-SS-11-2, Bimba, University Park, Illinois, USA) which was manually controlled through a physical on/off electric switch (Model#: R62-02653-02W, Leviton, Melville, New York, USA). When the electric switch was positioned off, the 3-

way valve would naturally release air to the exhaust pipe. If the electric switch was flipped on, the 3-way valve would electrically close the exhaust pipe port and open the 4-way valve port (Part#: N2-SCD-120-VAC, Bimba, University Park, Illinois, USA). When the port was open, the 4-way valve supplied air to the cylinder which physically moved the MRgRT lung insert. Additionally, the red and blue plastic nylon tubing (Part# 4HHC8, Granger, Lake Forest, Illinois, USA) attached to the 4-way valve were used to control the air flow supply on the cylinder. The blue tubing represented expiration whereas the red tubing represented inspiration. An electrical time delay counter (Model# IO23B01, Ebay Item# 232013288409, Ebay, San Jose, California, USA) was used to regulate the 4-way valve air flow direction. This 110V timer was programmed to fluctuate the air supply between the inhale (red) and exhale (blue) tubing every three seconds. Both exhale and inhale tubing were connected to a flow control knob (Part#: RAFK-2x2, Bimba, University Park, Illinois, USA). The knobs were used to manually control the speed at which the lung insert would move by adjusting the air flow pressure. The inhale (red) and exhale (blue) plastic tubing were connected to an MR safe cylinder (Part#: FOD-040.8-ABBMT, Bimba, University Park, Illinois, USA). The cylinder was modified with a custom brass piston to make it MR safe and was specially designed to connect to the HIPS lid. The piston physically moved the lung insert according to the air flow direction. When the red tubing supplied pressurized air, the piston would extend and cause the lung insert to move inferiorly. Vice versa, the piston would contract and move the lung insert superiorly when the blue tubing supplied pressurized air.

As illustrated in Figure 30, the equipment used in the pneumatic system was divided into two broad sections: MR safe and MR unsafe parts. The MR safe parts could be used inside the MRgRT treatment vault and included: the cylinder, the piston, the lung

insert and the plastic tubing. MR unsafe materials were required to stay outside the vault

and these parts were: the compressor, the 3-way valve, and the 4-way valve. The red and

blue plastic tubing were placed through the MR waveguide; thereby creating a physical

wall barrier between MR safe and MR unsafe parts of the pneumatic system. The cylinder

was screwed directly into the MRgRT thorax phantom and during treatment was placed

at the center of the bore.
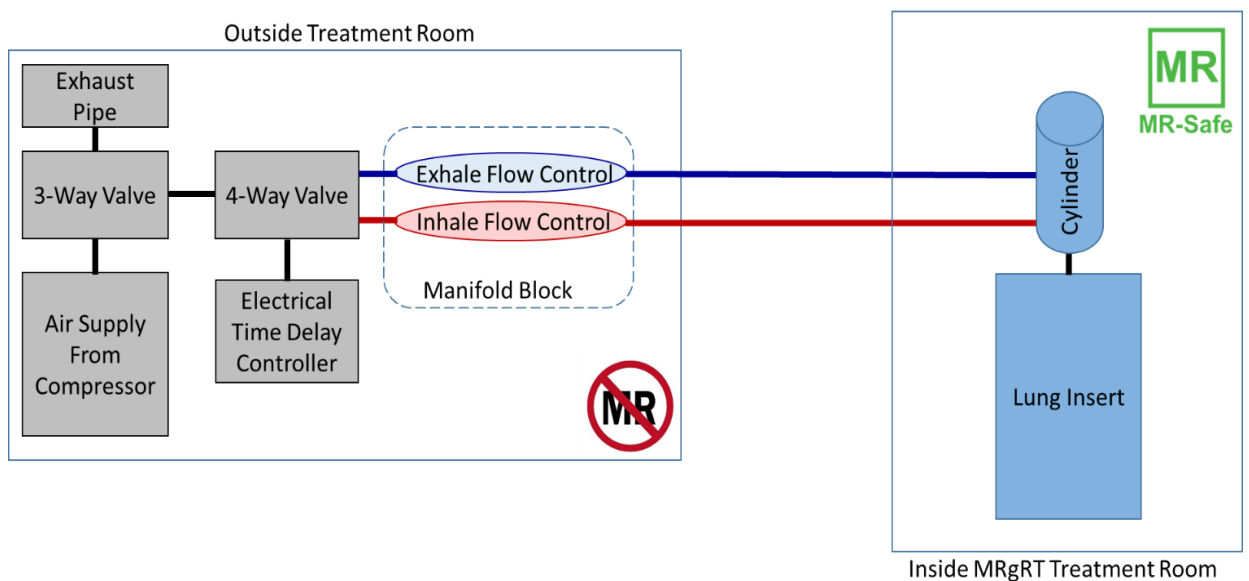
Figure 30: Schematic of the pneumatic system used to mimic lung motion in a MR environment. The pneumatic system was broadly divided into two sections: MR safe and MR unsafe parts. MR safe parts were allowed inside the treatment vault whereas MR unsafe parts were stored outside the treatment room. The MR unsafe parts consisted of the air compressor and parts used to regulate the air flow. The MR safe parts included the plastic air tubing and a custom cylinder. The two tubes were colored red and blue to distinguish the air flow used to move the cylinder's brass piston. The red tubing represented inspiration and blue tubing represented expiration.

5.3.3   Phantom Imaging

The MRgRT thorax phantom was imaged on a CT simulator and two MRgRT

systems using 1.5T and 0.35T magnetic field strengths. Under a GE Lightspeed CT

simulator (General Electric Company, New York, New York, USA), the phantom was

imaged using a breast protocol with scanning parameters of: DFOV= 500.0 mm, 120

kVp, 275 mA, and slice thickness=3mm. The MRgRT thorax phantom was imaged on a

1.5T Unity system using a T1-weighted sequence and had scanning parameters of: FA=

8°, TR= 8.0 ms, TE= 3.6 ms, ETL= 136, NEX=1. Using a 0.35T MRIdian ^{60}Co, the

MRgRT thorax phantom was scanned with a TrueFISP (true fast imaging with steady-

state free precession) sequence and had scanning parameters of: FA= 60°, TR= 3.33 ms,

TE= 1.43 ms, NEX=1. The MR scanning parameters from the Unity and MRIdian

systems are summarized in Table 20.

Parameters	ViewRay	Unity
MR Scanning Sequence	True Fast Imaging with Steady-state free Precession (TrueFISP)	T1-Weighted Gradient
FA	60°	8°
TR (ms)	3.33	8.0
TE (ms)	1.43	3.6
ETL	-	136
NEX	1	1

Table 20: MR images were captured on both the ViewRay and Unity systems. The ViewRay system acquired a true fast imaging with steady-state free precession image and the Unity system acquired a T1- weighted image. *TRUFI and TrueFISP are the same sequences but are under different names for different manufactures.

5.3.4   Dose Prescription

The dose prescriptions set for the MRgRT thorax phantom were the same

prescriptions used for IROC-Houston's conventional thorax phantom. In short, 95% and

99% of the primary tumor volume (PTV) were required to receive at least 6.0 Gy and 5.4

Gy, respectively. Excluding the PTV, 37% of the whole lung (i.e., both left and right

lung) was restricted to receive a maximum of 2.0 Gy. The spinal cord and heart had

maximum received dose limits of 5.0 Gy and 4.0 Gy, respectively. Additional dose

constraints limited 6.0 Gy and 4.5 Gy to 33% and 66% of the heart volume, respectively. IROC-Houston's dose prescriptions for the MRgRT thorax phantom are summarized in Table 21.

MRgRT Thorax Structure	Dose Prescription
PTV	$D_{95\%} \geq 6.0$ Gy $D_{99\%} \geq 5.4$ Gy
Whole Lung (Contralateral & Ipsilateral)	$D_{37\%} < 2.0$ Gy
OAR: Spinal Cord	$D_{0\%} \leq 5.0$ Gy
OAR: Heart	$D_{33\%} \leq 6.0$ Gy $D_{66\%} \leq 4.5$ Gy $D_{100\%} \leq 4.0$ Gy

Table 21: The dose prescription for the MRgRT thorax phantom. Both commissioning and feasibility studies used the same dose constraints.

5.3.5   Treatment Delivery

The MRgRT thorax phantom was reproduced using a 1.5T Unity system and then sent out to three institutions for an independent feasibility study. During the multi-institutional feasibility study, the MRgRT thorax phantom was irradiated using either an MRIdian Linac or an MRIdian ^{60}Co and Unity MRgRT system. The performance of both reproducibility and feasibility studies were evaluated based on an end-to-end test.

Double-loaded TLDs (ThermoFisher Scientific, Waltham, Massachusetts, USA) were read two weeks from the irradiation date to account for fading. These absolute dosimeters were read with the same method as IROC-Houston uses for its phantom studies. The amount of lithium fluoride powder was read using a Mettler AT261 DeltaRange (Mettler Toledo, Greifensee, Switzerland) scale and a Harshaw M3500 TLD reader (ThermoFisher Scientific, Waltham, Massachusetts, USA) was used to measure the light output. Additionally, the MRgRT thorax phantom used EBT3 film as relative

dosimeters. The intensity from the irradiated films was read on a photoelectron CCD microdensitometer (Photoelectron Corporation, North Billerica, Massachusetts, USA) and converted into dose using an in-house MATLAB program (The MathWorks, Inc., Natick, Massachusetts, USA).

The end-to-end tests for reproducibility and feasibility studies were analyzed by using the same two evaluation methods. These analytical methods included: 1) comparing measured TLD dose to expected plan and 2) performing a gamma analysis using a 7%/5mm criterion.

5.3.5.1 Reproducibility Study

During the reproducibility study, the MRgRT thorax phantom was irradiated three times on a 1.5T Unity system. The exterior thorax shell was filled with tap water and imaged on a GE Lightspeed CT simulator using a breast protocol. The parameters of this protocol were: DFOV= 500.0 mm, 120 kVp, 275 mA, and slice thickness= 3mm. The electron density data collected from the CT simulator was transferred to Monaco's Treatment Planning Software (TPS) (Elekta, Crawley, United Kingdom) and an IMRT plan was designed using 7 beams angles. All anatomical structures and TLD capsules were contoured and labelled accordingly.

The MRgRT thorax phantom was placed above a 15-degree inclining platform and was positioned in the center of the Unity's treatment couch. The surface coil did not properly fit over the phantom and platform; so, the Unity's body coil was used to capture a MR image. The treatment setup used in the reproducibility study for the thorax phantom is shown in Figure 31. New dosimeters were replaced in the thorax phantom after each irradiation. To reload new radiation detectors the treatment couch was moved out of the

bore, the pneumatic system was momentarily switched off to release pressurized air and the lung insert was removed from the phantom. Once the portable dosimeters were replaced, the insert and the pneumatic system were screwed back to the phantom, the pneumatic system was turned on, and the phantom was moved back into the center of the bore. A T1-weighted MR image was captured using scanning parameters of: FA= 8°, TR= 8.0 ms, TE= 3.6 ms, ETL= 136, NEX=1 after every irradiation. The treatment plan was re-optimized based on the MRgRT thorax's current position and then irradiated. Each irradiation took approximately 30 minutes to deliver all 7 beams. TLD capsules' maximum, minimum and mean doses were recorded, and the treatment plan was exported to further analyze the treatment performance.

Figure 31: The MRgRT Thorax Phantom setup up for the reproducibility study. The MRgRT body coil was used to capture an MR image.

5.3.5.2 **Feasibility Study**

The MRgRT thorax phantom was shipped to three institutions within the United States that either had an MRIdian ^{60}Co or an MRIdian Linac MRgRT

system. In addition to receiving the thorax phantom and the pneumatic system, each institution received from IROC-Houston detailed instructions describing how to use the motion system and the dose prescriptions requirement. Upon receiving the phantom, the institutions were required to perform an end-to-end test. This test required each institution to image the thorax phantom on a CT, create a treatment plan based on IROC-Houston's dose prescriptions, capture an MR image to verify treatment setup and, finally, irradiate the phantom. Since this end-to-end test was to demonstrate the ability to treat a moving target, IROC-Houston required each institution to use the pneumatic system during imaging and treatment stages. Institutions were allowed to emulate their typical MR workflow by choosing gantry angles, type of motion management, and any additional MR workflow components. Each institution was required to submit a digital copy of the treatment plan and record the expected TLDs' maximum, minimum, and mean dose. End to end tests were analyzed by evaluating the treatment plan to measured dose.

5.4 RESULTS

5.4.1 Phantom Imaging

As shown in Figure 32, the MRgRT thorax phantom was imaged on a GE CT simulator, and Unity and MRIdian MRgRT system. Internal structures and the disease site are clearly visible in all three images. The contralateral lung, heart, and spinal cord were constructed of non-MR visible materials. The absence of MR signal in these internal structures could be seen due to the contrast between the lack of signal surrounded by the MR signal from water. The ipsilateral lung and disease site were constructed of MR

visible materials and the contrast between these structures was visible on all three images. On the Unity system, the disease site appears brighter and has a higher spatial resolution which is attributed to the magnetic field strength and MR sequence, respectively. The Unity system used a T1-weighted sequence whereas the MRIdian system used a true fast imaging with a steady-state free precession (TrueFisp) sequence.
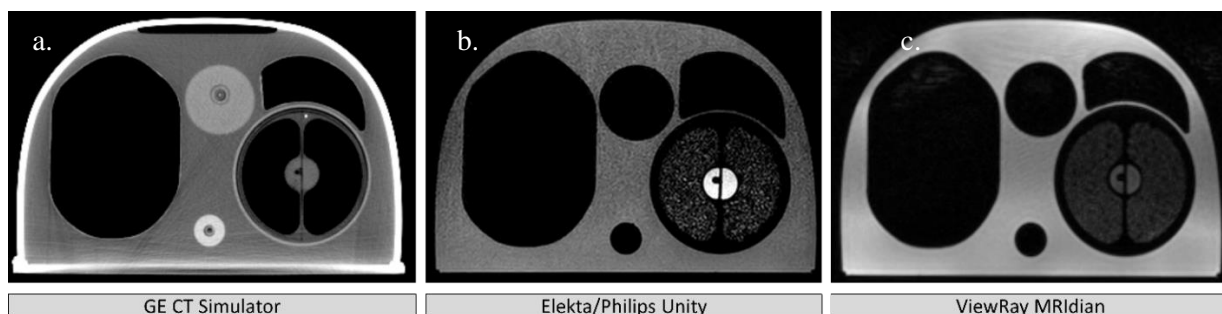
Figure 32: The MRgRT thorax phantom was filled with water and scanned on: (a) GE CT simulator, (b) Unity system's 1.5T MRI with a T1 sequence and (c) ViewRay's MRIdian ^{60}Co 0.35T system with a TrueFISP sequence. In all images, the OAR, primary and secondary PTV are clearly visible.

5.4.2 Treatment Delivery

In both the commissioning and the feasibility study, measured TLD dose was compared to predicted dose from the TPS. Table 22 and Table 23 display the ratios between measured and predicted dose under the commissioning and feasibility study, respectively. TLDs within the superior portion of the PTV had ratios of: 1.00, 1.01, and 1.00 and in the inferior portion had ratios of: 0.93, 0.98, and 0.96 for the commissioning study. Overall, the average ratios between measured and reported doses for superior and inferior PTVs locations were 1.00 and 0.96, respectively. The feasibility study showed greater agreement between measured and expected dose at the inferior PTV than did the commissioning study. The superior portion of the PTV had ratios of: 0.98, 1.03, 1.00, whereas the inferior portion had ratios of: 1.00, 1.00, and 0.98. TLDs that fall within 0.92

and 1.05 to reported dose were considered to pass IROC-Houston's TLD dose criterion. In both studies, TLD readings were within IROC-Houston's acceptable criteria.

TLD Location	Reproducibility Test			Average	Coefficient of Variance
	Unity 1-a	Unity 1-b	Unity 1-c		
PTV Superior	1.004	1.006	1.000	**1.004**	**0.3%**
PTV Inferior	0.934	0.982	0.961	**0.959**	**2.5%**

Table 22: The reproducibility test results of two PTV TLD positions. The left column represents TLD locations for doses calculated on Monaco's treatment planning software. The middle three columns represent the average TLD measured for each location and the percent standard deviation. The average ratios between measured and calculated dose are displayed in the right column. The TLD measurements were all within 4.1% of the reported TLD dose and the coefficient of variance was all within 2.5%.

Institution	Energy	PTV Superior	PTV Inferior
Unity 1	7 MV	1.00	0.96
ViewRay 2	6 MV	0.98	1.00
ViewRay 3	^{60}Co	1.03	1.00
ViewRay 4	^{60}Co	1.00	0.98
Average	**--**	**1.00**	**0.98**

Table 23: Feasibility study results for two TLD positions in the PTV for the MRgRT thorax phantom. The results display ratios between measured TLD dose and reported TLD dose from the institutions' treatment planning software.

IROC-Houston evaluated the treatment deliveries by performing an in-house gamma study on axial and sagittal films. The same gamma criteria (7%/5mm) used on IROC-Houston's conventional thorax phantom was also used to evaluate the MRgRT thorax phantom. A film was said to pass the gamma analysis if more than 80% of the pixels passed each axial and sagittal plane and if the combined average between the two films (sagittal and axial) resulted in at least 85% of pixels passing. Table 24 and Table 25 display the individual gamma pass rates for both the commissioning and the feasibility
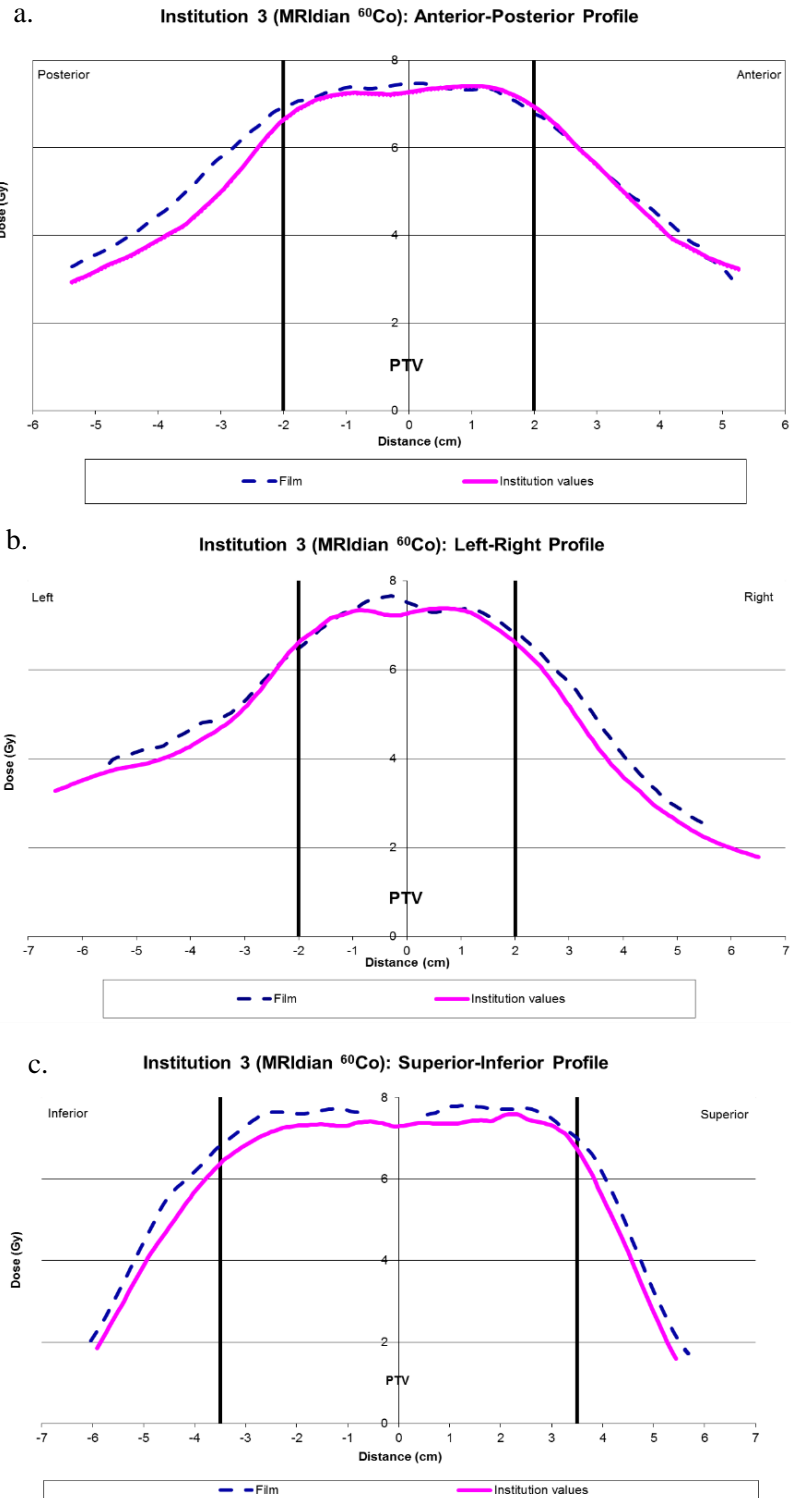
study, respectively. The commissioning study had individual passing rates of 89.0%, 96.8%, and 96.1% for axial films and 90.4%, 96.8%, and 90.9% for sagittal films. Individual passing rates for axial films were 97.9%, 96.7% and sagittal films were: 95.7% and 96.6% in the feasibility study. The combined average of pixels passing between axial and sagittal film in the commissioning study were 89.7%, 96.8%, 93.5% and were 96.8% and 96.7% in the feasibility study. Three dose profiles were generated in anterior-posterior, left-right, and superior-inferior orientations during gamma analysis. A typical set of dose profiles generated from the study is shown in Figure 33. Qualitatively, film dose profiles in all studies were in excellent agreement with their calculated dose profiles.

Institution	% Pixel Passing [7%/5mm]		
	Axial	Sagittal	Average Film Plane
Unity 1-a	89.0	90.4	89.7
Unity 1-b	96.8	96.8	96.8
Unity 1-c	96.1	90.9	93.5
Average	94.0	92.7	93.3

Table 24: The MRgRT thorax phantom was irradiated three times under a 1.5T Unity system. Axial and sagittal planes were evaluated based on 7%/5mm gamma criteria.

Institution	Energy	Pixel Passing		
		Axial	Sagittal	Average Film Plane
ViewRay 2	6 MV	97.9%	95.7%	96.8%
ViewRay 3	Co-60	96.7%	96.6%	96.7%
ViewRay 4[*]	Co-60	-	-	-
Average	-	97.3%	96.2%	96.8%

*Table 25: The feasibility study were evaluated using the same passing criteria as the commissioning study. IROC-Houston gamma passing criteria required individual film planes to have a greater than 80% passing rate and an overall passing rate of 85%. *Data unavailable from institution for analysis.*

a.

Institution 3 (MRIdian ^{60}Co): Anterior-Posterior Profile

b.

Institution 3 (MRIdian ^{60}Co): Left-Right Profile

c.

Institution 3 (MRIdian ^{60}Co): Superior-Inferior Profile

Figure 33: Dose profiles generated in the (a) anterior-posterior, (b) left-right, and (c) superior-inferior direction. These graphs compare dose profiles generated on film to those generated from the treatment planning. These graphs were generated from institution 3, but resemble the typical dose profiles generated from both the feasibility and the commissioning studies.

121

5.5 DISCUSSION

IROC-Houston's conventional thorax phantom was originally designed for CT-only workflows and was not intended to be used in MR environments. Two primary concerns with IROC-Houston's conventional thorax phantom that rendered the phantom insufficient for MRgRT systems. These concerns were: 1) PTV and surrounding tissues were indistinguishable in MR images and 2) the motion table contained ferromagnetic materials that classified the motion system as MR unsafe. It was critical that the disease site and surrounding tissues were distinguishable from one another since on-board MR imagers can track tumors during treatment. Since IROC-Houston's phantoms evaluated the institutions' ability to accurately deliver radiation, it was also important that the MRgRT thorax phantom simulate patient breathing. Having motion during imaging and radiation delivery allowed institutions to perform their normal MR clinical workflows and allowed them to determine methods to mitigate motion uncertainties (i.e., gating, tumor tracking, free breathing).

Several design modifications were performed to create an MRgRT lung insert which included: 1) creating four insert pieces, 2) equipping the insert with film pinpricks, and 3) construction of an exterior insert shell used to create a single unit. The MRgRT lung insert was constructed using a heterogeneous mixture which was composed of semi-solid petroleum jelly and miniature styrofoam balls. Unlike IROC-Houston's conventional lung insert, where the compressed cork was sculpted into place, the MRgRT lung insert could not simply be sculpted since the heterogeneous material was pliable. Each insert piece had an exterior shell constructed of HIPS and was used to create a rigid structure. The tumor was encapsulated in solid water to create a rigid structure. Solid water was used rather than HIPS for the tumor's exterior shell since liquid PVC plastic

chemically reacted to HIPS. Film pinpricks are traditionally used in IROC-Houston's phantoms to register the film's orientation relative to the phantom's position. Film pinpricks in IROC-Houston's conventional lung insert are created by drilling small holes through compress cork. Drilling a hole through the MRgRT lung insert was not efficient since the insert was made with a semi-solid mixture which would make reproducing the same pinprick location difficult. The insert was modified by securing small fine needles inside the external HIPS part. When the insert's pieces were combined, the small needles created small pinprick artifacts on the film which were used to register the film position. An exterior HIPS shell was created to combine the four individual lung insert pieces into a single unit. The exterior shell's lid was made with an aluminum rod used to connect the cylinder to the lung insert.

IROC-Houston is responsible for ensuring that quality is maintained within NCTN clinical trials. One-way IROC-Houston ensures quality is by sending off-site credentialing phantoms to test the cohesiveness between institutions. Since consistency is critical for the credentialing process, the MRgRT must use the same dose prescription and passing criteria as the conventional thorax phantom. Consistent dose prescriptions are also important when evaluating the treatment delivery. The commissioning study consistently showed larger discrepancies between inferior portions, most likely due to uncertainties occurring when creating the treatment plan. The thorax phantom only used free-breathing techniques and captured the PTV's position at a single point in time. The treatment most likely did not capture the entire movement and caused greater uncertainties.

The Unity system was not equipped with lasers inside the treatment vault. Rather, this MRgRT system captured MR images during every irradiation to account for any

setup discrepancies. Unlike conventional linear accelerators, the normal workflow for the Unity system is to fuse an MR image to a CT image and re-optimize the treatment plan based on the anatomical structures captured in the MR image. In the commissioning study, the thorax phantom was removed from the MRgRT bore and the lung insert was uninstalled after each irradiation. These changes could have introduced setup uncertainties which included 1) the treatment couch potentially stopped at a different location inside the bore or 2) the thorax phantom shifted from the original position once reinstalling the insert and pneumatic system. Without lasers in the vault, it was difficult to quantify any noticeable shifts between irradiations. To account for any setup uncertainties and capture the entire end-to-end workflow, an MR imager was captured after every irradiation and the treatment plan was re-optimized according to any new shifts.

Each part of the treatment workflow will have associated uncertainties. Since MRgRT and conventional linear accelerator systems have different workflows, they also will have different associated uncertainties. Some inherent uncertainties of an MRgRT system from treating a moving target on an MRgRT system would include: 1) MR/CT image registration, 2) potential minor MR effects on TLDs, 3) MR spatial accuracy, 4) real-time image guidance, and 5) re-optimization plans. The purpose of this study was not to quantify the source of uncertainties, but to allow these end-to-end studies to have similar uncertainties found in the clinic. This study showed that the Unity, the MRIdian ^{60}Co, and the MRIdian Linac systems consistently deliver expected treatments despite having multiple sources of uncertainties associated to each MRgRT system. Even though there were associated uncertainties in each step of the treatment process, the gamma results showed that these uncertainties played a minor role in the overall dose delivery.

5.6   CONCLUSION

In the future, NCI-sponsored clinical trials will begin to focus on the clinical impacts of MRgRT systems. The thorax region will be of particularly interest for MRgRT systems since new image guidance and online ART techniques could be used to improve lung tumor radiotherapy treatments. The MRgRT thorax phantom was carefully designed as a credentialing tool for MRgRT systems participating in NCTN clinical trials. OARs in the MRgRT thorax phantom were distinguishable in MR due to the contrast between the lack of signal from the internal structures and the surrounding MR signal from water. The MRgRT lung insert has a centrally located PTV surrounded by lung-mimicking tissue and was manufactured with tissue equivalent and MR/CT visible materials. Commissioning and feasibility studies were within IROC's 7%/5mm passing criteria, thus, demonstrating that the MRgRT thorax phantom could be used as a credentialing tool for NCI clinical trials. This study also showed that various MRgRT systems could deliver comparable IMRT dose plans for moving targets.

Chapter 6: Summary

6.1   GENERAL DISCUSSIONS AND CONCLUSIONS

The main purpose of this study was to design a stationary H&N and dynamic thorax anthropomorphic QA phantom that could be used as an end-to-end tool to credential institutions wishing to use an MRgRT device to participate in NCI-sponsored clinical trials. This study was completed in four independent aims. The first two aims were designed to determine materials and radiation detectors used in the anthropomorphic MRgRT phantoms. Once materials were chosen and detectors were characterized in 0.35T and 1.5T magnetic field environments, then the next two aims focused on designing, manufacturing and evaluating the anthropomorphic thorax and H&N phantoms.

The purpose of the first aim was to identify materials that could be used to manufacture the two MRgRT anthropomorphic phantoms. IROC-Houston had several material requirements which included: 1) simulate soft tissue or lung tissue dosimetrically, 2) have comparable HUs, 3) be visible in all aspects of the MRgRT workflow (i.e., MR and CT compatible), 4) endure harsh shipping conditions, 5) show longevity without additivities, 6) maintain physical structure over time (i.e., did not morph over time and had high melting points), 7) show ease in manipulating into tissue shapes and 8) hold radiation detectors in place. Before examining any dosimetric and imaging characteristics, all materials were first examined based on their physical characteristics. Materials that did not meet IROC-Houston's practical characteristics (i.e., had low melting points, used preservatives, or required refrigeration) were eliminated as

potential MRgRT materials. The remaining 80 materials were analyzed based on IROC-Houston's radiotherapy criterion. Most of the materials evaluated in MR and CT imagers showed comparable HU values as human tissue but were not visible in both T1-weighted and T2-weighted MR sequences. Silicone-based and synthetic gel-based materials were the most promising materials since they were compatible in MR and CT. Silicone-based materials did not dosimetrically compare to either soft tissue or lung tissue. The dosimetric discrepancies found in silicone-based materials were attributed to their high effective atomic numbers. Synthetic gel-based materials showed similar effective atomic numbers and dosimetrically resemble human tissue. The first aim found four materials (ClearBallistic Gel #20, Liquid PVC plastics, Superflab and an in-house petroleum jelly/styrofoam ball mixture) that met all of IROC-Houston's material requirements. Gel #20, and 100% Liquid PVC Plastic, and Superflab dosimetrically mimicked soft-tissue and the in-house petroleum jelly/styrofoam balls dosimetrically mimicked lung tissue (Figure 16 and Figure 17).

TLD and radiochromic films were characterized in ViewRay's MRIdian ^{60}Co and Elekta's Unity MRgRT systems in Aim 2. The same MRgRT system was used to characterize double-loaded TLD-100s and EBT3 film in the presence and absence of magnetic fields for the Unity and MRIdian configurations. TLDs were characterized in IROC-Houston's homogenous acrylic output blocks and two geometrical phantom slabs. A lung and head geometrical slab phantom was manufactured from materials recommended in Aim 1. The TLD reproducibility study showed negligible differences of 0.6% and 0.5% between TLDs irradiated in the presence and absence of MRIdian and Unity configurations, respectively. Similarly, TLDs irradiated in geometrical phantom slabs also showed less than 1.4% differences. A larger discrepancy was seen in the

geometrical head phantom slab for the Unity configuration. This discrepancy resulted from having to change the HIPS exterior wall to solid water between irradiations. TLD comparisons using acrylic blocks and geometrical slab phantoms were all within the 2.3% TLD uncertainty and were comparable to previous studies (Table 9)[65]. If a magnetic field dosimetrically affected the dose deposition in double-loaded TLDs, they were smaller than the 2.3% TLD uncertainty and were indistinguishable from the readout uncertainty.

In addition to double-loaded TLDs, the geometrical phantoms were used to characterize EBT3 films in the presence and absence of a magnetic field for both MRIdian and Unity systems. Relative beam profiles were measured on the EBT3 films and were validated from virtual beam profiles generated on GEANT4. The DTA between measured and generated beam profiles were compared on the Unity system. The Unity configuration had excellent agreement between measured and generated film, thus demonstrating that a 1.5T magnetic field environment did not affect radiochromic EBT3 film (Table 10 and Figure 21). The measured and simulated beam profiles on the MRIdian configuration had greater discrepancies than the Unity configuration. Greater agreement was found on the Unity configuration since the point-source file was provided by Elekta. A generic ^{60}Co phase-space data was used to simulate MRIdian's proprietary system. Using a generic ^{60}Co phase-space data caused greater discrepancies since the MRIdian treatment head could not be simulated completely due to unavailability of proprietary information. The greatest discrepancy between measured and simulated beam profiles were most apparent in the penumbra region. The simulated penumbra was broader due to only simulating a single MLC set. EBT3 was validated in a 0.35T environment by comparing the DTA between 0T/0.35T for measured beam profiles to

DTA between 0T/0.35T of Monte Carlo generated beam profiles (Table 11 and Figure 22). This validation showed negligible differences between the film shift; thus, concluding that a 0.35T environment does not affect EBT3 films.

Aim 3 used results from the previous two aims to construct anthropomorphic thorax and H&N phantoms using materials and dosimeters previously characterized in Aim 1 and Aim 2 (Figure 23 and Figure 28). Gel-based materials used in the MRgRT inserts were more difficult to manufacture than solid hydrogen-lacking materials used in IROC-Houston's conventional inserts. Creating film pinprick locations and forming complex structures from gel-based materials was a challenging aspect during the manufacturing process. Film pinpricks were created by either drilling small holes into the insert's thicker exterior wall or by attaching permeant fine needles into the insert's exterior shell. Complex internal structures, constructed from gel-based materials, were manufactured in a multi-step process. The construction process consisted of melting the materials and pouring them into a pre-constructed custom mold. To eliminate bubbles induced in the pouring process, the molds were placed into a vacuum until the melted materials had solidified at room temperature. All gel-based materials were encapsulated with either solid water or HIPS to create a rigid and reproducible structure. Solid water was used to encapsulate materials that were shown to previously chemically react to and degrade HIPS. Due to the cost of solid water, materials that did not chemically react were encapsulated with HIPS rather than solid water. The MRgRT inserts' hard exterior shells provided a rigid structure that could withstand hard shipping conditions.

Designing and manufacturing a motion system used for the MRgRT thorax phantom was also included in Aim 3. The two MR safe motions systems considered for the MRgRT thorax phantom was to use either a piezoelectric motor or a pneumatic

system. MR safe piezoelectric motors were made with fragile ceramic materials that usually had a limited workload capability. Since IROC-Houston equipment frequently endures rough shipping and handling conditions it was not ideal to have a fragile motor that could easily break during transit. A pneumatic system was an appropriate motion system since it was durable and had a high workload capability. The pneumatic system was designed with two major sections: MR safe and MR unsafe components (Figure 30). The waveguide, built into all MRgRT suites, was used to separate the two sections. Thus, MR unsafe components were positioned outside and the MR safe parts were positioned inside the treatment room. The pneumatic system's cylinder was an integral part of the motion system since it needed to be MR safe and was positioned at the center of the magnet. Commercially available aluminum cylinders were not completely MR safe since most were manufactured with a stainless steel piston. An aluminum cylinder was bought and the stainless steel piston was replaced with a custom made brass piston, thus, allowing to be used in center of the MR bore.

After developing two phantoms in Aim 3, the MRgRT thorax and H&N phantoms were irradiated and their dose deliveries were evaluated in Aim 4. Evaluations were done by conducting a single institutional commissioning study and a multi-institutional feasibility study. In these studies, TLDs and EBT3 films were used to compare the actual treatment to anticipated treatment and were evaluated using the same criteria used in IROC-Houston's conventional phantoms. The passing criteria for the conventional thorax and H&N phantoms were 7%/5mm and 7%/4mm, respectively. All studies passed IROC-Houston's criteria for the H&N (Table 15-Table 18) and thorax (Table 22-Table 25) phantom, thus demonstrating these phantoms were affective end-to-end QA tools

which could be used to credential institutions participating in NCI-sponsored clinical trials.

The simplistic breathing pattern from the pneumatic system could have been a weakness in this work. The pneumatic system was designed such that every three seconds the phantom would move into either exhale or inhale positions. While this pneumatic system was used to represent lung breathing, it did not fully mimic breathing patterns from a lung cancer patient. To fully mimic breathing patterns from a typical lung patient, the pneumatic system would need to program a series of irregular lung movements. This pneumatic system was IROC-Houston's first MR safe motion system and was originally designed with manual flow control knobs. The flow control knobs were physically adjusted to create the speed at which the lung insert would move. These manual flow control knobs could be replaced with programmable flow control knobs which could be used to create various breathing patterns.

Another limitation of this work was the amount of institutions that participated in the feasibility studies. These studies were restricted to MRgRT systems in the United States, thus, reducing any time delays caused from shipping overseas and having to go through customs. At the time of this study there were only a few MRgRT systems in the United States which were fully installed and were working in the clinic. The feasibility study consisted of institutions who initially agreed to participate in both phantom studies. Some institutions, who had an MRgRT system, were not very receptive and either did not provide all necessary items (i.e., exported treatment plan, reported dose) for the evaluation studies, were undergoing an upgrade, was newly installed or had exported corrupted treatment data that could not completely be analyzed. Since the Unity system was new, only a handful of people were allowed to use the MRgRT system. The

feasibility study did not include MD Anderson since the same person who was required to operate the Unity system during the commissioning study was the same person who would have completed the feasibility study. Despite the small cohort, the ones that did participate in the feasibility studies passed IROC-Houston's passing criterion.

The goal of the MRgRT thorax and H&N phantom was to evaluate each institution's complete MRgRT radiotherapy workflow. Every component of the multi-step treatment workflow had an associated uncertainty. The purpose of the end-to-end test was not to quantify or identify the source of each specific uncertainty but rather evaluate the overall radiotherapy process. Based on the phantom irradiations, the end-to-end feasibility studies demonstrated that the MRIdian ^{60}Co, MRIdian Linac and Unity MRgRT systems could accurately deliver radiation plans. These studies also showed that on-board MR imagers were able to verify treatment setup and track tumors on the MRgRT phantoms. Lastly, the phantom's irradiation performance did not show a vendor dependence, thus demonstrating that the MRIdian and Unity systems can cohesively deliver IMRT plans to treat the MRgRT phantoms.

The hypothesis of this project was that a homogeneous H&N and dynamic heterogeneous thoracic anthropomorphic phantom could be designed to evaluate MRgRT systems and would have agreements between the measured and calculated doses within ±7%/4mm and ±7%/5mm, respectively. Based on the information obtained from this work the hypothesis was met by: 1) identifying tissue equivalent materials which were MR/CT visible, 2) characterizing EBT3 and TLDs in the presence of a 0.35T and 1.5T magnetic field 3) designing and manufacturing a homogenous H&N and a dynamic heterogeneous thorax anthropomorphic MRgRT phantom and 4) performing a commissioning and a feasibility study on both phantoms.

6.2 FUTURE WORK

One potential avenue of future research would include modeling the MRIdian treatment head more realistically. While the treatment head configuration on the MRIdian ^{60}Co system is proprietary, one could attempt to mimic the treatment head by applying two MLCs within a generic ^{60}Co Monte Carlo model. The user would have to estimate the location of the two MLCs within the model. Even with approximate MLC locations the simulated penumbra would better represent the actual penumbras seen on a MRIdian system. Potentially, one could simulate the beam profiles better by using a phase-space file provided by Viewray. While this would be the best scenario to simulate the MRIdian beam profiles this would be more difficult to achieve since this would require collaborating with ViewRay and asking them to provide the phase space data.

Another broad area of future work would include making several other anthropomorphic phantoms for MRgRT systems. This future work could be completed by either: making modification to IROC-Houston's phantoms to adjust for the MR component workflows or design new anatomical phantoms used for the MRgRT systems. IROC-Houston currently has a conventional pelvis phantom that is only visible in CT. This phantom could be constructed with materials suggested in the Steinmann et al. 2018 study to create an MRgRT pelvic phantom. Other anatomical phantoms could be created using MRgRT materials. For example, an MRgRT pancreas phantom could be extremely useful since ViewRay launched a multi-center prospective clinical trial for pancreatic tumors.

Modifying the current MRgRT thorax phantom to address auto contouring and online ART techniques could also be another future research area. Rather than having a single insert, two inserts could be designed, manufactured and used in the credentialing

process. The original insert would represent a patient's tumor in the beginning of treatment and the second insert would have a smaller PTV that represented the same tumor after several fractionations. The original insert would have the same end-to-end treatment methodology as the MRgRT thorax phantom and would be used to capture a CT image, create an IMRT plan accordingly, verify a treatment setup using an MR imager and irradiate the phantom. The second insert would be used to test automatic contouring and online ART techniques. After the original insert was irradiated, it would be removed and the second insert, with the smaller PTV, would be inserted into the phantom. While the phantom was on the treatment couch, the institution would perform their online ART workflow where they would have to auto contour the smaller PTV, adjust the treatment plan, re-calculate the treatment plan, verify treatment plan and irradiate the phantom with the new insert.

Appendix A: Beam Profile
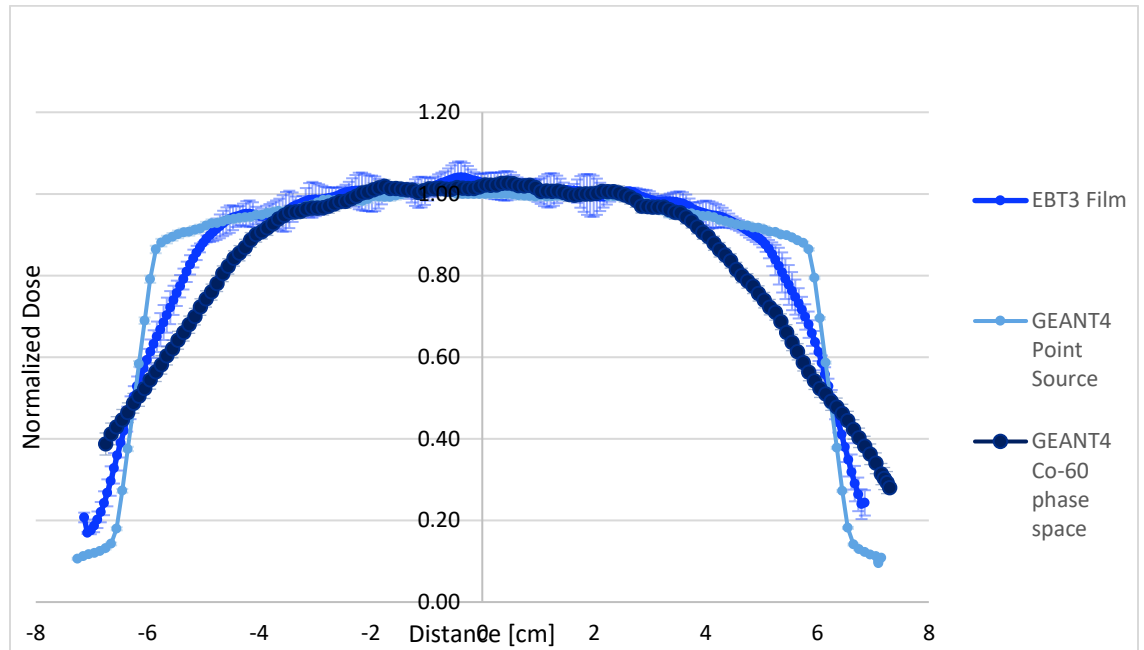
Figure 34: Beam profiles generated under the geometrical head phantom 0T configuration for the MRIdian beam. Averaged measured EBT3 beam profile compared to simulate beam profiles on Monte Carlo.
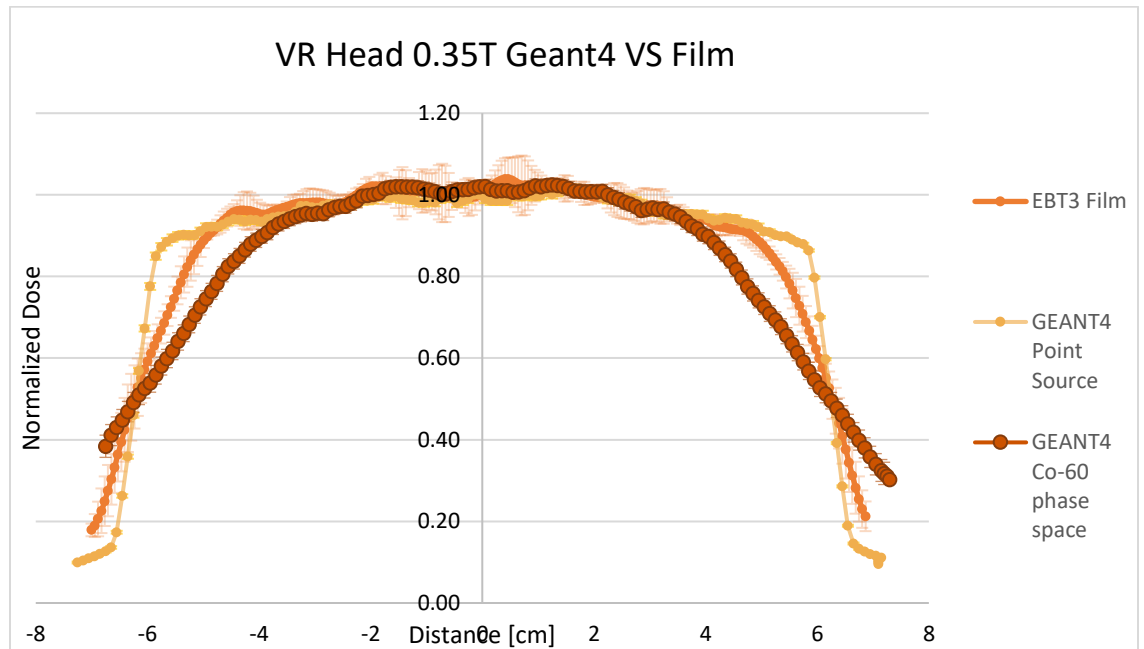
Figure 35: Beam profiles generated under the geometrical head phantom 0.35T configuration for the MRIdian beam. Averaged measured EBT3 beam profile compared to simulate beam profiles on Monte Carlo.
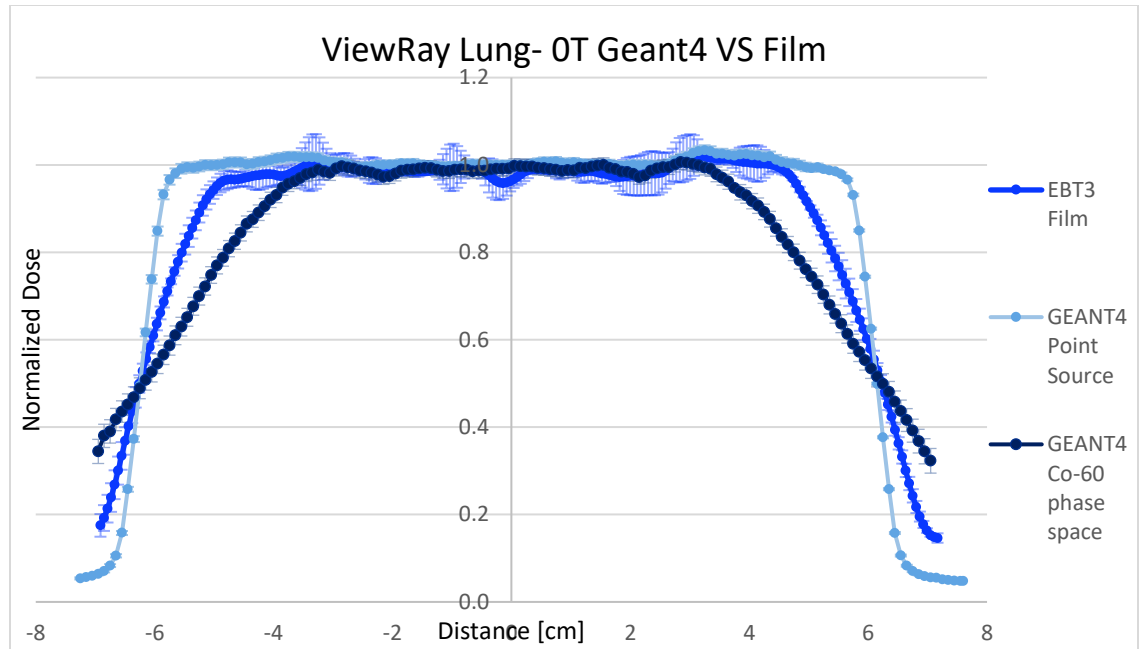
Figure 36: Beam profiles generated under the geometrical lung phantom 0T configuration for the MRIdian beam. Averaged measured EBT3 beam profile compared to simulate beam profiles on Monte Carlo.
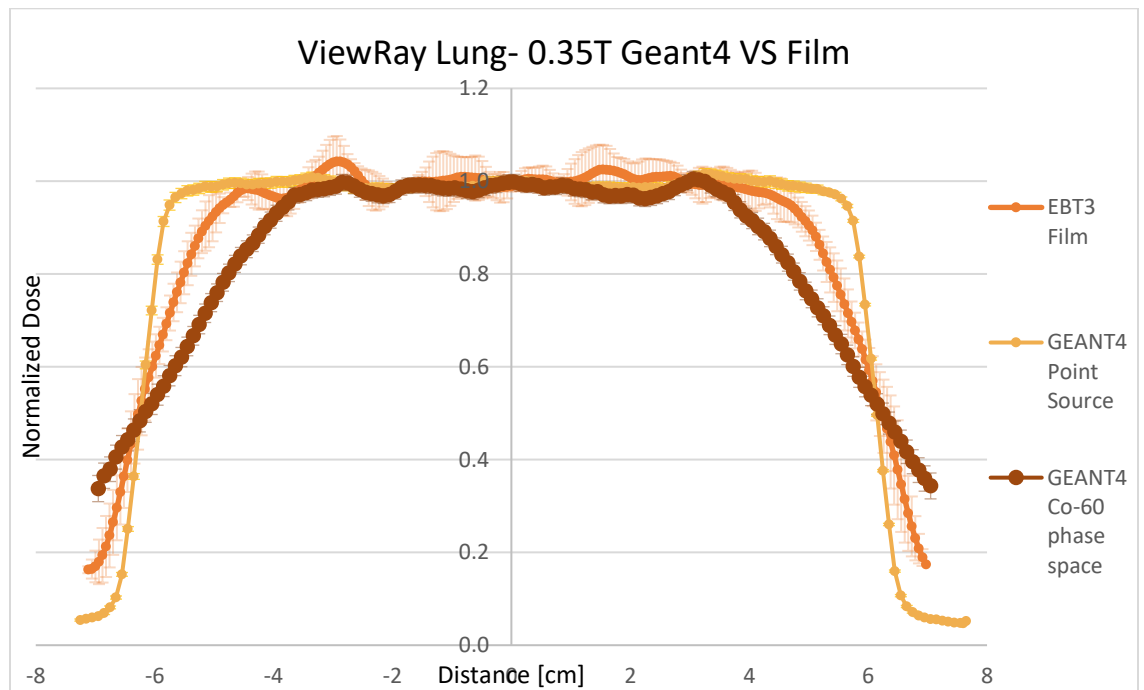
Figure 37: Beam profiles generated under the geometrical lung phantom 0.35T configuration for the MRIdian beam. Averaged measured EBT3 beam profile compared to simulate beam profiles on Monte Carlo.

Appendix B: Dose Profile

6.2.1   MRgRT Head & Neck: Left-Right
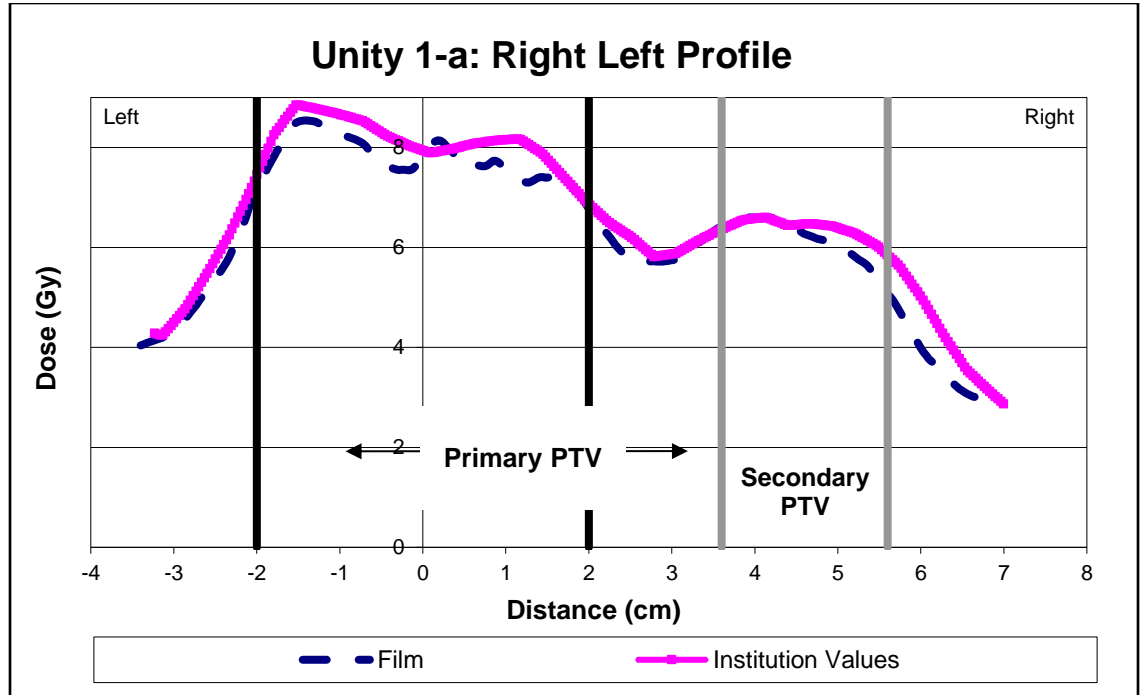
Figure 38: Left-right dose profile from Unity 1-a (7MV/1.5T) of the commissioning study using the MRgRT H&N phantom.
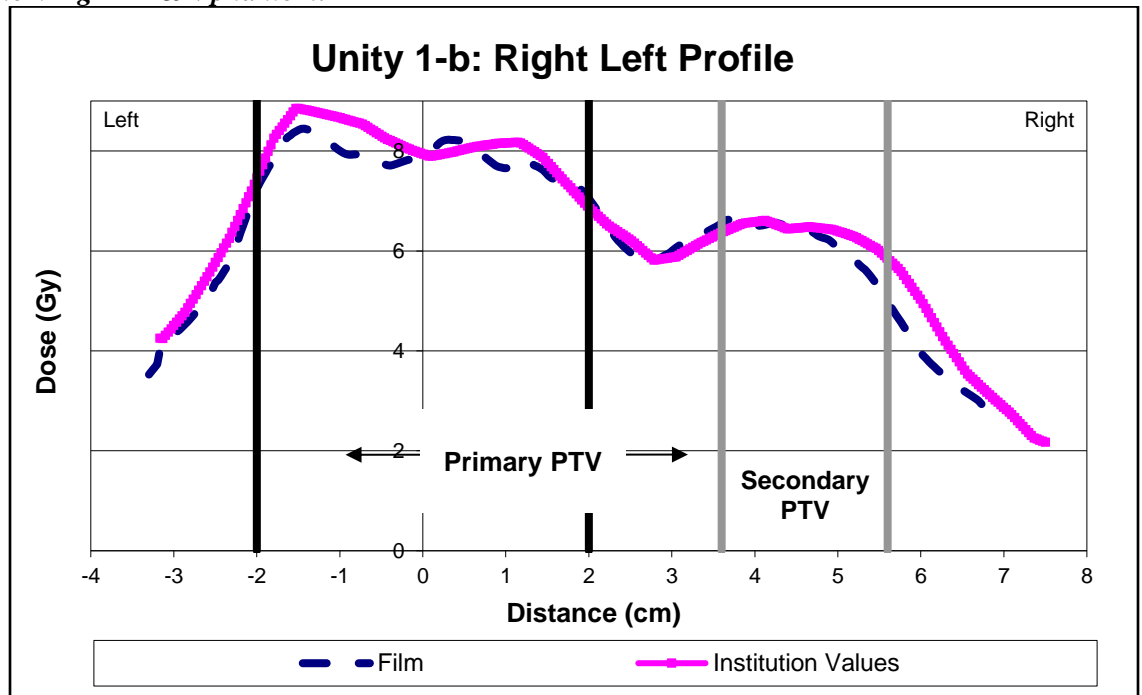
Figure 39: Left-right dose profile from Unity 1-b (7MV/1.5T) of the commissioning study using the MRgRT H&N phantom.
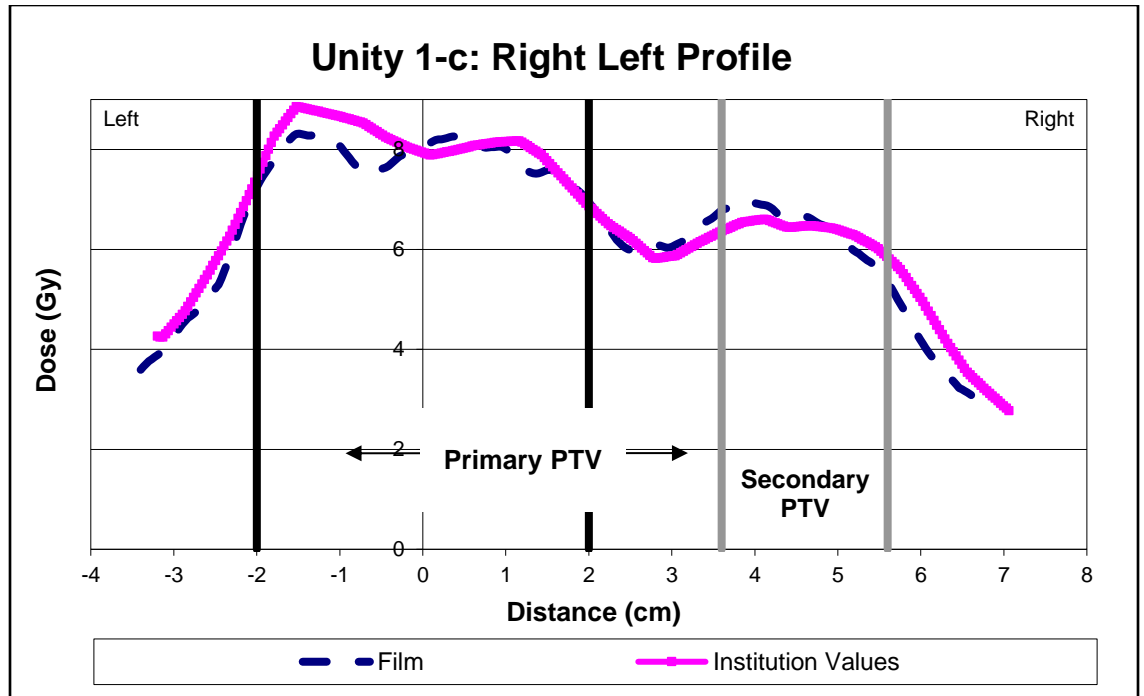
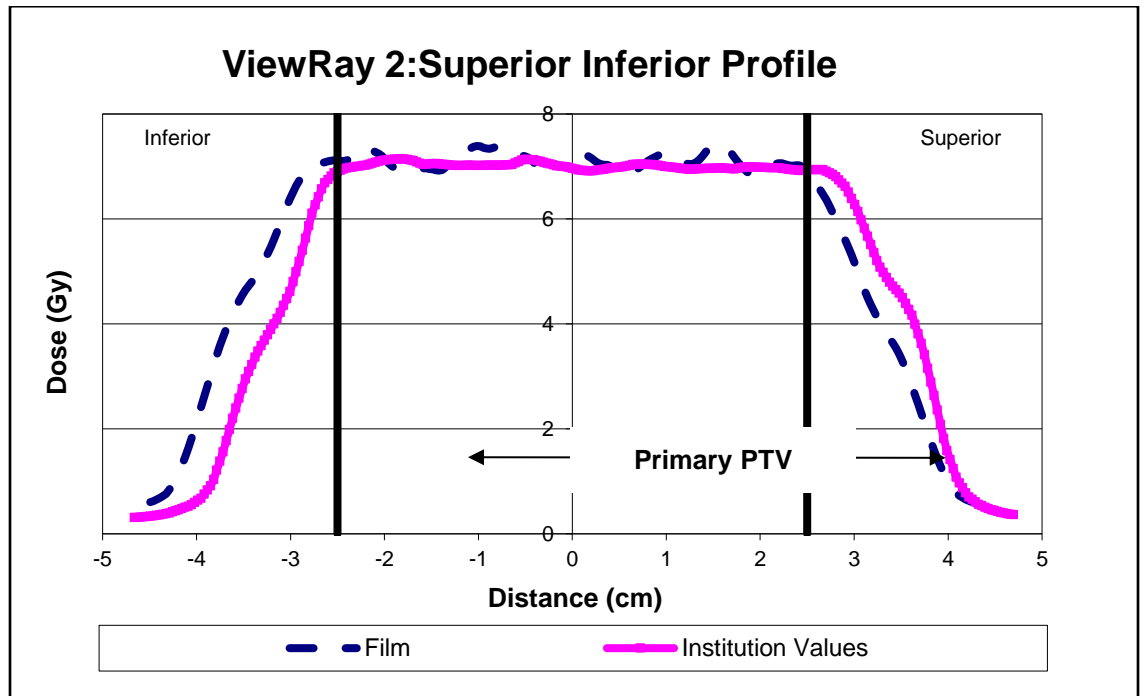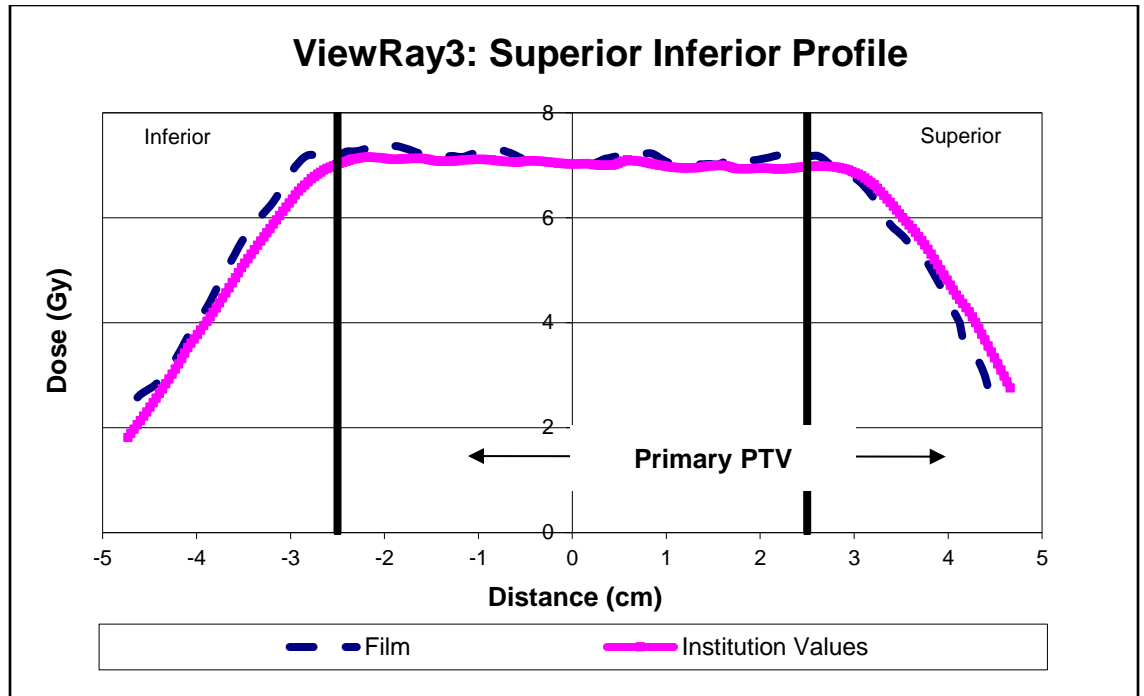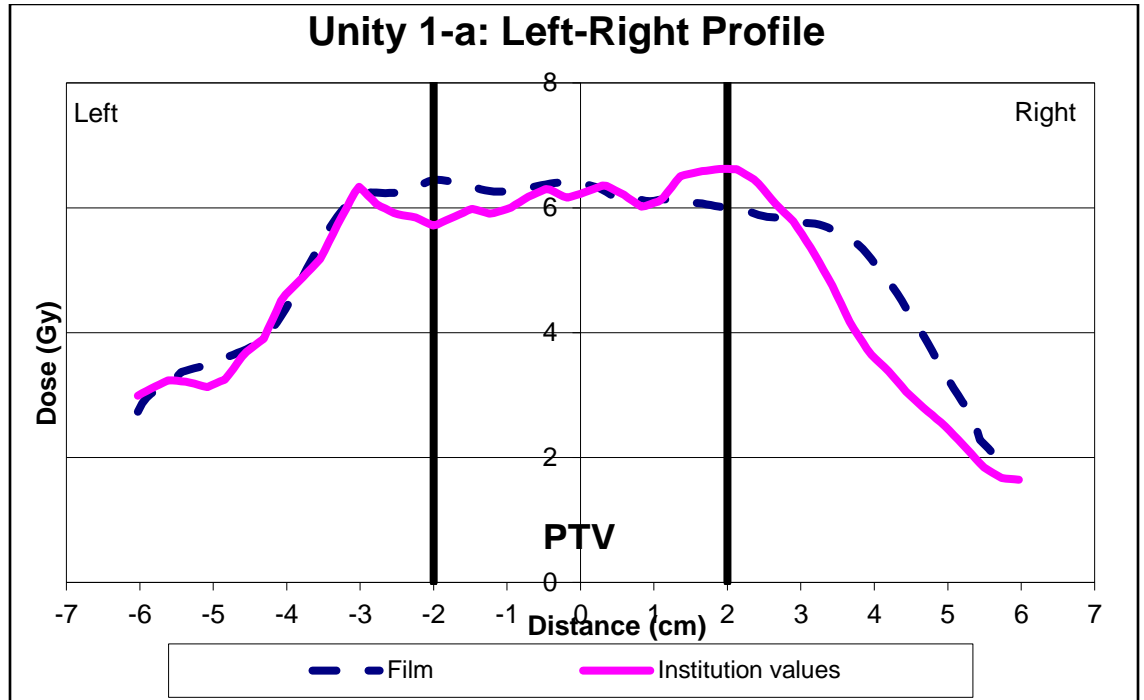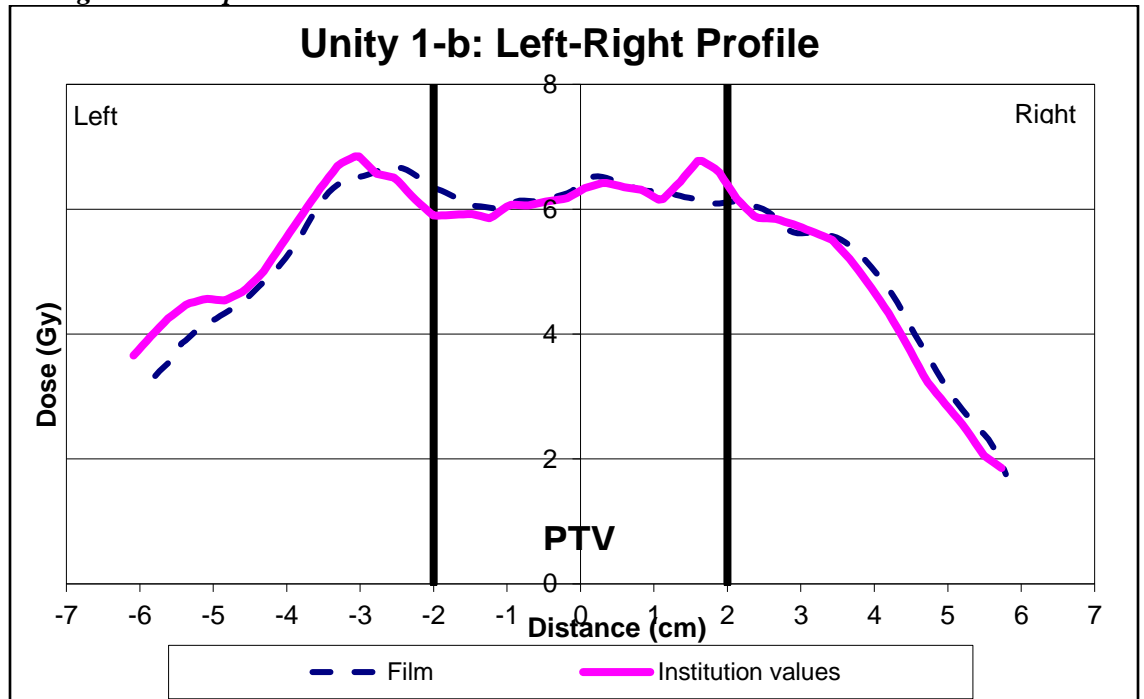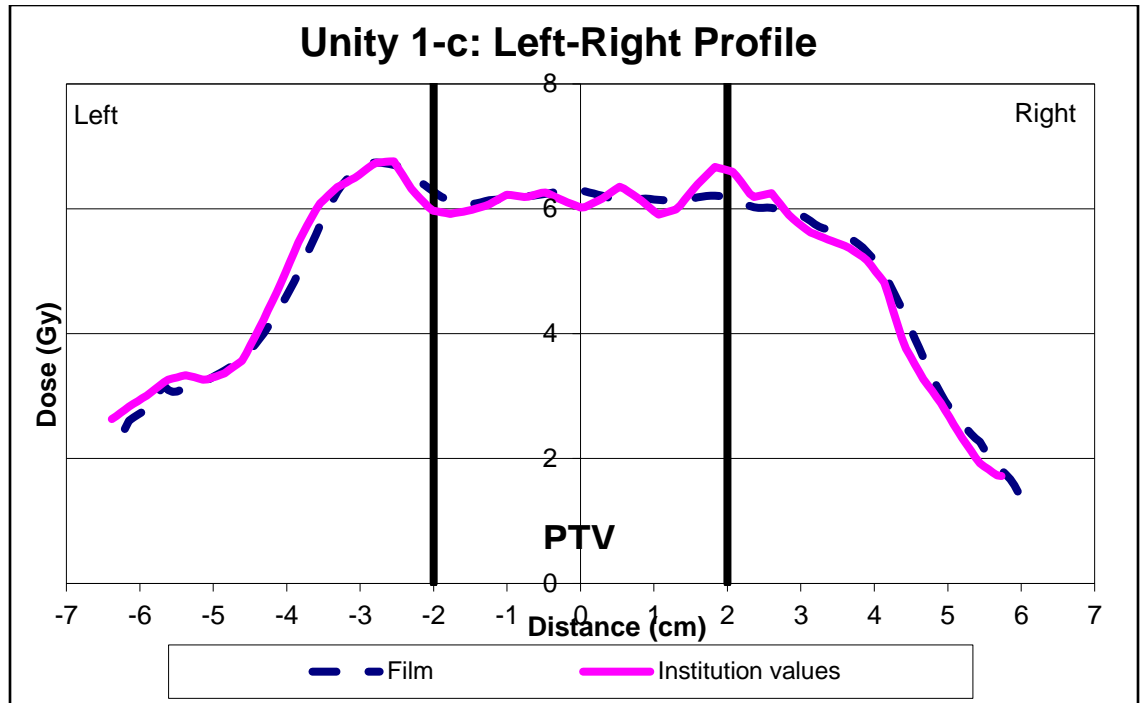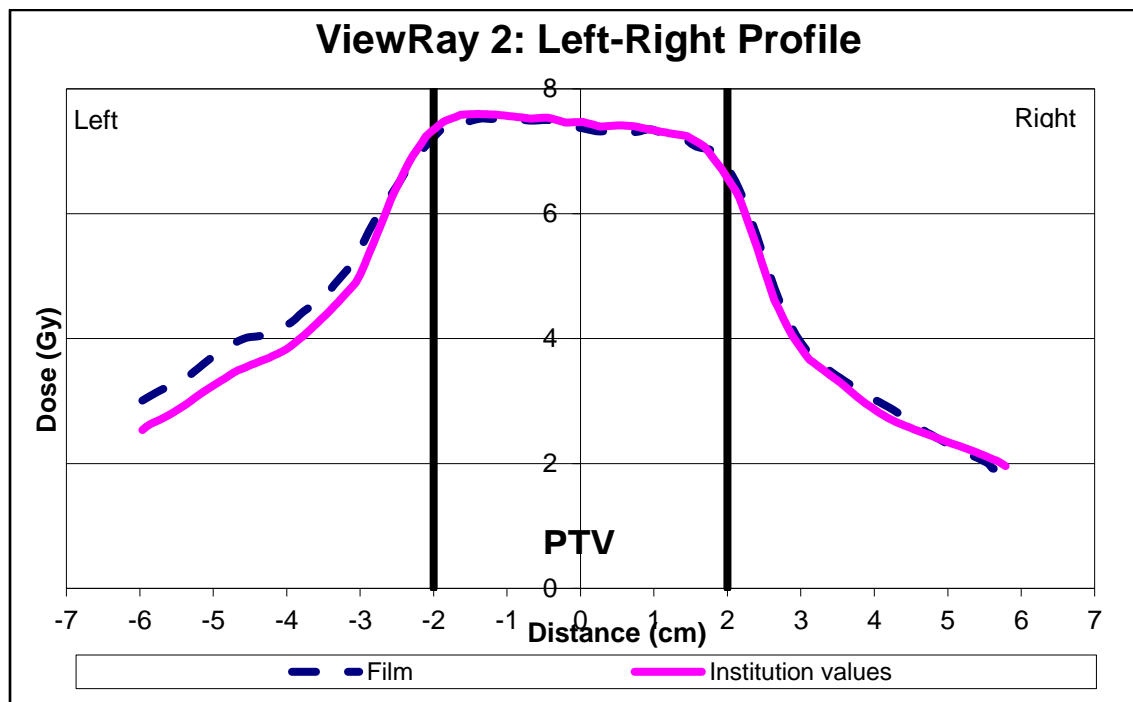*Figure 40: Left-right dose profile from Unity 1-c (7MV/1.5T) of the commissioning study using the MRgRT H&N phantom.*
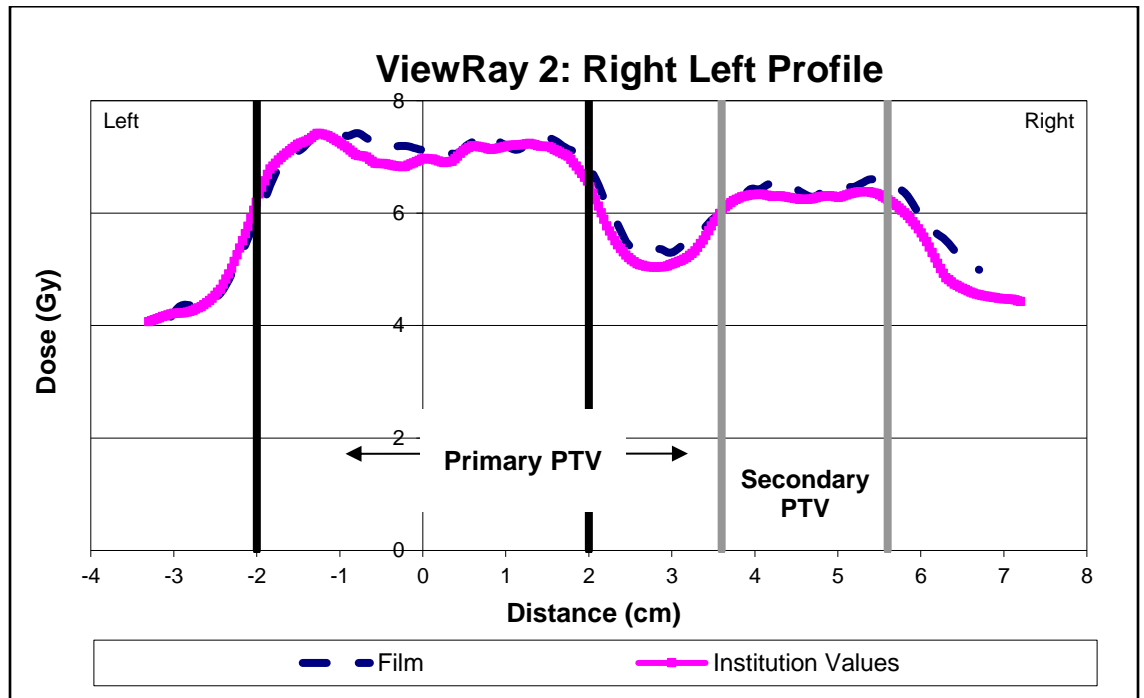
Figure 41: Left-right dose profile from ViewRay2 (6MV/0.35T) of the feasibility study using the MRgRT H&N phantom.
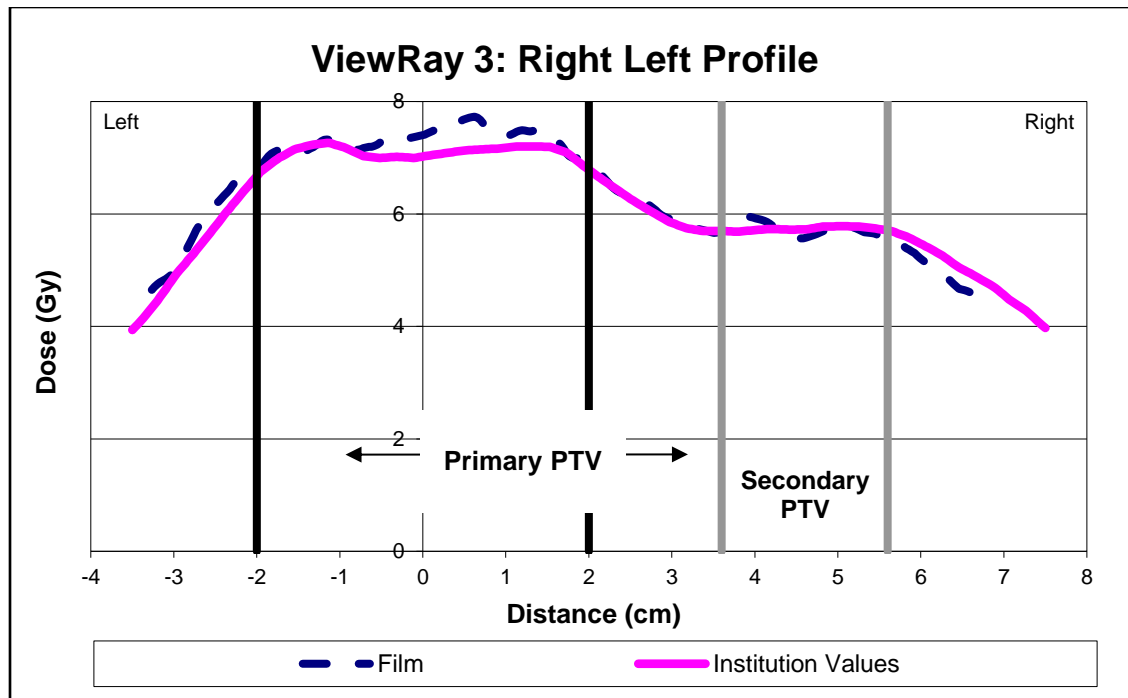
Figure 42: Left-right dose profile from ViewRay3 (60Co/0.35T) of the feasibility study using the MRgRT H&N phantom.
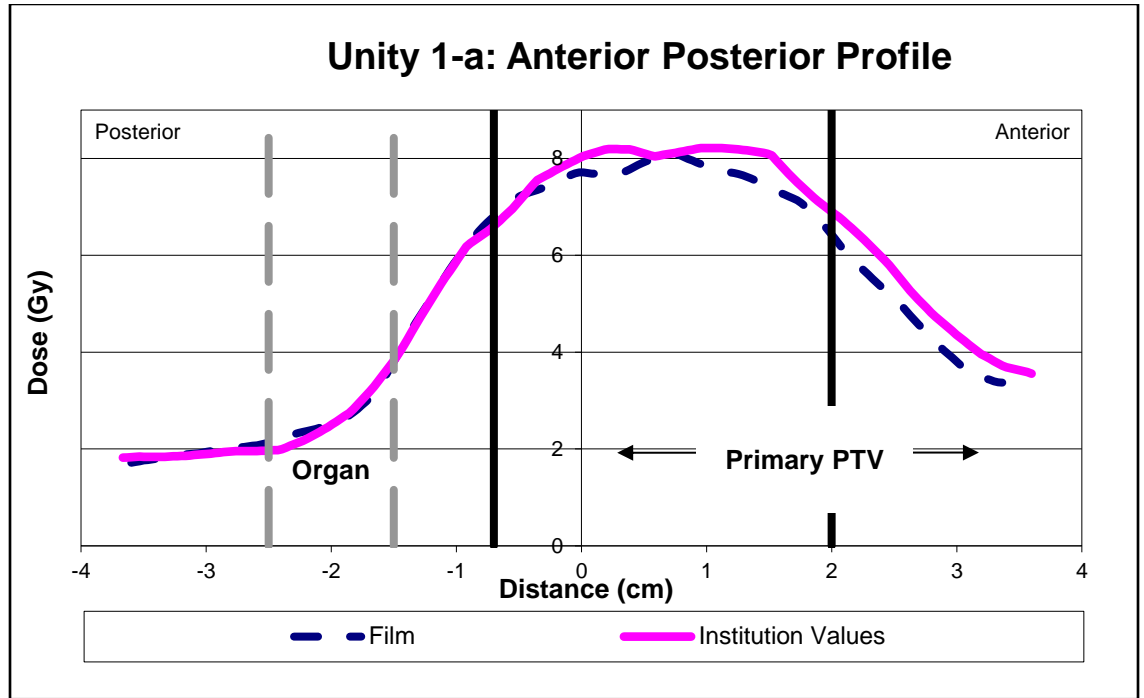
Figure 43: Anterior-posterior dose profile from Unity 1-a (7MV/1.5T) of the commissioning study using the MRgRT H&N phantom.
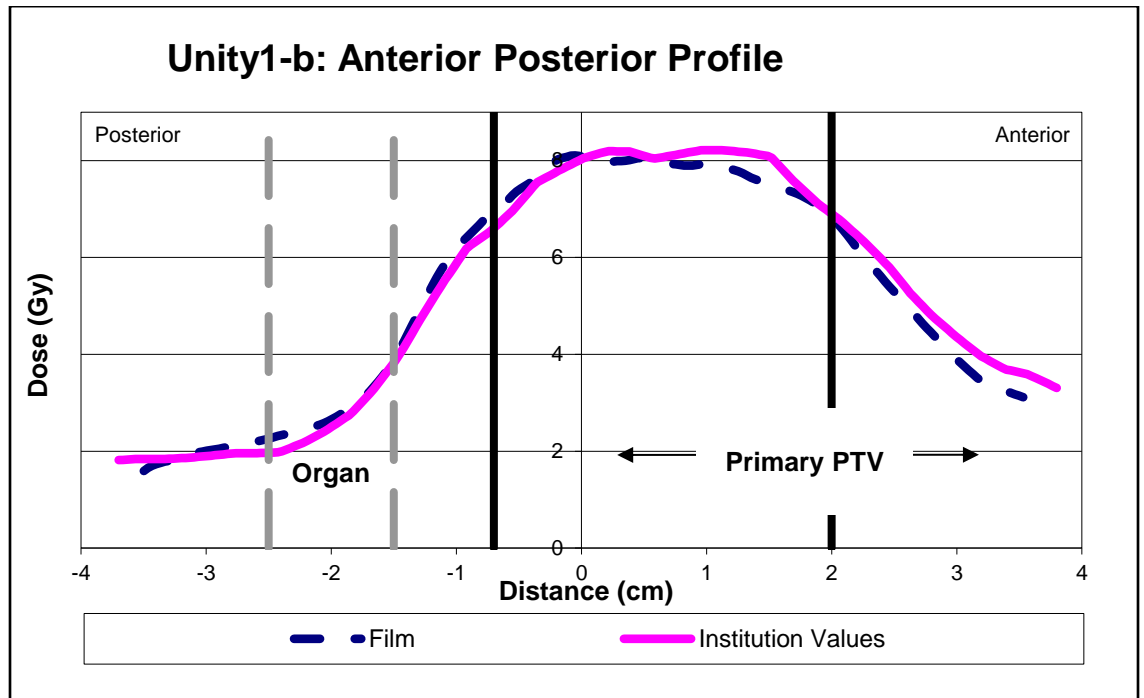
Figure 44: Anterior-posterior dose profile from Unity 1-b (7MV/1.5T) of the commissioning study using the MRgRT H&N phantom.
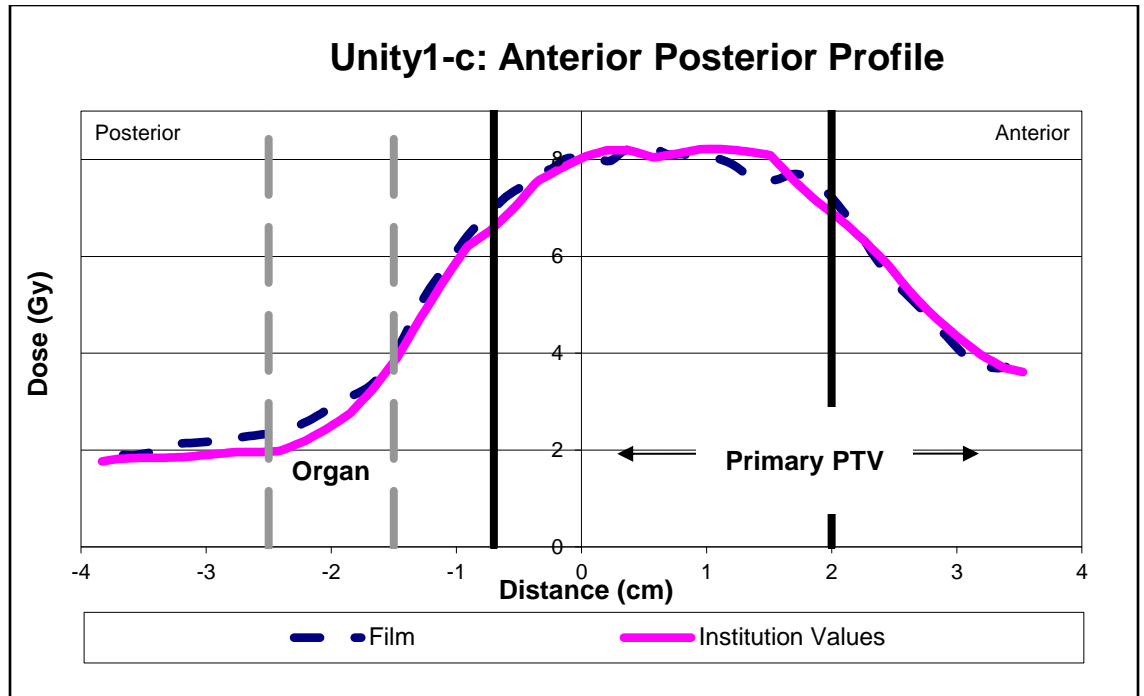
Figure 45: Anterior-posterior dose profile from Unity 1-c (7MV/1.5T) of the commissioning study using the MRgRT H&N phantom.
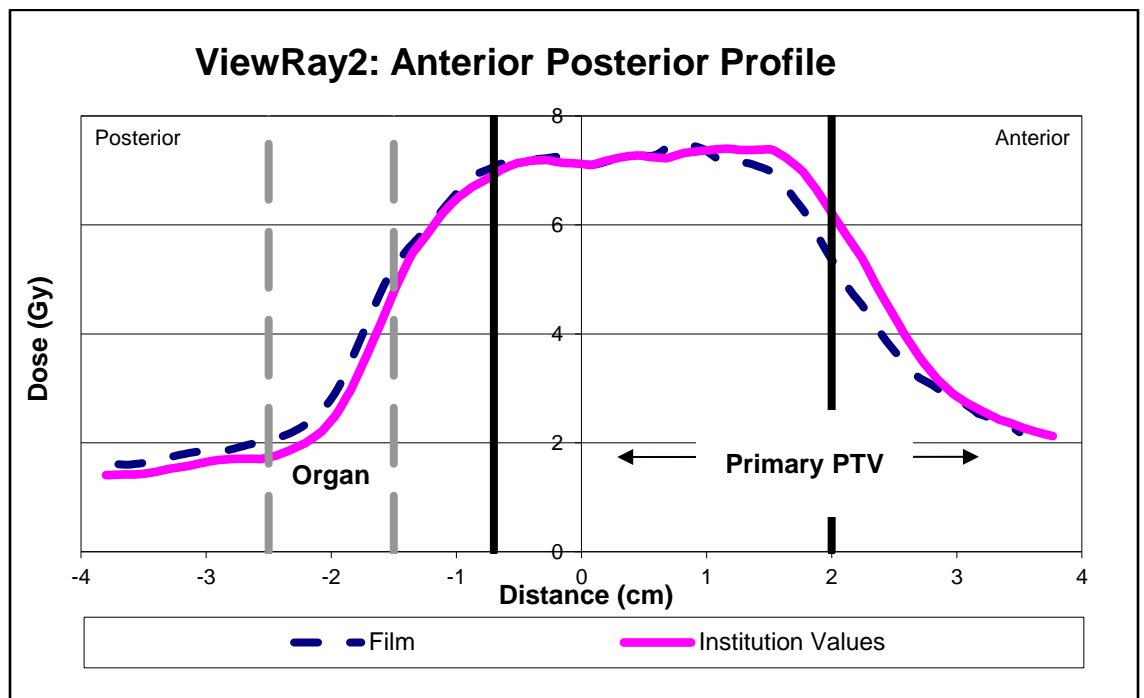
Figure 46: Anterior-posterior dose profile from ViewRay2 (6MV/0.35T) of the feasibility study using the MRgRT H&N phantom.
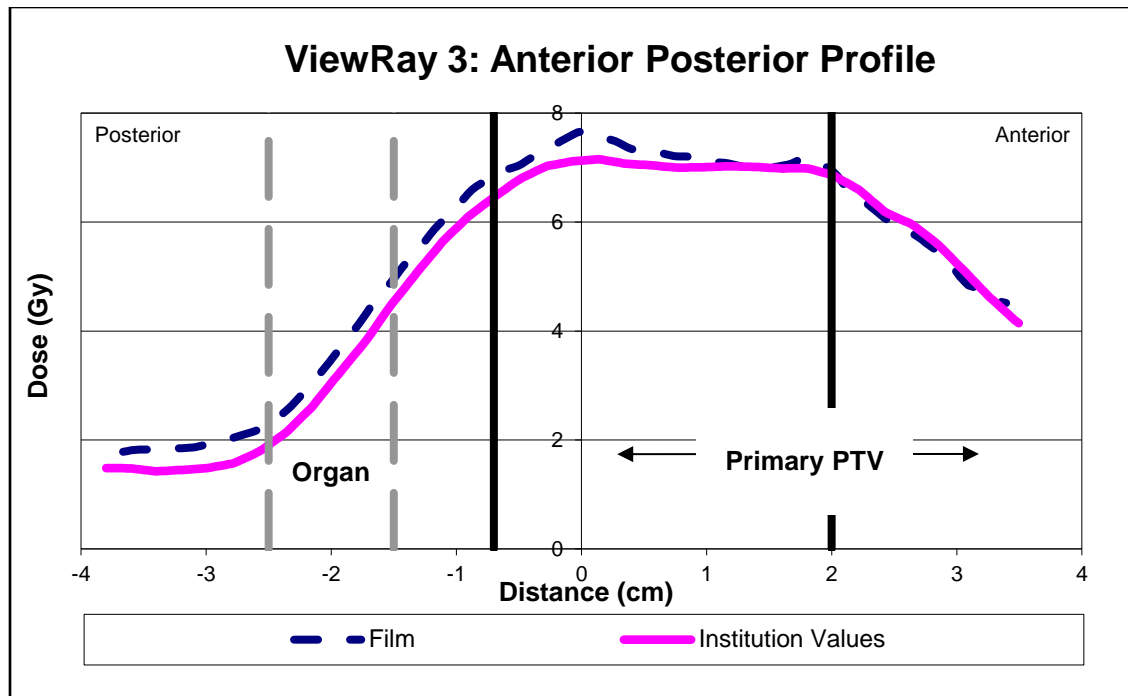
Figure 47: Anterior-posterior dose profile from ViewRay3 (60Co/0.35T) of the feasibility study using the MRgRT H&N phantom.

6.2.3 MRgRT Head & Neck: Superior-Inferior
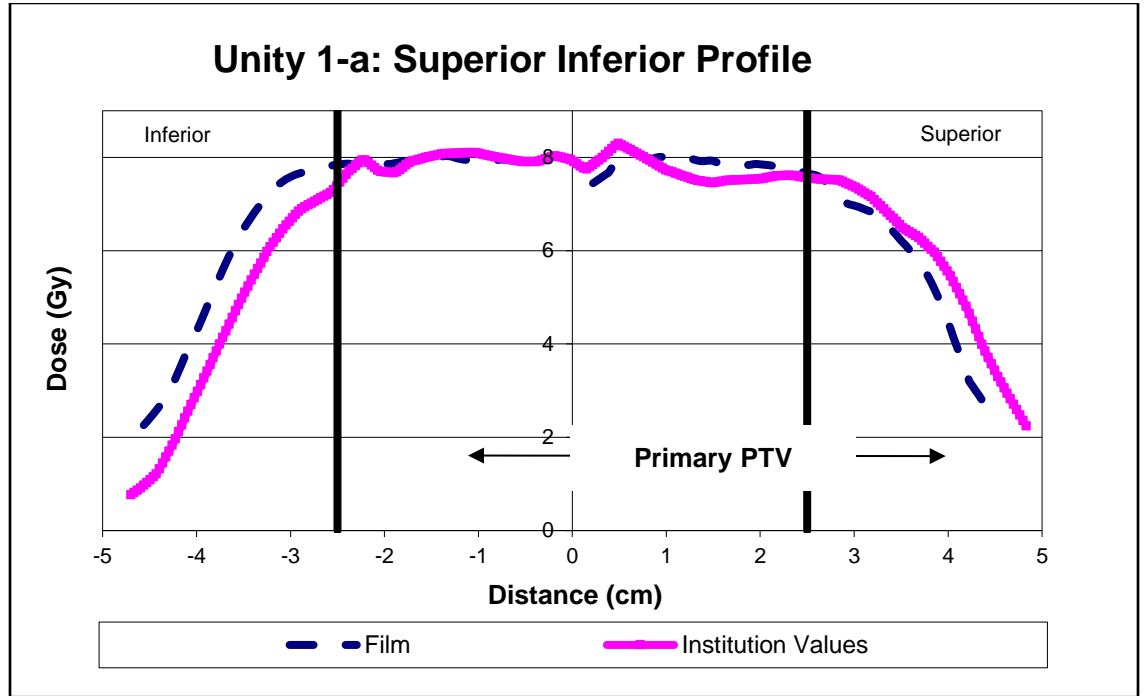
Figure 48: Superior-inferior dose profile from Unity 1-a (7MV/1.5T) of the commissioning study using the MRgRT H&N phantom.
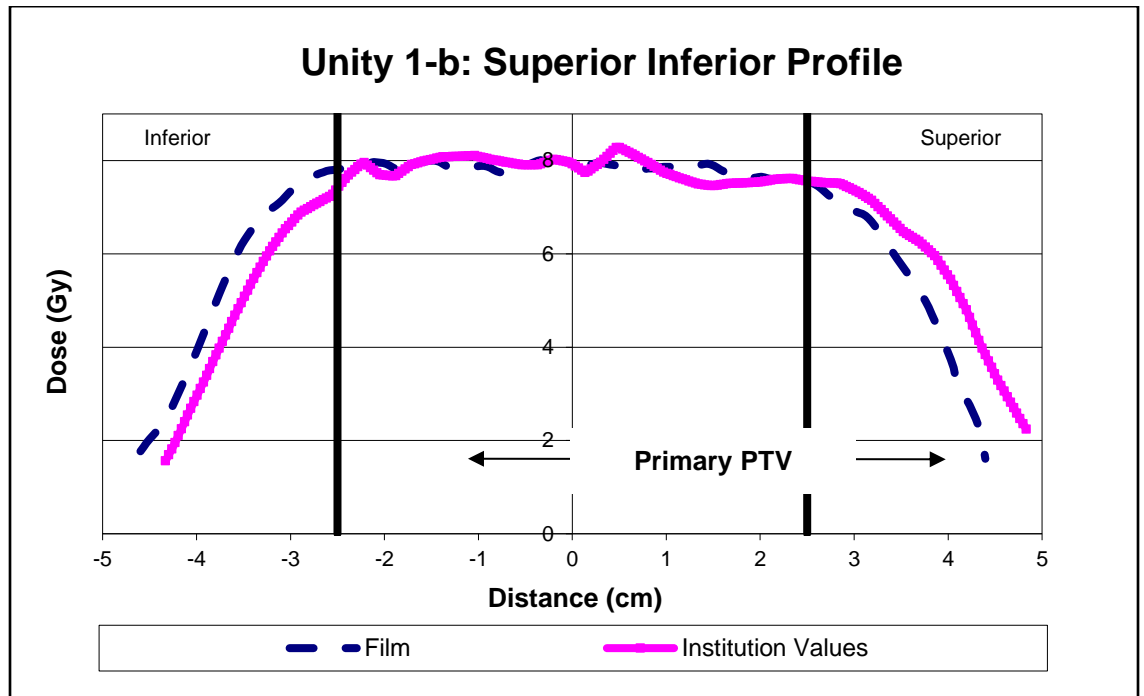
Figure 49: Superior-inferior dose profile from Unity 1-b (7MV/1.5T) of the commissioning study using the MRgRT H&N phantom.
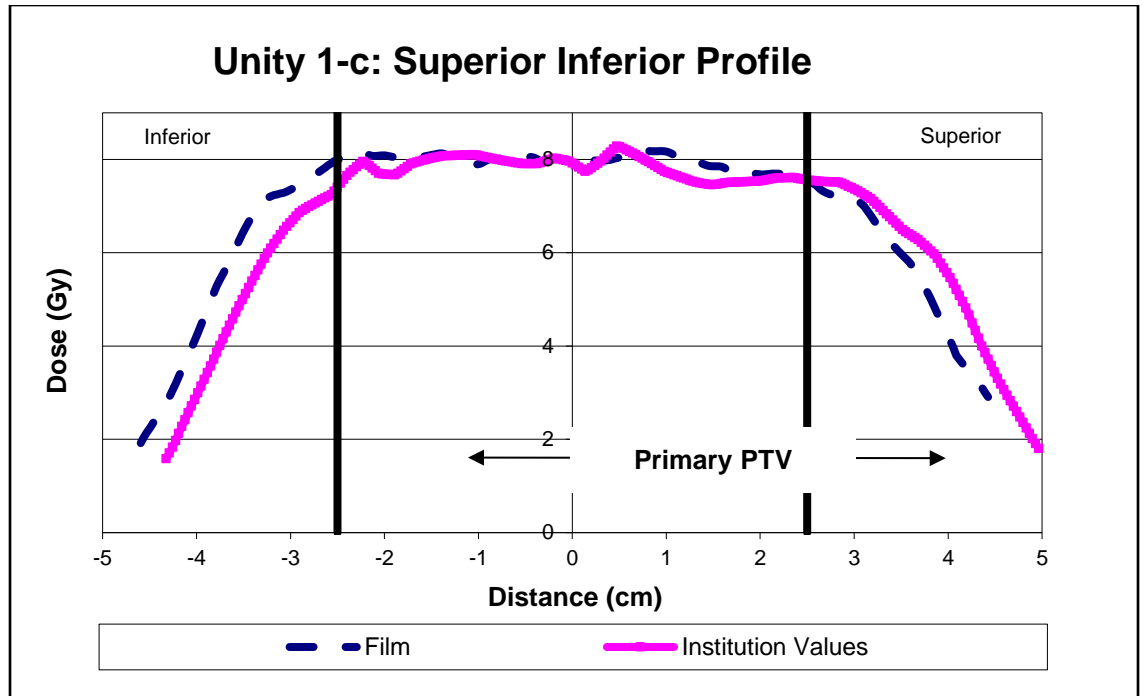
Figure 50: Superior-inferior dose profile from Unity 1-c (7MV/1.5T) of the commissioning study using the MRgRT H&N phantom.

Figure 51: Superior-inferior dose profile from ViewRay2 (6MV/0.35T) of the feasibility study using the MRgRT H&N phantom.
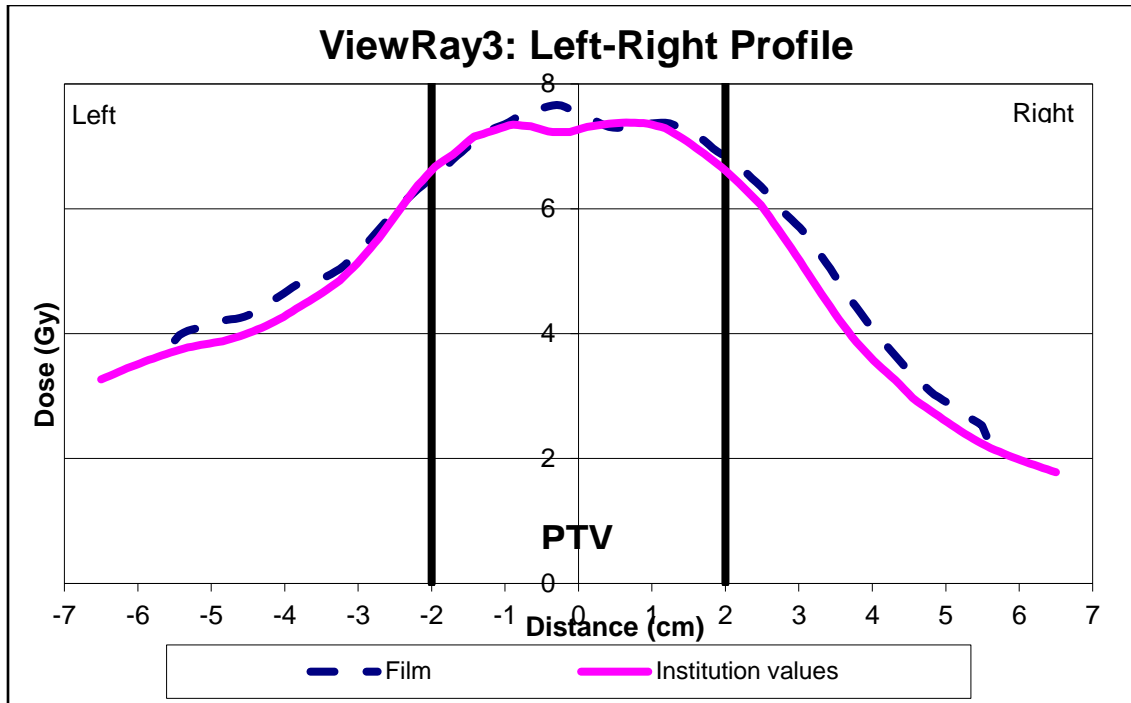
Figure 52: Superior-inferior dose profile from ViewRay3 (60Co/0.35T) of the feasibility study using the MRgRT H&N phantom.
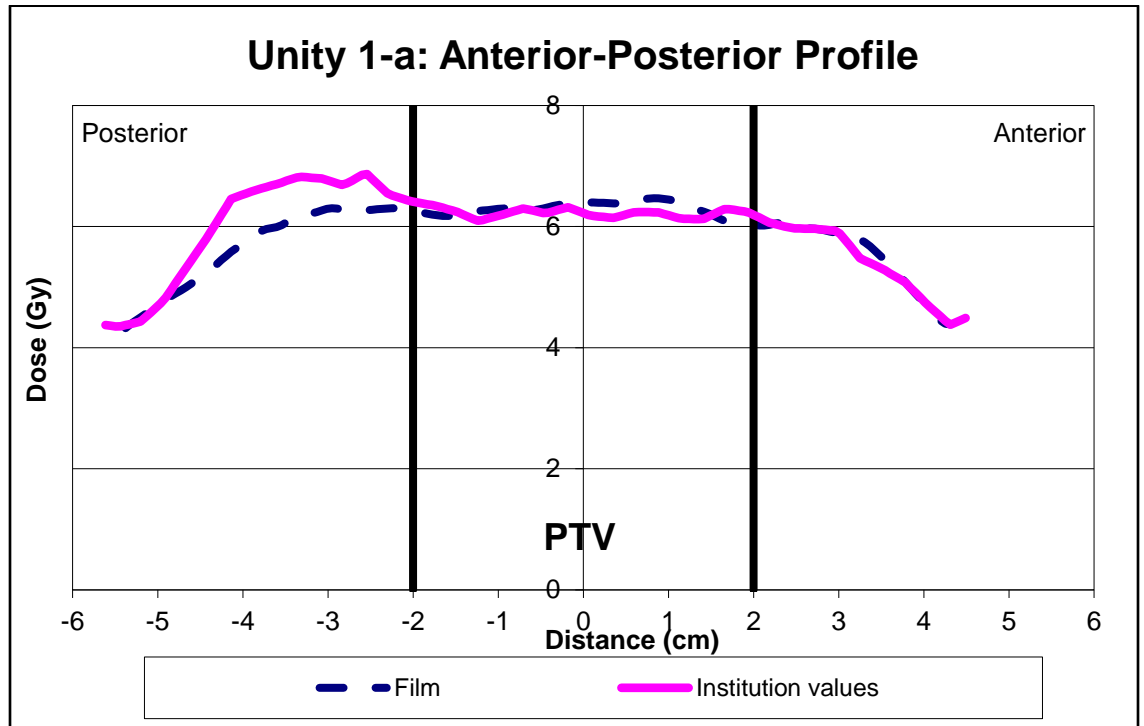
6.2.4 MRgRT Thorax: Left-Right Film Profiles

Figure 53: Left-right dose profile from Unity 1-a (7MV/1.5T) of the commissioning study using the MRgRT thorax phantom.
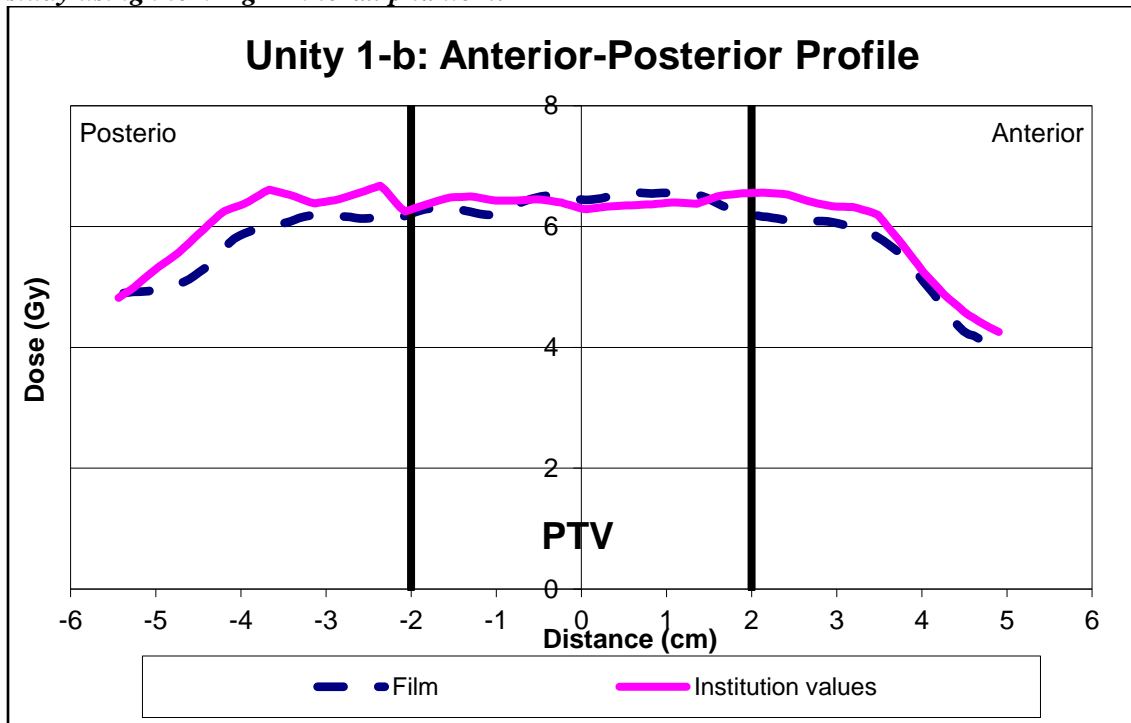

Figure 54: Left-right dose profile from Unity 1-b (7MV/1.5T) of the commissioning study using the MRgRT thorax phantom.
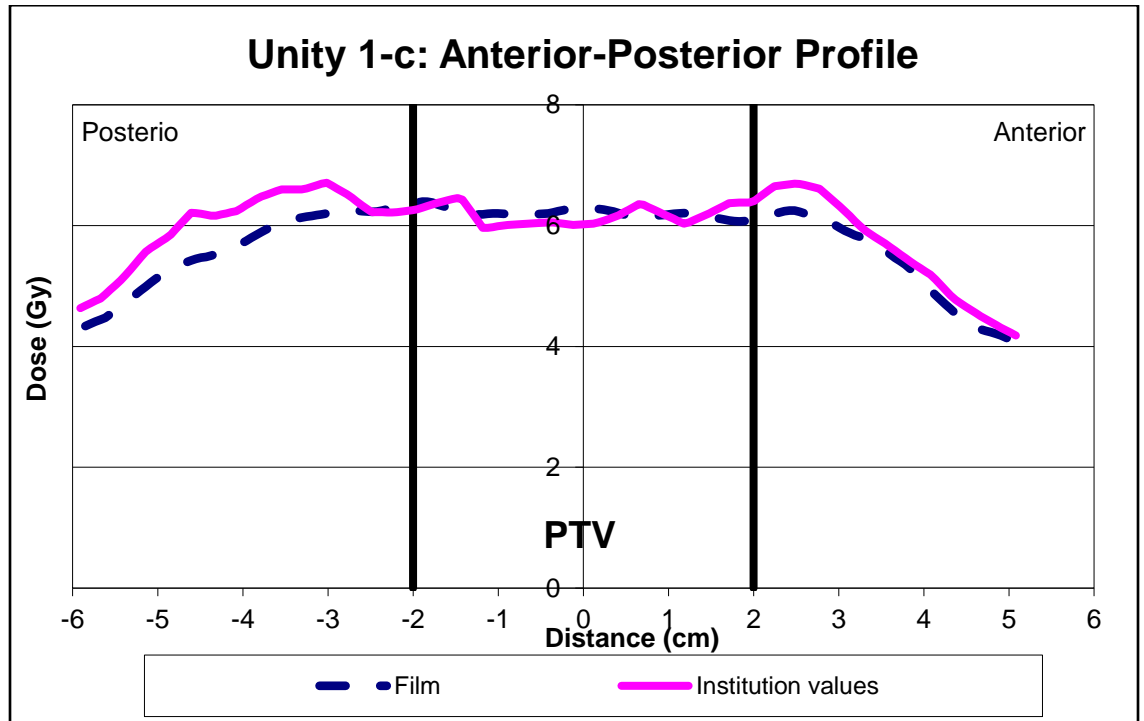
Figure 55: Left-right dose profile from Unity 1-c (7MV/1.5T) of the commissioning study using the MRgRT thorax phantom.

Figure 56: Left-right dose profile from ViewRay2 (6MV/0.35T) of the feasibility study using the MRgRT thorax phantom.

Figure 57: Left-right dose profile from ViewRay3 (60Co/0.35T) of the feasibility study using the MRgRT thorax phantom.

Figure 58: Anterior-posterior dose profile from Unity 1-a (7MV/1.5T) of the commissioning study using the MRgRT thorax phantom.
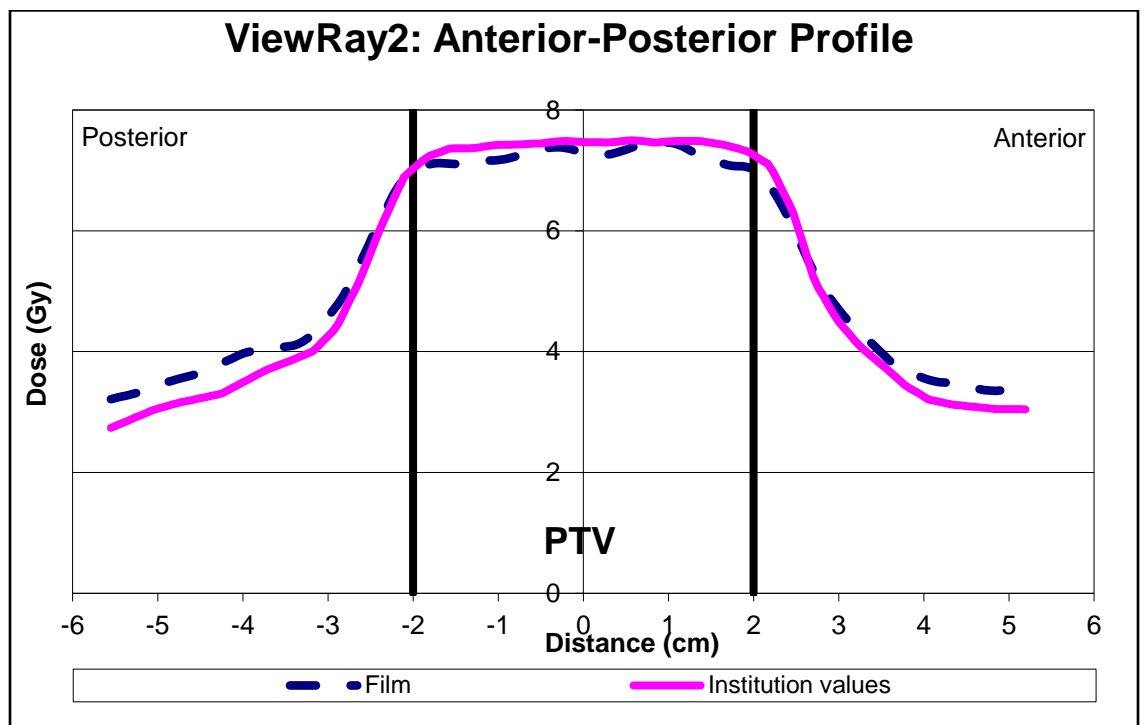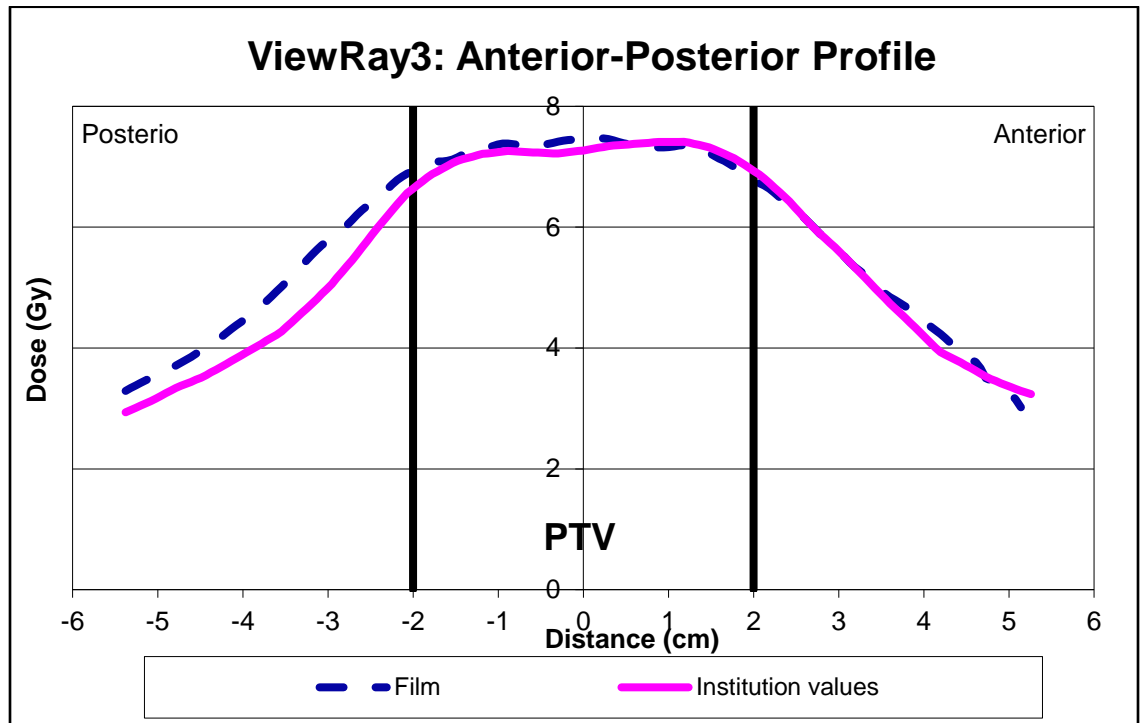

Figure 59: Anterior-posterior dose profile from Unity 1-b (7MV/1.5T) of the commissioning study using the MRgRT thorax phantom.

Figure 60: Anterior-posterior dose profile from Unity 1-c (7MV/1.5T) of the commissioning study using the MRgRT thorax phantom.

Figure 61: Anterior-posterior dose profile from ViewRay2 (6MV/0.35T) of the feasibility study using the MRgRT thorax phantom

Figure 62: Anterior-posterior dose profile from ViewRay3 (60Co/0.35T) of the feasibility study using the MRgRT thorax phantom
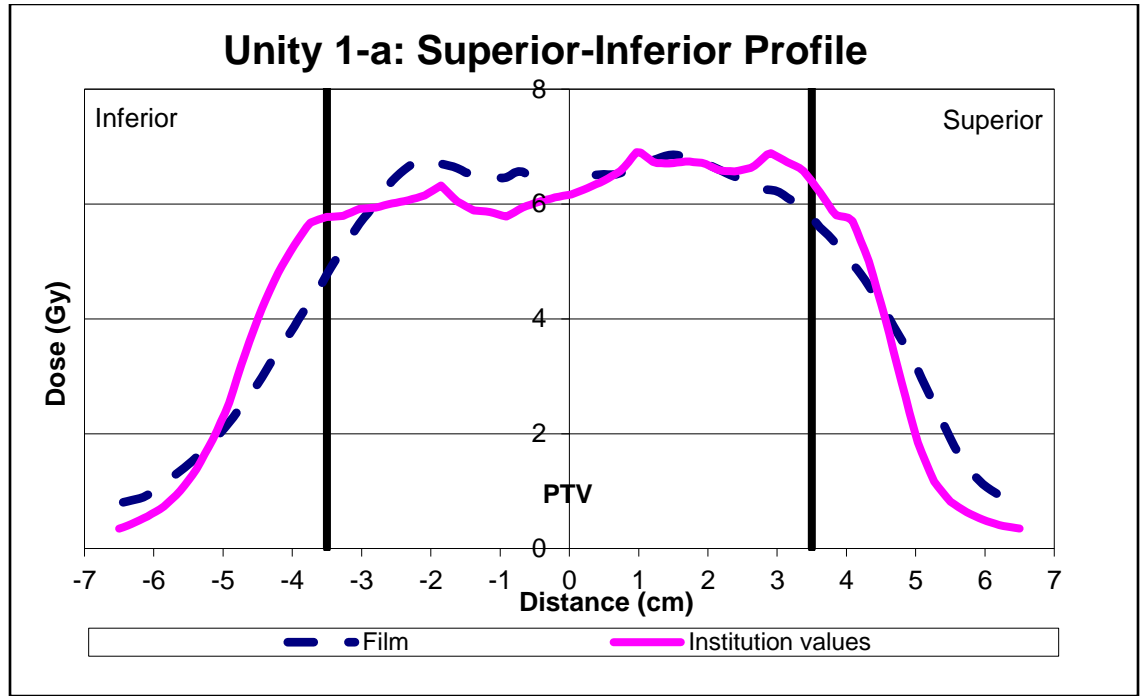
Figure 63: Superior-inferior dose profile from Unity 1-a (7MV/1.5T) of the commissioning study using the MRgRT thorax phantom.
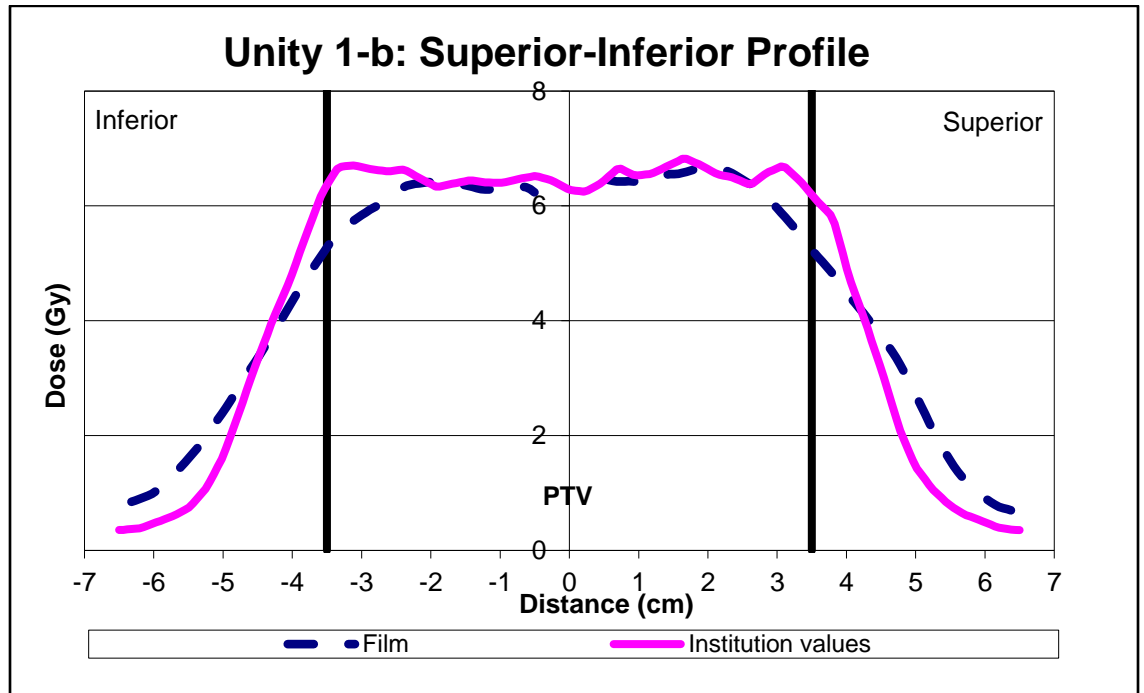

Figure 64: Superior-inferior dose profile from Unity 1-b (7MV/1.5T) of the commissioning study using the MRgRT thorax phantom.
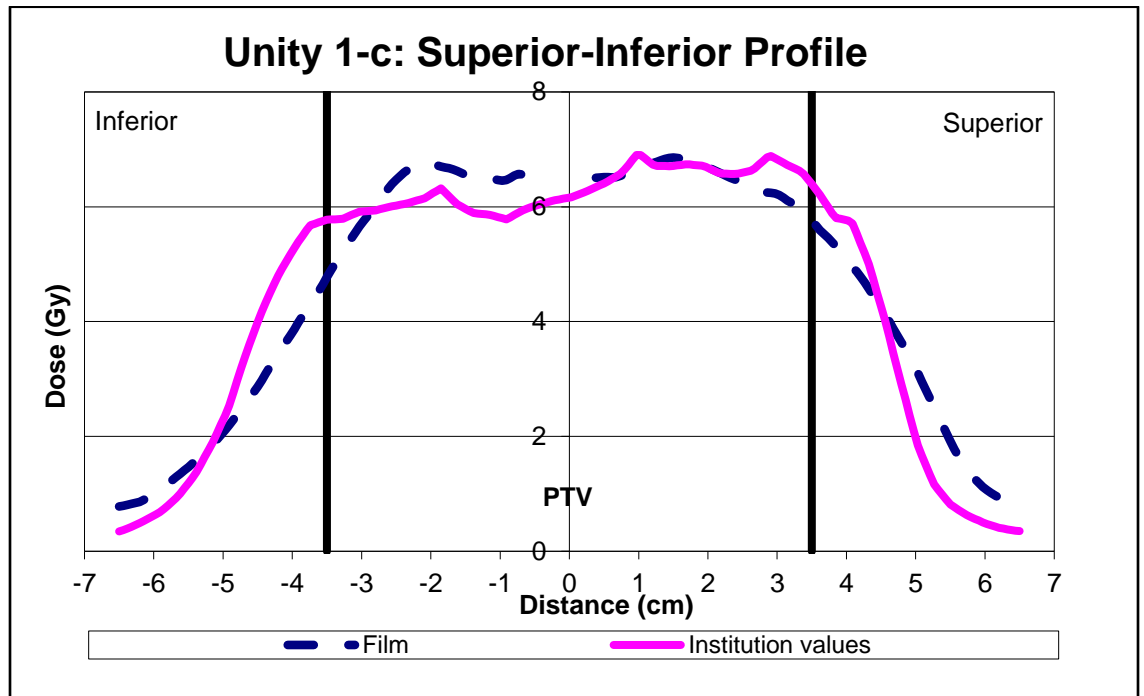
Figure 65: Superior-inferior dose profile from Unity 1-c (7MV/1.5T) of the commissioning study using the MRgRT thorax phantom.
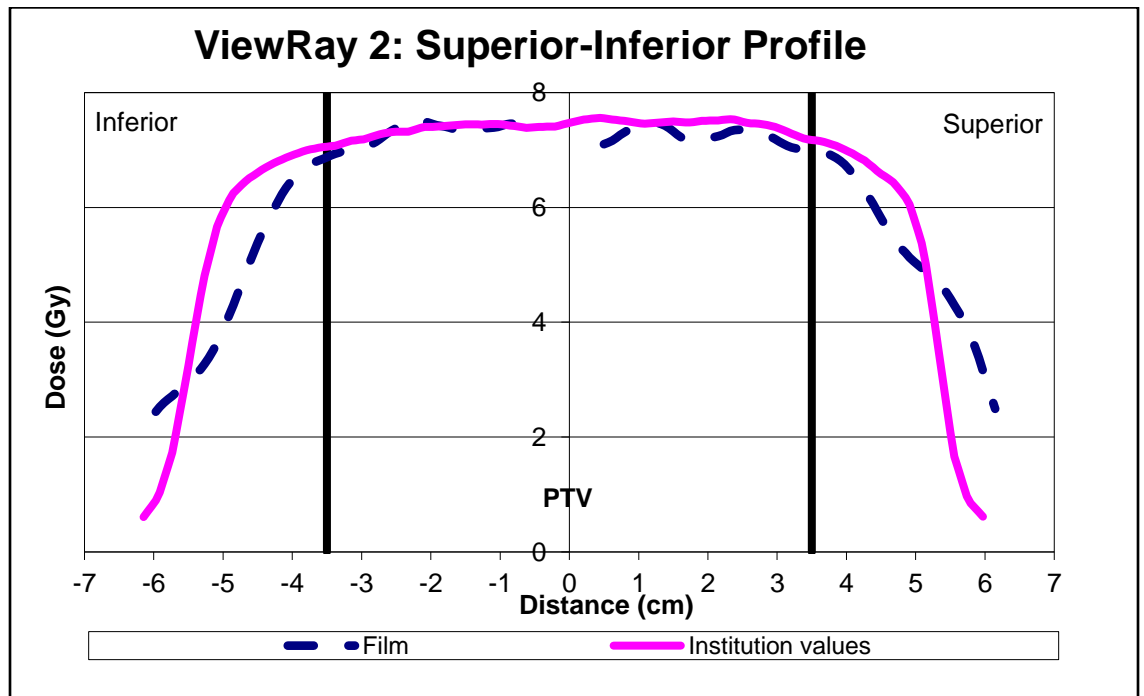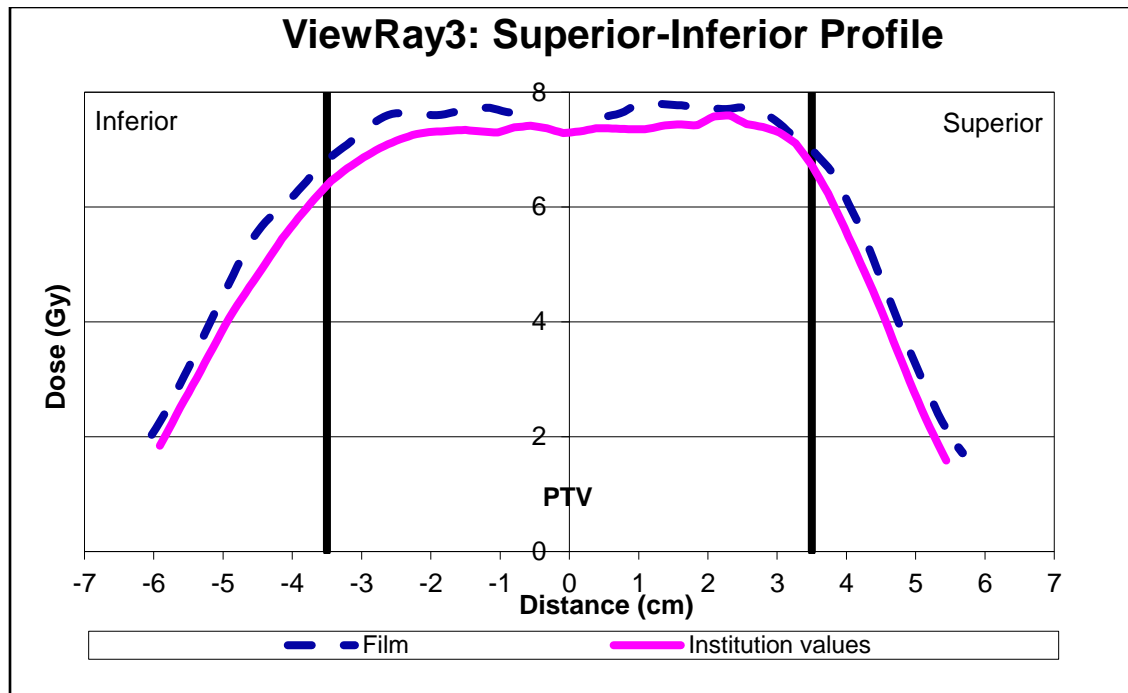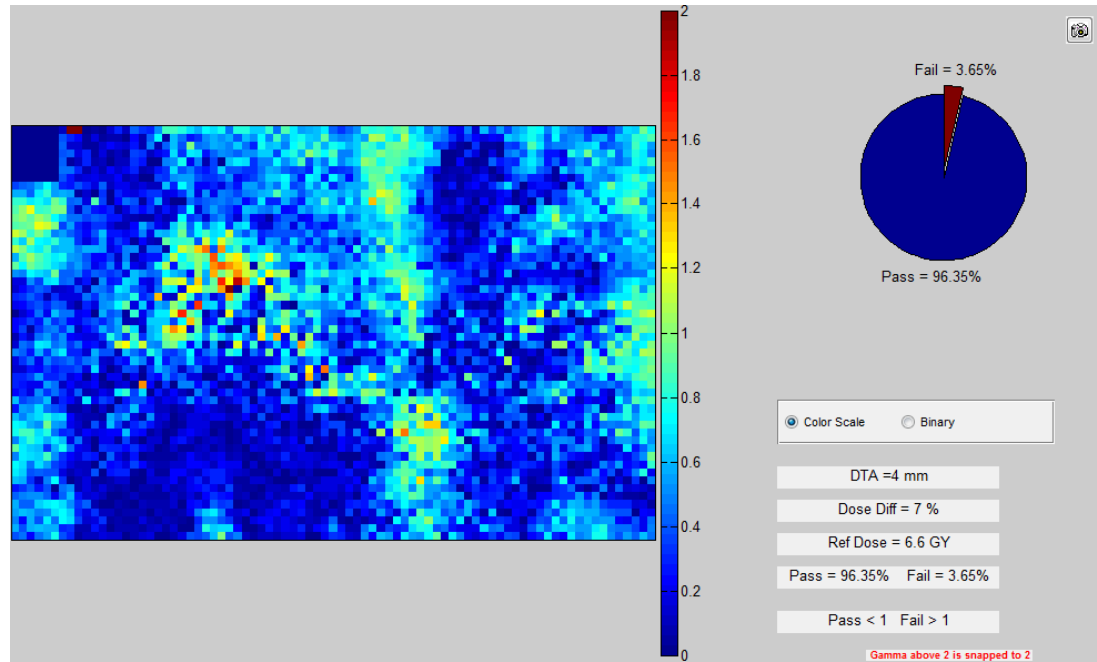

Figure 66: Superior-inferior dose profile from ViewRay2 (6MV/0.35T) of the feasibility study using the MRgRT thorax phantom.

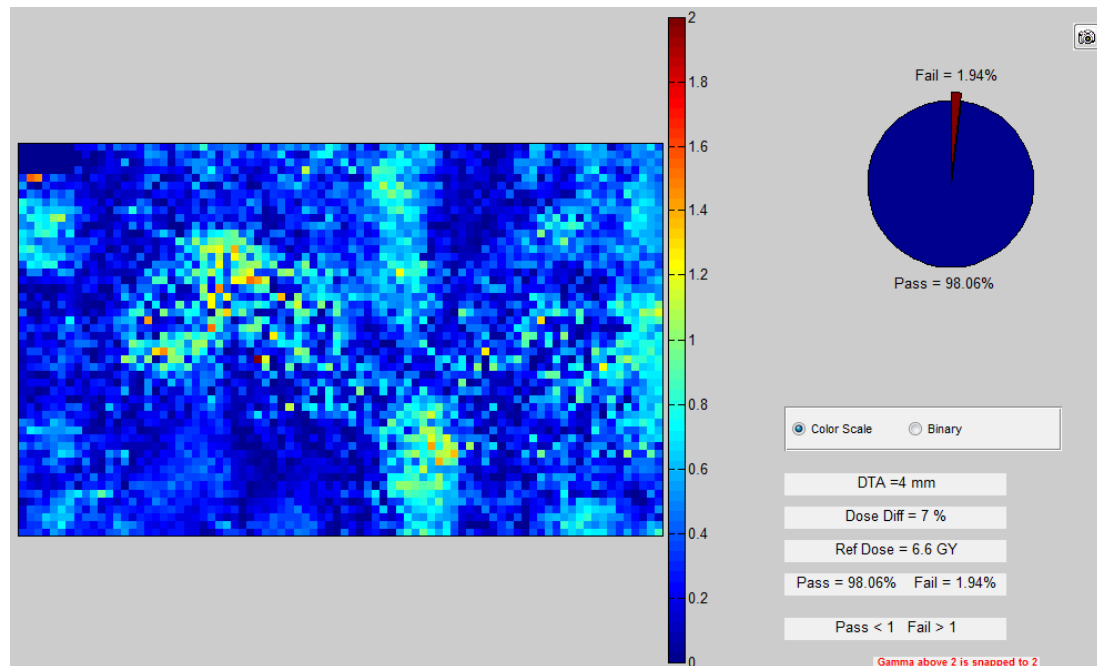*Figure 67: Superior-inferior dose profile from ViewRay3 (60Co/0.35T) of the feasibility study using the MRgRT thorax phantom.*

Appendix C: Gamma Analysis

6.2.7   MRgRT Head & Neck: Axial

Figure 68: The commissioning study for the MRgRT H&N phantom. Unity 1-a axial film had 96.4% pixels passing.

Figure 69: The commissioning study for the MRgRT H&N phantom. Unity 1-b axial film had 98.1% pixels passing.

Figure 70: The commissioning study for the MRgRT H&N phantom. Unity 1-c axial film had 99.1% pixels passing.

Figure 71: The feasibility study for the MRgRT H&N phantom. ViewRay 2 axial film had 97.9% pixels passing.

Figure 72: The feasibility study for the MRgRT H&N phantom. ViewRay 3 axial film had 96.7% pixels passing.
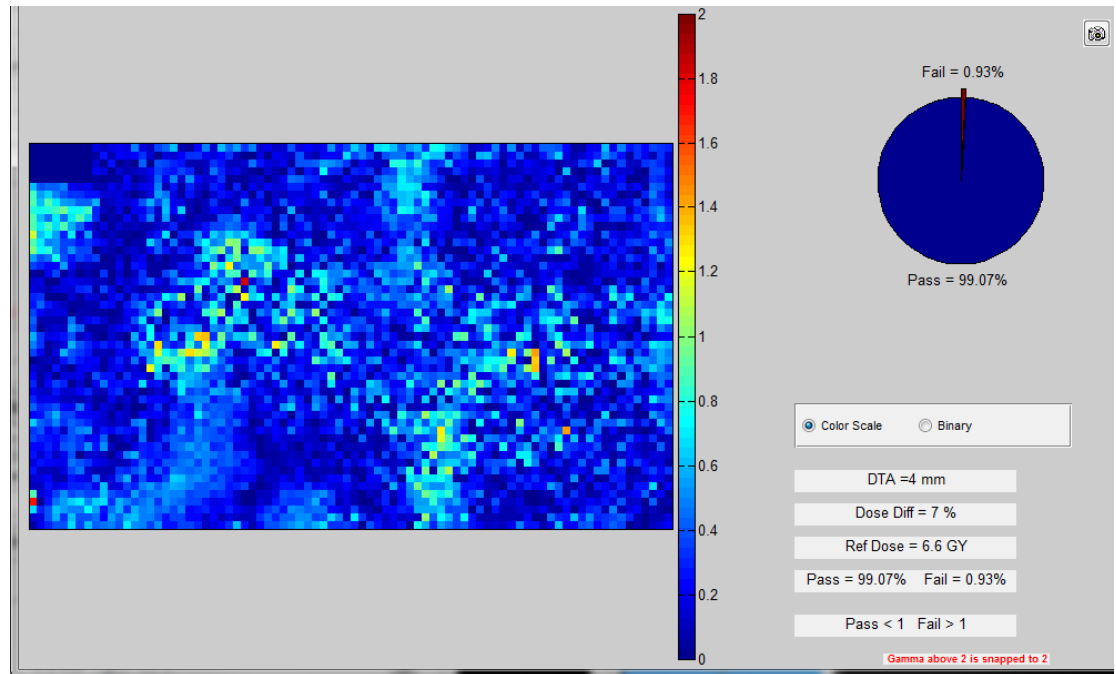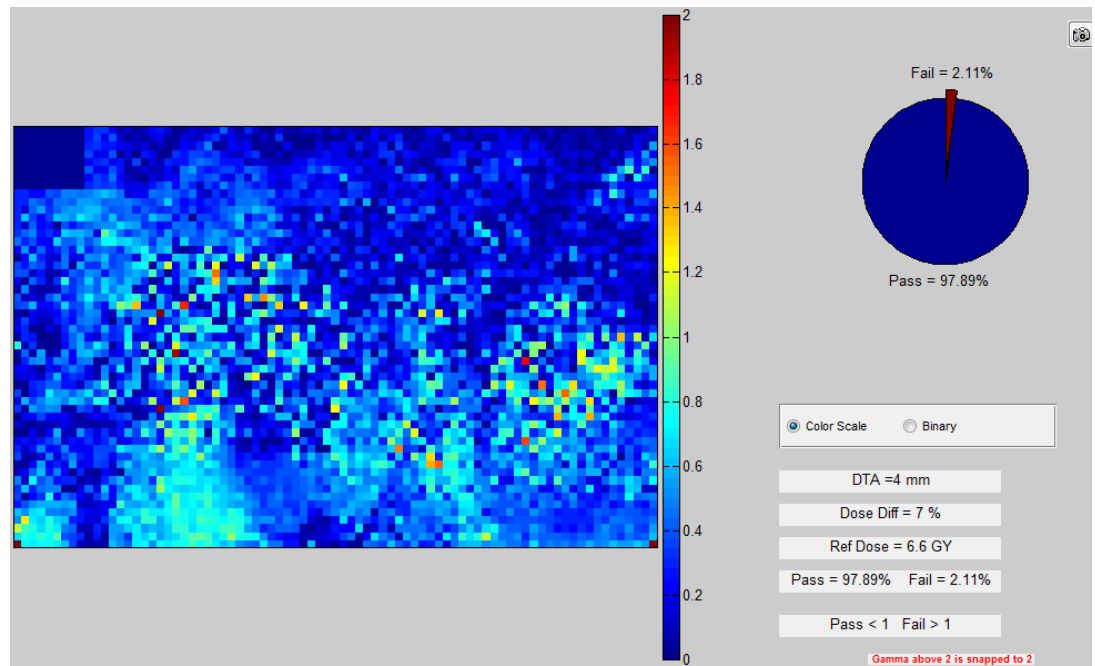
6.2.8 MRgRT Head & Neck: Sagittal

Figure 73: The commissioning study for the MRgRT H&N phantom. Unity 1-a sagittal film had 89.9% pixels passing.

Figure 74: The commissioning study for the MRgRT H&N phantom. Unity 1-b sagittal film had 89.9% pixels passing.

Figure 75: The commissioning study for the MRgRT H&N phantom. Unity 1-c sagittal film had 89.2% pixels passing.

Figure 76: The feasibility study for the MRgRT H&N phantom. ViewRay 2 sagittal film had 95.7% pixels passing.

Figure 77: The feasibility study for the MRgRT H&N phantom. ViewRay 3 sagittal film had 96.6% pixels passing.

6.2.9   MRgRT Thorax: Axial

Figure 78: The commissioning study for the MRgRT Thorax phantom. Unity 1-a axial film had 89.0% pixels passing.
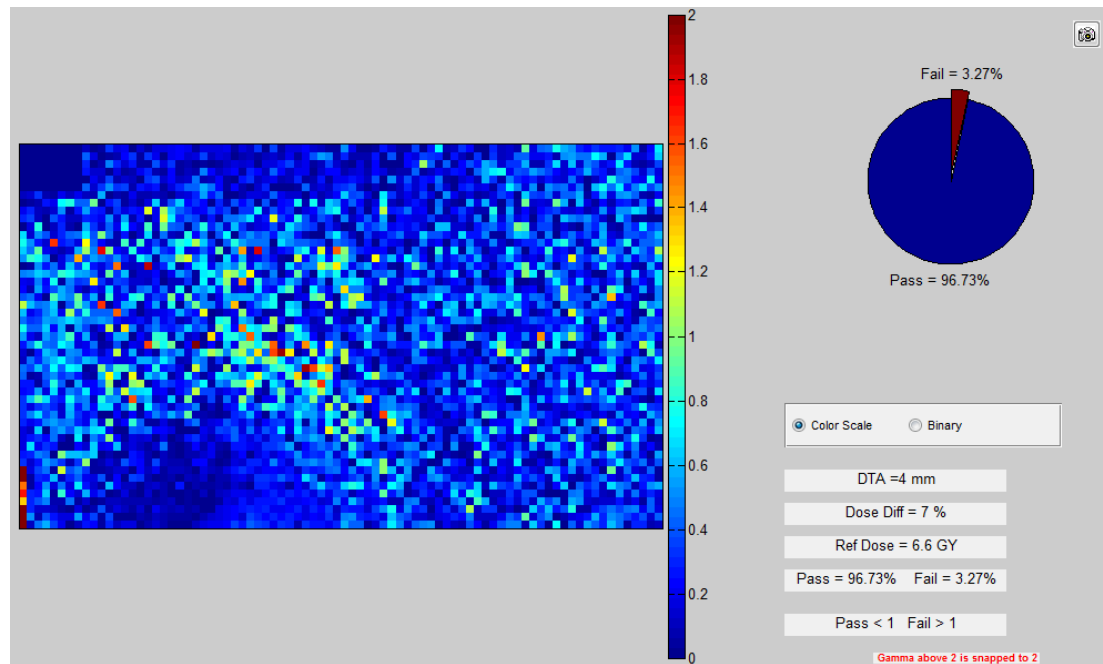

Figure 79: The commissioning study for the MRgRT Thorax phantom. Unity 1-b axial film had 97.2% pixels passing.
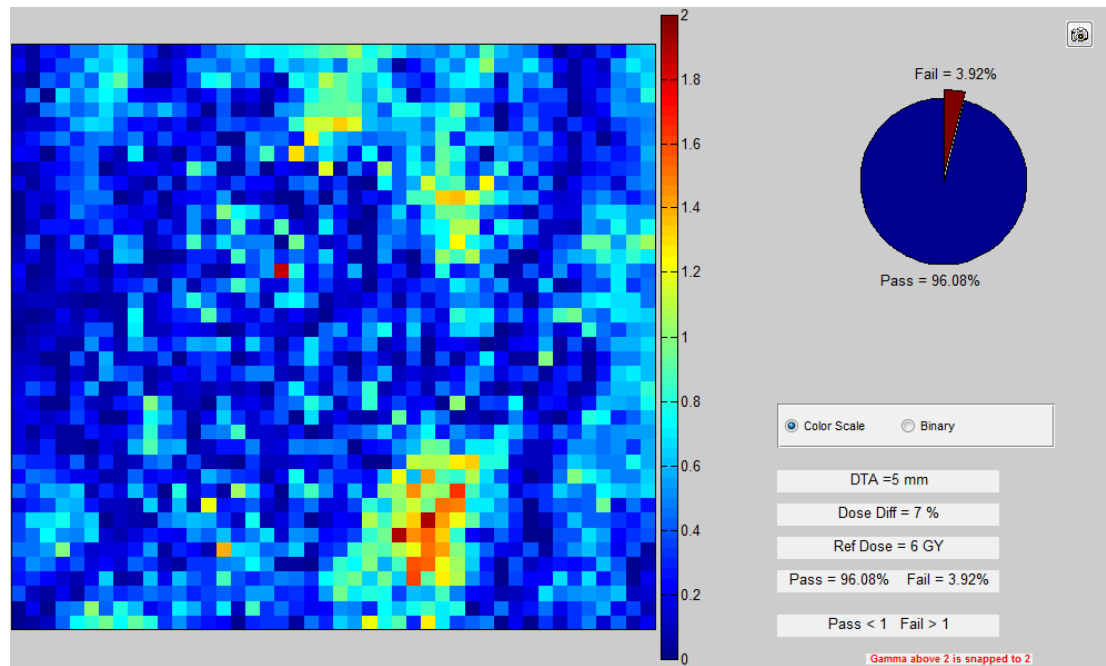
Figure 80: The commissioning study for the MRgRT Thorax phantom. Unity 1-c axial film had 96.1% pixels passing.
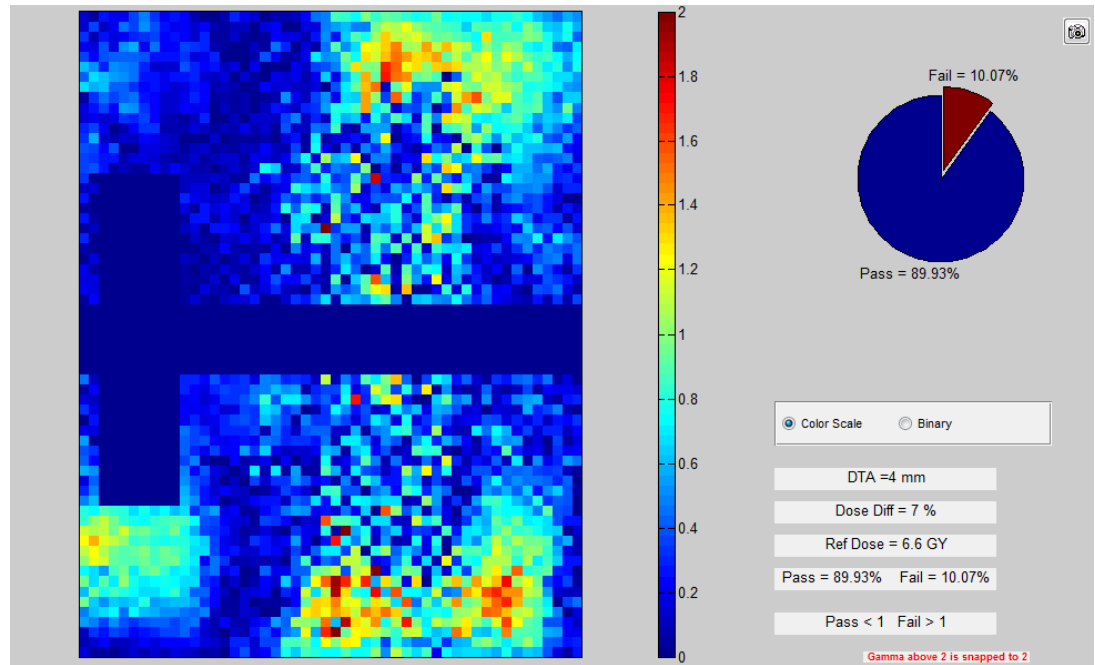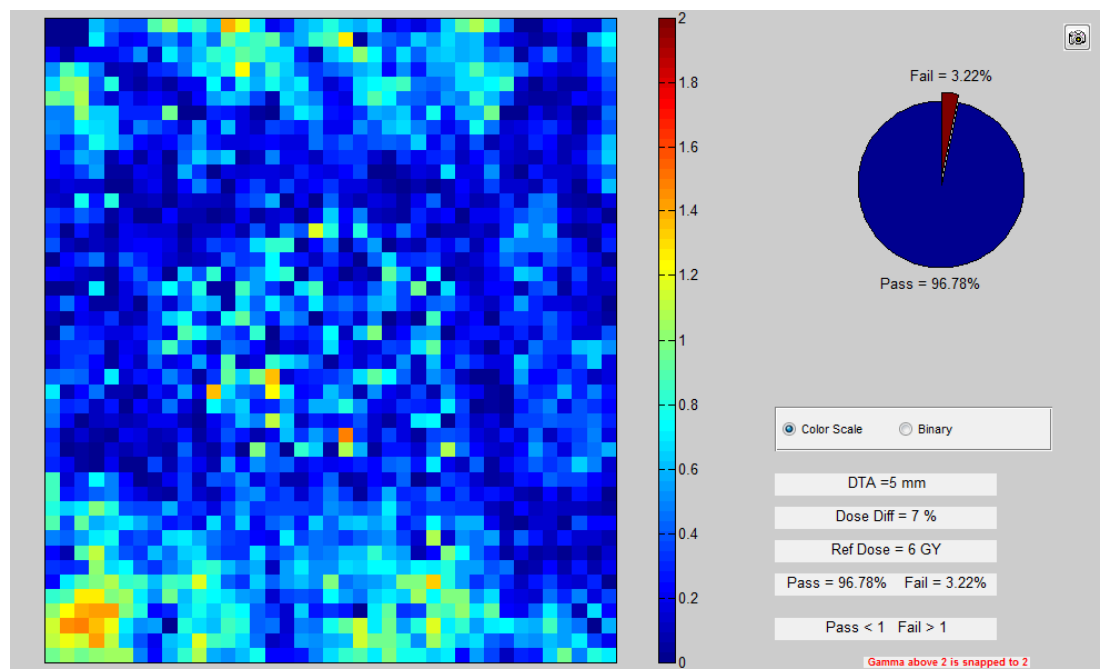

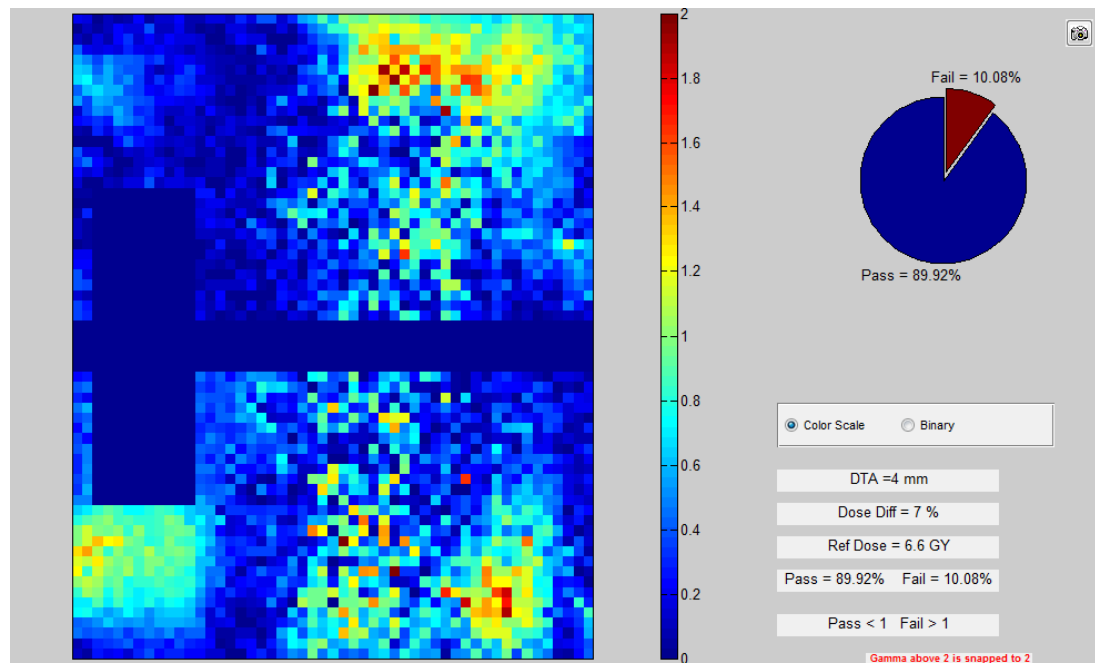*Figure 81: The feasibility study for the MRgRT Thorax phantom. ViewRay 2 axial film had 96.8% pixels passing.*
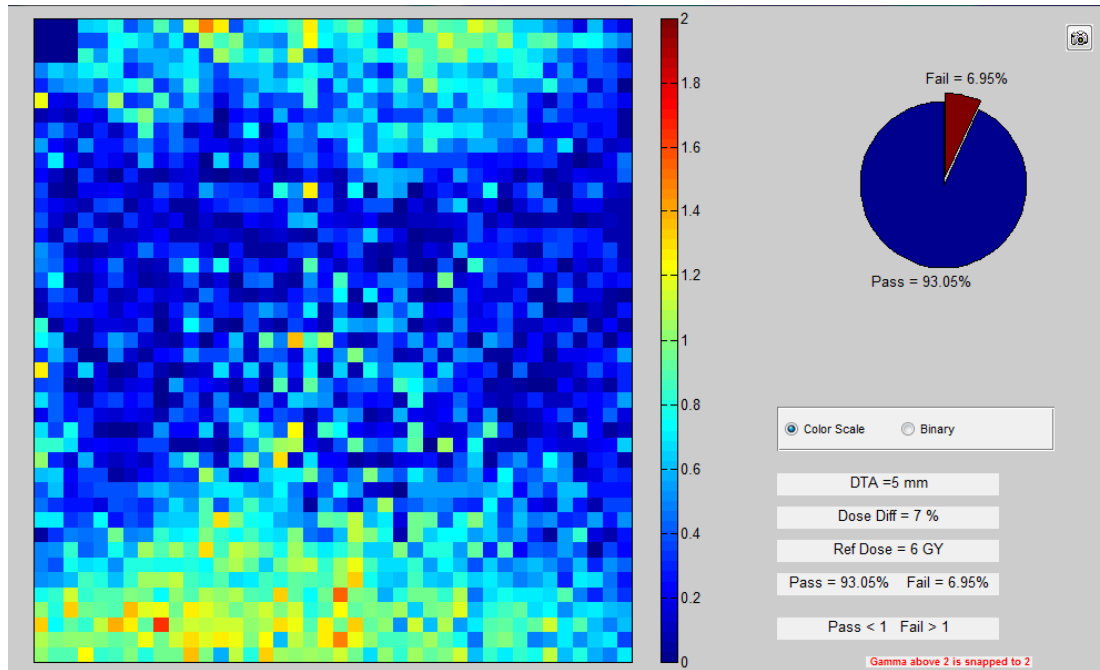
Figure 82: The feasibility study for the MRgRT Thorax phantom. ViewRay 3 axial film had 93.1% pixels passing.
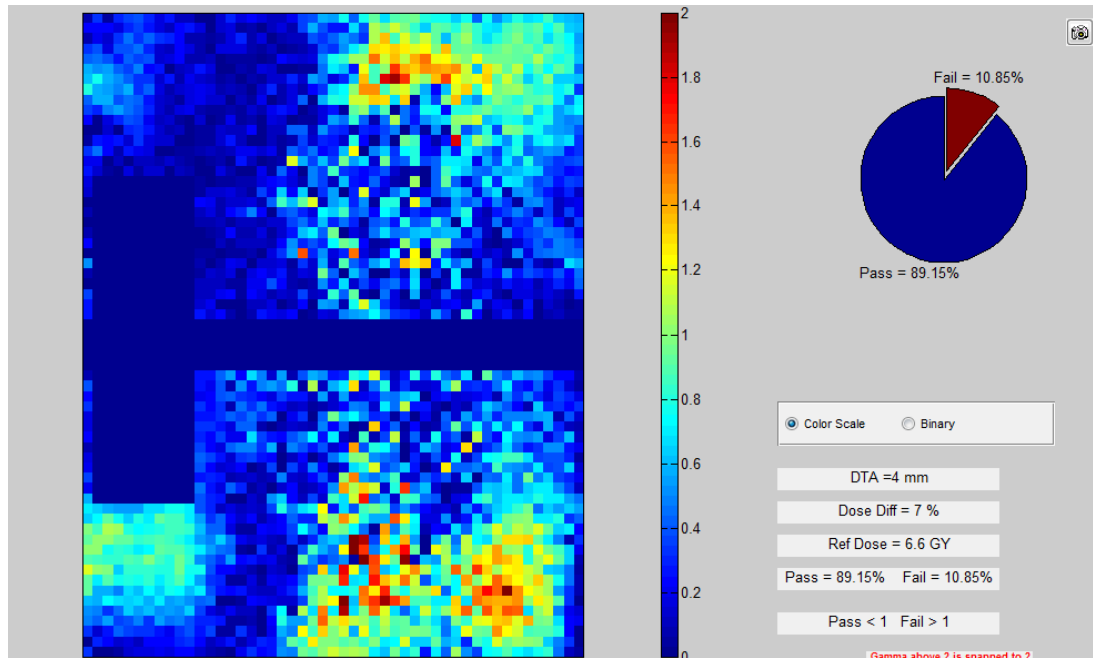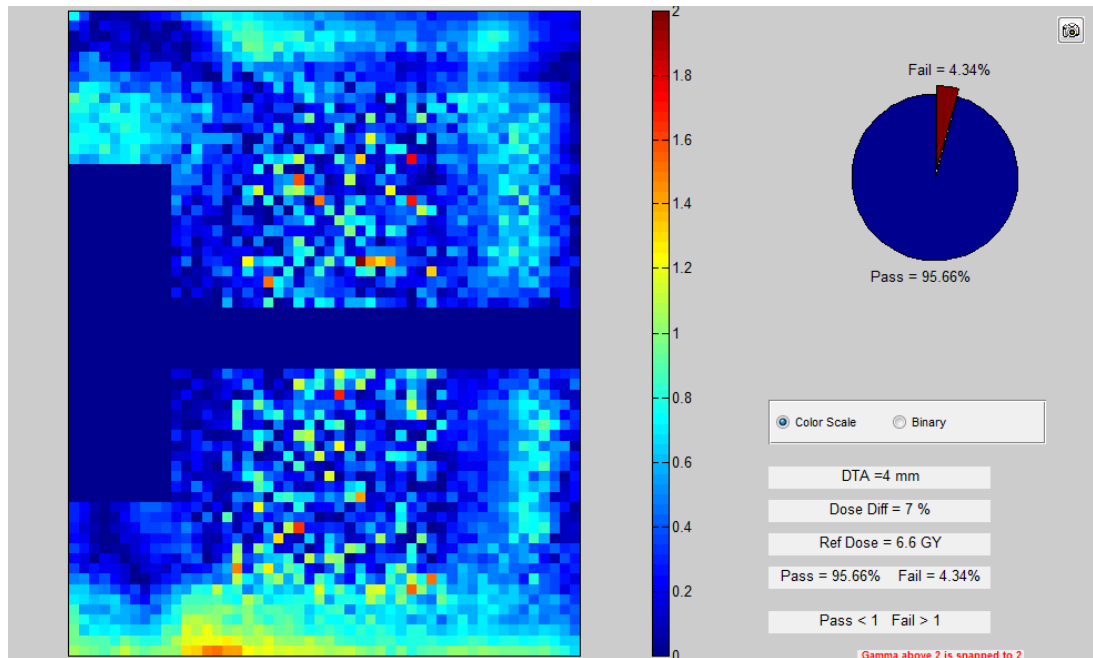
MRgRT Thorax: Sagittal
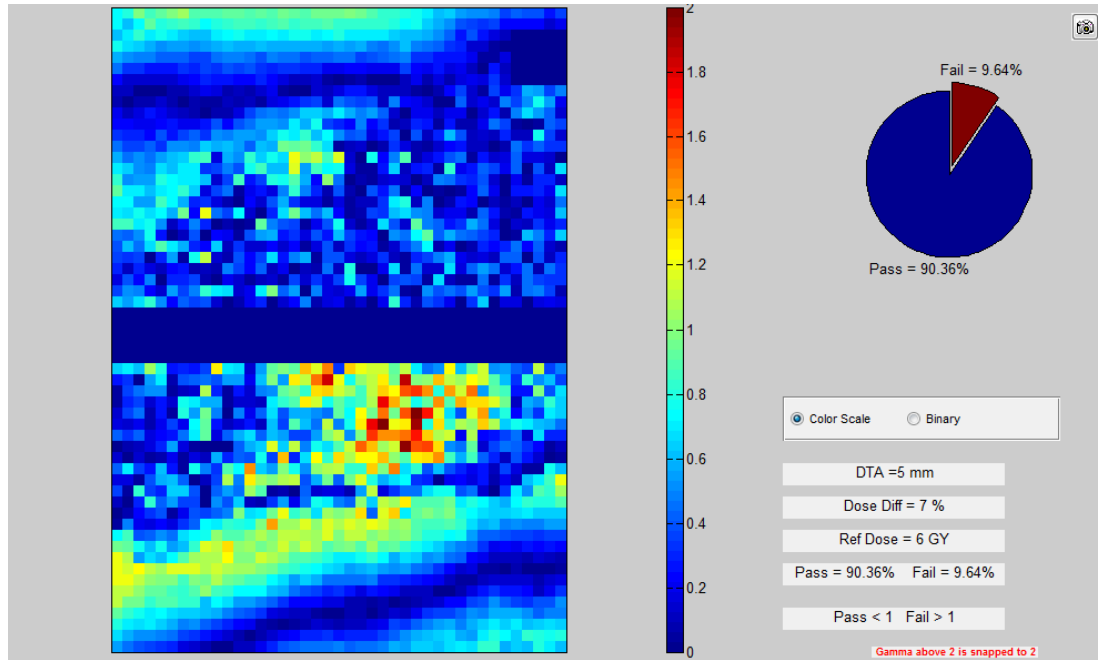
Figure 83: The commissioning study for the MRgRT Thorax phantom. Unity 1-a sagittal film had 90.4% pixels passing.
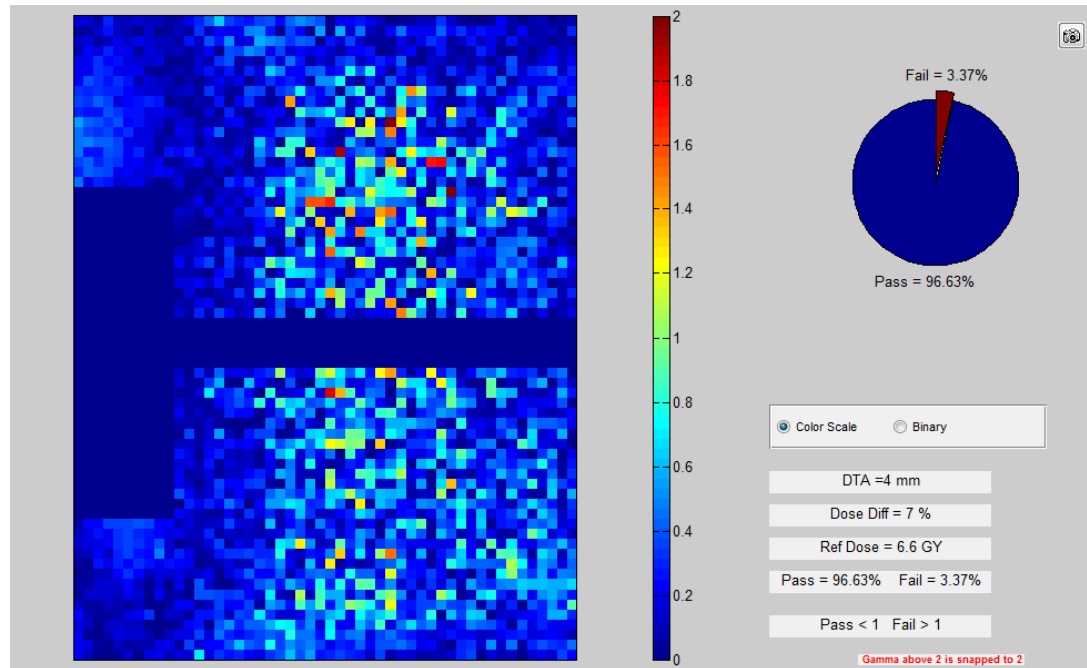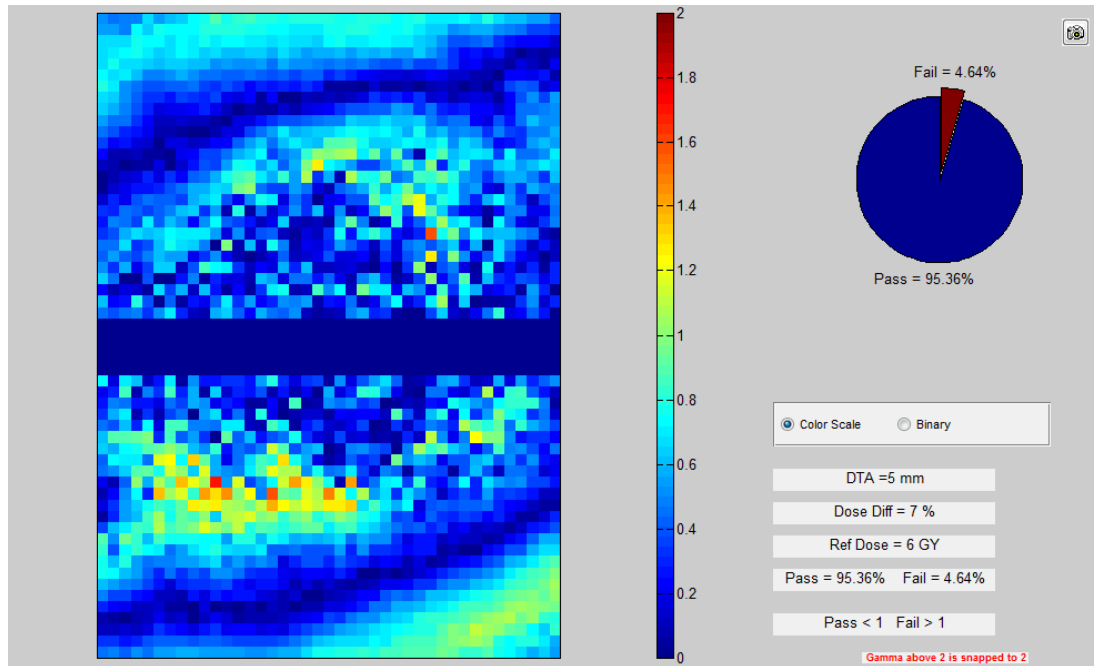

Figure 84: The commissioning study for the MRgRT Thorax phantom. Unity 1-b sagittal film had 95.4% pixels passing.
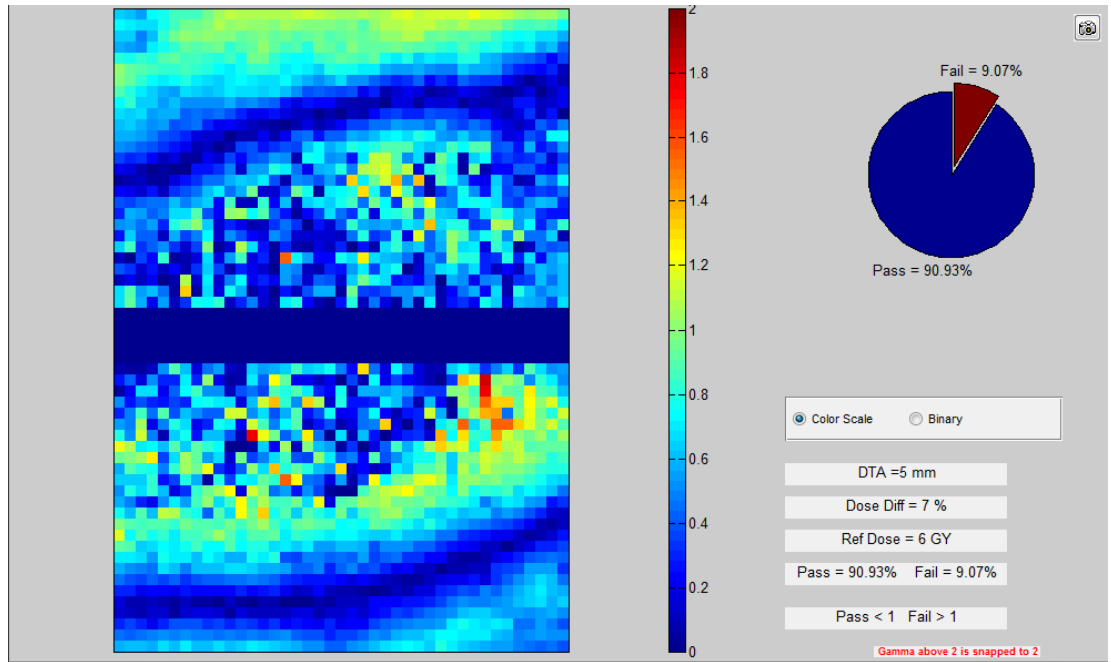
Figure 85: The commissioning study for the MRgRT Thorax phantom. Unity 1-c sagittal film had 90.9% pixels passing.
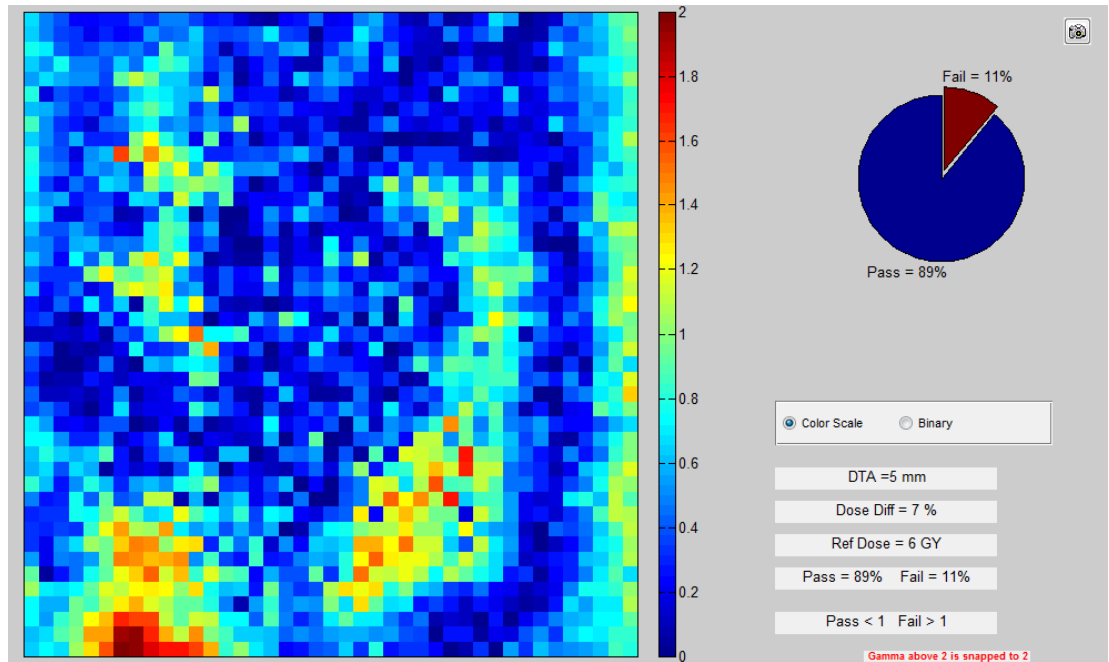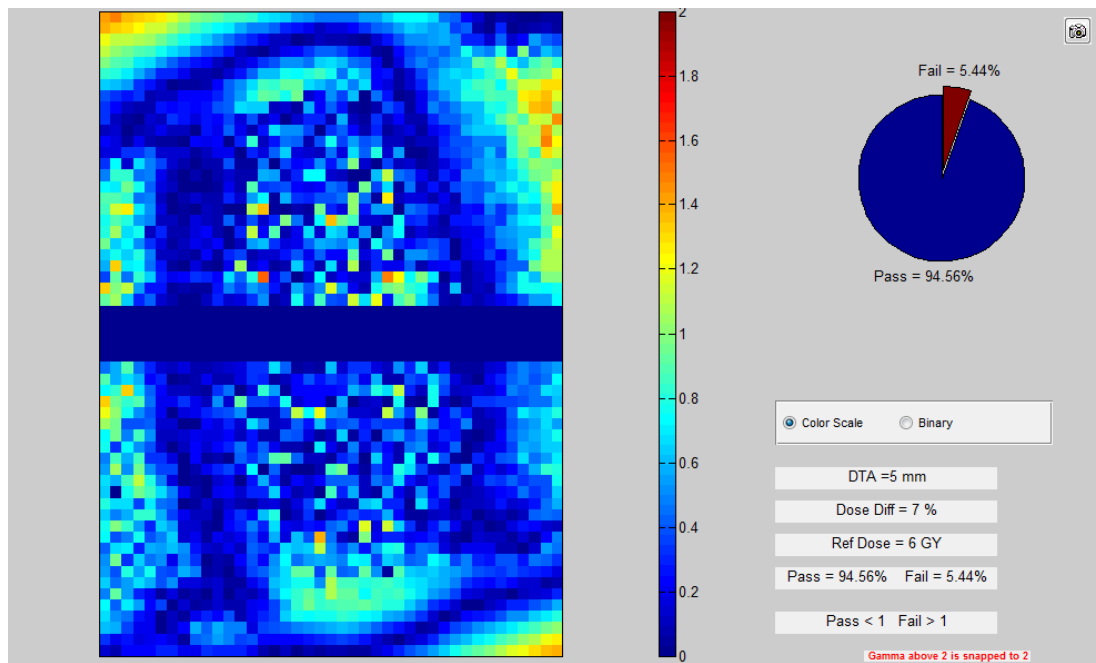

Figure 86: The feasibility study for the MRgRT Thorax phantom. ViewRay 2 sagittal film had 94.6% pixels passing.
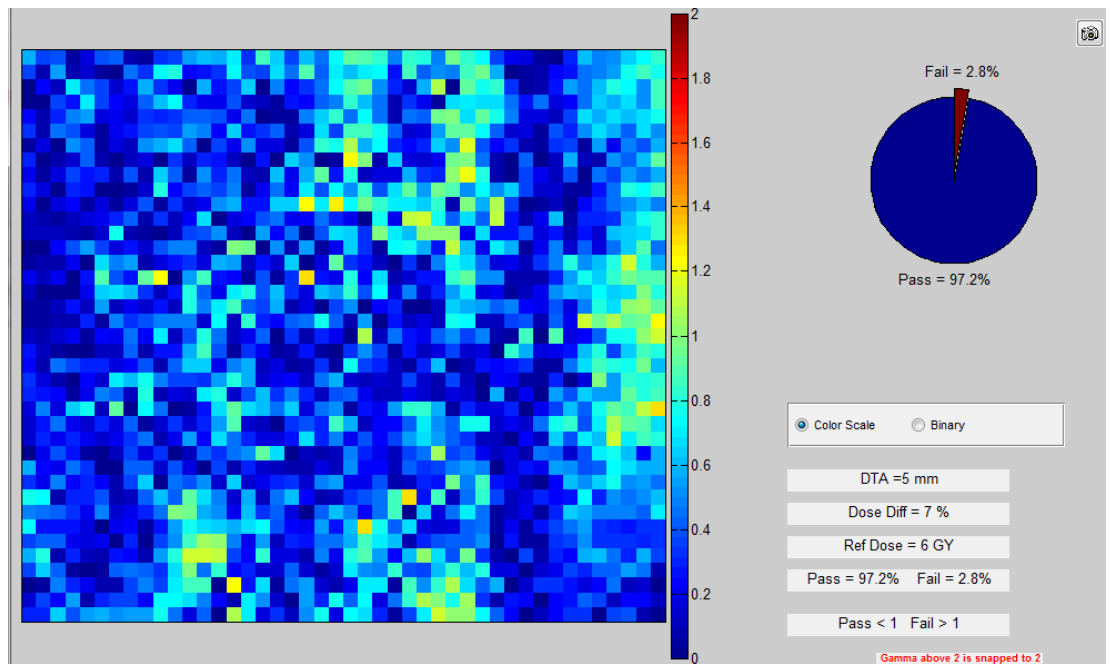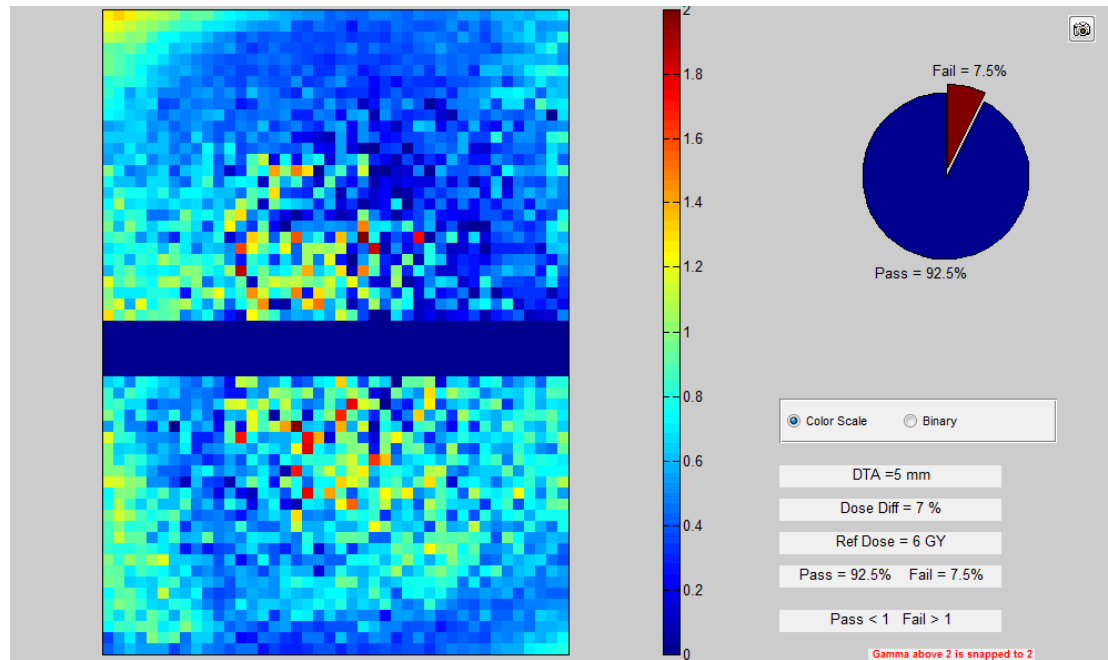
Figure 87: The feasibility study for the MRgRT Thorax phantom. ViewRay 3 sagittal film had 92.5% pixels passing.

Bibliography

1. Chen, G.T., Sharp, G.C., and Mori, S. (2009). A review of image-guided radiotherapy. Radiol Phys Technol 2, 1-12.

2. Dawson, L.A., and Sharpe, M.B. (2006). Image-guided radiotherapy: rationale, benefits, and limitations. The lancet oncology 7, 848-858.

3. Franzone, P., Fiorentino, A., Barra, S., Cante, D., Masini, L., Cazzulo, E., Todisco, L., Gabriele, P., Garibaldi, E., and Merlotti, A. (2016). Image-guided radiation therapy (IGRT): practical recommendations of Italian Association of Radiation Oncology (AIRO). La radiologia medica 121, 958-965.

4. School, A.A.o.P.i.M.S., Curran, B.H., Balter, J.E., and Chetty, I.J. (2006). Integrating New Technologies Into the Clinic: Monte Carlo and Image-guided Radiation Therapy : Proceedings of the American Association of Physicists in Medicine Summer School, University of Windsor, Windsor, Ontario, Canada, June 18-22, 2006.(Medical Physics Pub.).

5. Timmerman, R.D., and Xing, L. (2012). Image-Guided and Adaptive Radiation Therapy.(Wolters Kluwer Health).

6. Hayat, M.A. (2007). Cancer Imaging: Instrumentation and Applications.(Elsevier Science).

7. Goyal, S., and Kataria, T. (2014). Image guidance in radiation therapy: techniques and applications. Radiology research and practice 2014.

8. Li, X.A. (2011). Adaptive Radiation Therapy.(CRC Press).

9. Noel, C.E., Parikh, P.J., Spencer, C.R., Green, O.L., Hu, Y., Mutic, S., and Olsen, J.R. (2015). Comparison of onboard low-field magnetic resonance imaging versus

onboard computed tomography for anatomy visualization in radiotherapy. Acta Oncologica 54, 1474-1482.

10. Jaffray, D.A., Carlone, M.C., Milosevic, M.F., Breen, S.L., Stanescu, T., Rink, A., Alasti, H., Simeonov, A., Sweitzer, M.C., and Winter, J.D. (2014). A facility for magnetic resonance-guided radiation therapy. Semin Radiat Oncol 24, 193-195.

11. Keall, P.J., Barton, M., Crozier, S., Australian Mri-Linac Program, i.c.f.I.I.I.C.C.C.L.H.S.U.U.o.N.Q.S.W.S., and Wollongong. (2014). The Australian magnetic resonance imaging-linac program. Semin Radiat Oncol 24, 203-206.

12. Lagendijk, J.J., Raaymakers, B.W., and van Vulpen, M. (2014). The magnetic resonance imaging-linac system. Semin Radiat Oncol 24, 207-209.

13. Fallone, B.G. (2014). The rotating biplanar linac-magnetic resonance imaging system. Semin Radiat Oncol 24, 200-202.

14. Lagendijk, J.J., van Vulpen, M., and Raaymakers, B.W. (2016). The development of the MRI linac system for online MRI-guided radiotherapy: a clinical update. J Intern Med 280, 203-208.

15. Mutic, S., and Dempsey, J.F. (2014). The ViewRay system: magnetic resonance-guided and controlled radiotherapy. Semin Radiat Oncol 24, 196-199.

16. Saracen, M. (2016). First Scientific Presentations on ViewRay's MRIdian Linac Technology. In, M. Saracen, ed. (Cleveland, Ohio.

17. Whelan, B., Gierman, S., Holloway, L., Schmerge, J., Keall, P., and Fahrig, R. (2016). A novel electron accelerator for MRI-Linac radiotherapy. Med Phys 43, 1285-1294.

18. Baillie, D., Fallone, B.G., and Steciw, S. (2017). Design and simulation of a short, variable-energy 4 to 10 MV S-band linear accelerator waveguide. Medical physics.

19. St Aubin, J., Steciw, S., and Fallone, B. (2010). The design of a simulated in-line side-coupled 6 MV linear accelerator waveguide. Medical physics 37, 466-476.

20. Baillie, D., Aubin, J.S., Fallone, B., and Steciw, S. (2015). FEM design and simulation of a short, 10 MV, S-band Linac with Monte Carlo dose simulations. Medical physics 42, 2044-2053.

21. Wachowicz, K., Tadic, T., and Fallone, B. (2012). Geometric distortion and shimming considerations in a rotating MR-linac design due to the influence of low-level external magnetic fields. Medical physics 39, 2659-2668.

22. Saracen, M. (2017). First Patients Treated with ViewRay's MRIdian Linac System at Henry Ford Health System. In, M. Saracen, ed. (Cleveland, Ohio.

23. Raaymakers, B.W., Jurgenliemk-Schulz, I.M., Bol, G.H., Glitzner, M., Kotte, A., van Asselen, B., de Boer, J.C.J., Bluemink, J.J., Hackett, S.L., Moerland, M.A., et al. (2017). First patients treated with a 1.5 T MRI-Linac: clinical proof of concept of a high-precision, high-field MRI guided radiotherapy treatment. Phys Med Biol 62, L41-L50.

24. Lagendijk, J.J., Raaymakers, B.W., Raaijmakers, A.J., Overweg, J., Brown, K.J., Kerkhof, E.M., van der Put, R.W., Hardemark, B., van Vulpen, M., and van der Heide, U.A. (2008). MRI/linac integration. Radiother Oncol 86, 25-29.

25. Raaymakers, B.W., Lagendijk, J.J., Overweg, J., Kok, J.G., Raaijmakers, A.J., Kerkhof, E.M., van der Put, R.W., Meijsing, I., Crijns, S.P., Benedosso, F., et al.

(2009). Integrating a 1.5 T MRI scanner with a 6 MV accelerator: proof of concept. Phys Med Biol 54, N229-237.

26. (2017). Elekta Unity, transformative magnetic resonance radiation therapy (MR/RT) system, debuts at ESTRO 36. In. (Vienna, Austria.

27. Zagoudis, J. (2015). MRI Brings New Vision to Radiation Therapy. In. (Imaging Technology News.

28. (2015). The MRIdian Advantage. In. (Oakwood Village, OH, ViewRay.

29. Davis, R. (2017). Department of Radiation Oncology to install MRIdian Linac system. In Department News. (St. Louis.

30. (2017). MRIdian Linac Advantage. In ViewRay. (Oakwood Village, OH

31. Metcalfe, P., Liney, G., Holloway, L., Walker, A., Barton, M., Delaney, G., Vinod, S., and Tome, W. (2013). The potential for an enhanced role for MRI in radiation-therapy treatment planning. Technology in cancer research & treatment 12, 429-446.

32. Raaijmakers, A.J., Raaymakers, B.W., and Lagendijk, J.J. (2008). Magnetic-field-induced dose effects in MR-guided radiotherapy systems: dependence on the magnetic field strength. Phys Med Biol 53, 909-923.

33. Raaijmakers, A.J., Raaymakers, B.W., and Lagendijk, J.J. (2005). Integrating a MRI scanner with a 6 MV radiotherapy accelerator: dose increase at tissue-air interfaces in a lateral magnetic field due to returning electrons. Phys Med Biol 50, 1363-1376.

34. Raaijmakers, A.J. (2008). MR-guided radiotherapy: magnetic field dose effects. University Medical Center Utrecht, Utrecht, Netherlands.

35. O'Brien, D.J., Roberts, D.A., Ibbott, G.S., and Sawakuchi, G.O. (2016). Reference dosimetry in magnetic fields: formalism and ionization chamber correction factors. Med Phys 43, 4915.

36. O'Brien, D., Schupp, N., Pencea, S., Dolan, J., and Sawakuchi, G. (2017). Dosimetry in the presence of strong magnetic fields. In Journal of Physics: Conference Series. (IOP Publishing), p 012055.

37. O'Brien, D.J., and Sawakuchi, G.O. (2017). Monte Carlo study of the chamber-phantom air gap effect in a magnetic field. Med Phys 44, 3830-3838.

38. Khan, F.M., and Gibbons, J.P. (2014). Khan's The Physics of Radiation Therapy.(Wolters Kluwer Health).

39. Knoll, G.F. (2000). Radiation Detection and Measurement.(Wiley).

40. El-Hafez, A.A., Yasin, M., and Sadek, A. (2011). GCAFIT—A new tool for glow curve analysis in thermoluminescence nanodosimetry. Nuclear Instruments and Methods in Physics Research Section A: Accelerators, Spectrometers, Detectors and Associated Equipment 637, 158-163.

41. Taylor, M. (2011). Robust determination of effective atomic numbers for electron interactions with TLD-100 and TLD-100H thermoluminescent dosimeters. Nuclear Instruments and Methods in Physics Research Section B: Beam Interactions with Materials and Atoms 269, 770-773.

42. Kirby, T., Hanson, W., and Johnston, D. (1992). Uncertainty analysis of absorbed dose calculations from thermoluminescence dosimeters. Medical physics 19, 1427-1433.

43. Das, I.J. (2017). Radiochromic Film: Role and Applications in Radiation Dosimetry.(CRC Press).

44. (2018). GAFCHROMIC (TM) Dosimetry Media Type EBT-3. In Web (http://wwwgafchromiccom/documents/EBT3_Specificationspdf). (

45. Molineu, A., Hernandez, N., Nguyen, T., Ibbott, G., and Followill, D. (2013). Credentialing results from IMRT irradiations of an anthropomorphic head and neck phantom. Medical physics 40.

46. Palta, J.R., Deye, J.A., Ibbott, G.S., Purdy, J.A., and Urie, M.M. (2004). Credentialing of institutions for IMRT in clinical trials. International Journal of Radiation Oncology* Biology* Physics 59, 1257-1259.

47. Lecchi, M., Fossati, P., Elisei, F., Orecchia, R., and Lucignani, G. (2008). Current concepts on imaging in radiotherapy. Eur J Nucl Med Mol Imaging 35, 821-837.

48. Bol, G.H., Lagendijk, J.J., and Raaymakers, B.W. (2015). Compensating for the impact of non-stationary spherical air cavities on IMRT dose delivery in transverse magnetic fields. Phys Med Biol 60, 755-768.

49. Arumugam, S., Sidhom, M., Truant, D., Xing, A., Udovitch, M., and Holloway, L. (2017). Variable angle stereo imaging for rapid patient position correction in an in-house real-time position monitoring system. Phys Med 33, 170-178.

50. Prior, P., Chen, X., Botros, M., Paulson, E.S., Lawton, C., Erickson, B., and Li, X.A. (2016). MRI-based IMRT planning for MR-linac: comparison between CT- and MRI-based plans for pancreatic and prostate cancers. Phys Med Biol 61, 3819-3842.

51. Brock, K.K., and Dawson, L.A. (2014). Point: Principles of magnetic resonance imaging integration in a computed tomography-based radiotherapy workflow. Semin Radiat Oncol 24, 169-174.

52. Paulson, E.S., Erickson, B., Schultz, C., and Allen Li, X. (2015). Comprehensive MRI simulation methodology using a dedicated MRI scanner in radiation oncology for external beam radiation treatment planning. Med Phys 42, 28-39.

53. Nyholm, T., and Jonsson, J. (2014). Counterpoint: Opportunities and challenges of a magnetic resonance imaging-only radiotherapy work flow. Semin Radiat Oncol 24, 175-180.

54. Torresin, A., Brambilla, M.G., Monti, A.F., Moscato, A., Brockmann, M.A., Schad, L., Attenberger, U.I., and Lohr, F. (2015). Review of potential improvements using MRI in the radiotherapy workflow. Z Med Phys 25, 210-220.

55. Liney, G.P., and Moerland, M.A. (2014). Magnetic resonance imaging acquisition techniques for radiotherapy planning. Semin Radiat Oncol 24, 160-168.

56. Ruschin, M., Davidson, S.R., Phounsy, W., Yoo, T.S., Chin, L., Pignol, J.P., Ravi, A., and McCann, C. (2016). Technical Note: Multipurpose CT, ultrasound, and MRI breast phantom for use in radiotherapy and minimally invasive interventions. Med Phys 43, 2508.

57. Gallas, R.R., Hunemohr, N., Runz, A., Niebuhr, N.I., Jakel, O., and Greilich, S. (2015). An anthropomorphic multimodality (CT/MRI) head phantom prototype for end-to-end tests in ion radiotherapy. Z Med Phys 25, 391-399.

58. Niebuhr, N.I., Johnen, W., Guldaglar, T., Runz, A., Echner, G., Mann, P., Mohler, C., Pfaffenberger, A., Jakel, O., and Greilich, S. (2016). Technical Note: Radiological properties of tissue surrogates used in a multimodality deformable pelvic phantom for MR-guided radiotherapy. Med Phys 43, 908-916.

59. Followill, D.S., Evans, D.R., Cherry, C., Molineu, A., Fisher, G., Hanson, W.F., and Ibbott, G.S. (2007). Design, development, and implementation of the radiological

physics center's pelvis and thorax anthropomorphic quality assurance phantoms. Med Phys 34, 2070-2076.

60. Molineu, A., Followill, D.S., Balter, P.A., Hanson, W.F., Gillin, M.T., Huq, M.S., Eisbruch, A., and Ibbott, G.S. (2005). Design and implementation of an anthropomorphic quality assurance phantom for intensity-modulated radiation therapy for the Radiation Therapy Oncology Group. Int J Radiat Oncol Biol Phys 63, 577-583.

61. Singh, S.P., Singh, J., and Saha, K. (2015). Measurement and analysis of physical and climatic distribution environment for air package shipment. Packaging Technology and Science 28, 719-731.

62. Raaymakers, B.W., Raaijmakers, A.J., Kotte, A.N., Jette, D., and Lagendijk, J.J. (2004). Integrating a MRI scanner with a 6 MV radiotherapy accelerator: dose deposition in a transverse magnetic field. Phys Med Biol 49, 4109-4118.

63. Kirkby, C., Stanescu, T., Rathee, S., Carlone, M., Murray, B., and Fallone, B.G. (2008). Patient dosimetry for hybrid MRI-radiotherapy systems. Med Phys 35, 1019-1027.

64. Tchistiakova, E., Kim, A., Song, W., and Pang, G. (2017). MR-safe personal radiation dosimeters. Journal of applied clinical medical physics 18, 180-184.

65. Mathis, M., Wen, Z., Tailor, R., Sawakuchi, G., Flint, D., Beddar, S., and Ibbott, G. (2014). SU-E-T-368: Effect of a Strong Magnetic Field On Select Radiation Dosimeters. Medical Physics 41, 309-309.

66. Wen, Z., Alvarez, P., and Ibbott, G. (2015). SU-E-J-208: Feasibility Study On Using Small Plastic Phantoms for Auditing Radiation Output of MR-Linac Systems. Medical physics 42, 3313-3313.

67. Reynoso, F.J., Curcuru, A., Green, O., Mutic, S., Das, I.J., and Santanam, L. (2016). Technical Note: Magnetic field effects on Gafchromic-film response in MR-IGRT. Medical Physics 43, 6552-6556.

68. Reyhan, M.L., Chen, T., and Zhang, M. (2015). Characterization of the effect of MRI on Gafchromic film dosimetry. Journal of applied clinical medical physics 16, 325-332.

69. Roed, Y., Lee, H., Pinsky, L., and Ibbott, G. (2017). PO-0763: Characterizing the response of Gafchromic EBT3 film in a 1.5 T magnetic field. Radiotherapy and Oncology 123, S403.

70. Barten, D., Van Battum, L., Hoffmans, D., and Heukelom, S. (2017). OC-0231: The suitability of radiochromic film in 0.35 T magnetic field CO-60 compared with conventional 6MV. Radiotherapy and Oncology 123, S115-S116.

71. Delfs, B., Schoenfeld, A.A., Poppinga, D., Kapsch, R.P., Jiang, P., Harder, D., Poppe, B., and Looe, H.K. (2018). Magnetic fields are causing small, but significant changes of the radiochromic EBT3 film response to 6 MV photons. Phys Med Biol 63, 035028.

72. Steinmann, A., Stafford, R.J., Sawakuchi, G., Wen, Z., Court, L., Fuller, C.D., and Followill, D. (2018). Developing and characterizing MR/CT-visible materials used in QA phantoms for MRgRT systems. Med Phys 45, 773-782.

73. Ahmad, S.B., Sarfehnia, A., Paudel, M.R., Kim, A., Hissoiny, S., Sahgal, A., and Keller, B. (2016). Evaluation of a commercial MRI Linac based Monte Carlo dose calculation algorithm with GEANT4. Med Phys 43, 894-907.

74. Oborn, B.M., Metcalfe, P.E., Butson, M.J., Rosenfeld, A.B., and Keall, P.J. (2012). Electron contamination modeling and skin dose in 6 MV longitudinal field MRIgRT: Impact of the MRI and MRI fringe field. Med Phys 39, 874-890.

75. Oborn, B.M., Metcalfe, P.E., Butson, M.J., and Rosenfeld, A.B. (2010). Monte Carlo characterization of skin doses in 6 MV transverse field MRI-linac systems: effect of field size, surface orientation, magnetic field strength, and exit bolus. Med Phys 37, 5208-5217.

76. Oborn, B.M., Metcalfe, P.E., Butson, M.J., and Rosenfeld, A.B. (2009). High resolution entry and exit Monte Carlo dose calculations from a linear accelerator 6 MV beam under the influence of transverse magnetic fields. Med Phys 36, 3549-3559.

77. Mora, G.M., Maio, A., and Rogers, D.W. (1999). Monte Carlo simulation of a typical 60Co therapy source. Med Phys 26, 2494-2502.

78. Kry, S. (2018). The Clinical Use of Luminescent Dosimeters. In Report of AAPM Task Group 191-AAPM Recommendations on the Clinical Use of Luminescent Dosimeters (

79. Lee, H.B., G.; Ibbott G. (2018). Beam Output Changes After Magnet Ramp Down in a 1.5 T Pre-Clinical MR-Linac. In Therapy SNAP Oral Abstract. (AAPM 60th Annual Meeting.

80. Fischer-Valuck, B.W., Henke, L., Green, O., Kashani, R., Acharya, S., Bradley, J.D., Robinson, C.G., Thomas, M., Zoberi, I., and Thorstad, W. (2017). Two-and-a-half-year clinical experience with the world's first magnetic resonance image guided radiation therapy system. Advances in radiation oncology 2, 485-493.

81. Pathmanathan, A.U., van As, N.J., Kerkmeijer, L.G., Christodouleas, J., Lawton, C.A., Vesprini, D., van der Heide, U.A., Frank, S.J., Nill, S., and Oelfke, U. (2018). Magnetic Resonance Imaging-Guided Adaptive Radiation Therapy: A "Game Changer" for Prostate Treatment? International Journal of Radiation Oncology• Biology• Physics 100, 361-373.

82. Bruijnen, T., Stemkens, B., Terhaard, C., Lagendijk, J., Raaijmakers, C., and Tijssen, R. (2018). MRI-Based Radiation Therapy: Intrafraction Motion Quantification of Head and Neck Tumors Using Cine Magnetic Resonance Imaging. International Journal of Radiation Oncology• Biology• Physics 100, 1358.

83. Khoo, V.S., Dearnaley, D.P., Finnigan, D.J., Padhani, A., Tanner, S.F., and Leach, M.O. (1997). Magnetic resonance imaging (MRI): considerations and applications in radiotherapy treatment planning. Radiotherapy and Oncology 42, 1-15.

84. Ibbott, G.S., Molineu, A., and Followill, D.S. (2006). Independent evaluations of IMRT through the use of an anthropomorphic phantom. Technology in cancer research & treatment 5, 481-487.

85. Tonigan, J. (2011). Evaluation of Intensity Modulated Radiation Therapy (IMRT) Delivery Error Due to IMRT Treatment Plan Complexity and Improperly Matched Dosimetry Data. Masters, The University of Texas M. D. Anderson Cancer Center Houston, TX.

86. Low, D.A., Harms, W.B., Mutic, S., and Purdy, J.A. (1998). A technique for the quantitative evaluation of dose distributions. Medical physics 25, 656-661.

87. Soliman, A.S., Burns, L., Owrangi, A., Lee, Y., Song, W.Y., Stanisz, G., and Chugh, B.P. (2017). A Realistic Phantom for Validating MRI-based Synthetic CT Images of the Human Skull. Medical physics.

88. Cunningham, J., and Glide-hurst, C. (2017). End-To-End Phantom Evaluation for Transition From MR/CT Combined to MR-Only Workflow: SU-I-GPD-J-84.[Abstract]. Medical Physics 44, 2818.

89. Hoogcarspel, S., Kerkmeijer, L., Lagendijk, J., Van Vulpen, M., and Raaymakers, B. (2016). Development of An End-To-End Chain Test for the First-In-Man MR-Guided Treatments with the MRI Linear Accelerator by Using the Alderson Phantom: SU-F-J-150 [Abstract]. Medical physics 43, 3442-3442.

90. Price, R.G., Kim, J.P., Zheng, W., Chetty, I.J., and Glide-Hurst, C. (2016). Image guided radiation therapy using synthetic computed tomography images in brain cancer. International Journal of Radiation Oncology• Biology• Physics 95, 1281-1289.

91. Lamb, J.M., Ginn, J.S., O'Connell, D.P., Agazaryan, N., Cao, M., Thomas, D.H., Yang, Y., Lazea, M., Lee, P., and Low, D.A. (2017). Dosimetric validation of a magnetic resonance image gated radiotherapy system using a motion phantom and radiochromic film. J Appl Clin Med Phys 18, 163-169.

92. Saracen, M. (2014). ViewRay Announces World's First Patients Treated Using MRI-Guided Radiation Therapy. In ViewRay Newsroom. (Cleveland, Ohio, ViewRay.

Vita

Angela Kay Steinmann was born in Naples, Florida, the daughter of Bradford Wayne Steinmann and Brenda Sue Skinner Steinmann. After completing her work at Gulf Coast High School in May 2007, she was fortunate to attend Stetson University in a Deland, Florida. During the summer before her last year of undergraduate study, Angela participated in a Research Experience for Undergraduates (REU) at the University of Michigan where she worked on a toy Monte Carlo simulation for an international high energy collaborative research group. On May 2011 she received the degree of Bachelor of Science, Magna Cum Laude, with a major in Physics and a minor in General Business at Stetson University. Angela moved to Ann Arbor, Michigan summer of 2011 to attending the University of Michigan's Applied Physics graduate program. In May 2013, she successful completed a Master of Science in Applied Physics. Angela was accepted as a fellow for the Med-Into-Grad Howard Hughes Medical Institute and moved down to Houston, Texas that summer. Eagar to be the first in her family to obtain a PhD, Angela entered The University of Texas MD Anderson Cancer Center's Medical Physics PhD graduate program in August 2013.

Permanent Address:

3725 27th Ave SW
Naples, Florida 34117